Rep. Prog. Phys., Vol. 41, 1978. Printed in Great Britain

Electron tunnelling spectroscopy

E L WOLF

Ames Laboratory, US Department of Energy, and Department of Physics, Iowa State University, Ames, Iowa 50011, USA

Abstract

The probability $|\psi|^2$ of finding a conduction electron a distance t outside a metal even at very low temperatures is not zero, but is governed by the metal's work function ϕ through an exponential law $|\psi|^2 \sim \exp(-2\kappa t)$, with $\kappa \simeq (2m/\hbar^2)^{1/2}\,\phi^{1/2}$. This basic consequence of quantum mechanics makes possible measurable electrical currents between two conductors separated by a sufficiently thin uniform (~ 20 Å) insulator. The energy-spectroscopic information that can be, and has been, derived from careful measurement of the current–voltage (I–V) relation in such experiments is the subject of the present review.

In probably the most important application of the technique Giaever in 1960 demonstrated that when one member of the junction is superconducting, the differential conductance $\mathrm{d}I/\mathrm{d}V$ as a function of bias energy eV directly measures the density of quasiparticle excitations of the superconductor. Such data are shown to permit the most complete characterisation of the strong coupling superconducting state that is presently available, and have contributed in a most important way to our present understanding of superconductivity and superconductors.

A second type of energy spectroscopy, that of inelastic excitation thresholds, observed in the second derivative $\mathrm{d}^2I/\mathrm{d}V^2$, was demonstrated initially by Esaki (1958) in phonon spectroscopy of semiconductor tunnel diodes. This method, which has become known as inelastic electron tunnelling spectroscopy (IETS), has provided information on a variety of elementary excitations in normal systems, including, for example plasmons, magnons, and an extremely sensitive vibrational spectroscopy of molecular additions to the tunnelling barrier.

The subject matter of this review from its origin before 1960 to the present is so intimately related to the phenomenon of superconductivity including its microscopic origins that the relevant basic concepts are introduced in sufficient detail to make the article self-contained, even for the reader not previously familiar with superconductivity. Finally, the present state of the field is assessed and some guesses are hazarded as to those areas most likely to lead to important future advances.

This review was received in January 1978.

0034–4885/78/0009–1439 $05.00

Contents

1. Introduction and scope

While the phenomenon of single-particle tunnelling, basic to a quantum-mechanical understanding of matter, had been invoked early on in theories of nuclear beta decay (Gamow 1928, Gurney and Condon 1929) and electric field emission into vacuum (Fowler and Nordheim 1928), its exploitation in solid-state capacitor-like structures with ultra-thin dielectric spacing to provide a low-energy (0–5 eV) spectroscopy of the elementary excitations of solids was initiated by Esaki's invention (1958) of the tunnelling p–n semiconductor diode, and given great impetus by Giaever's studies (1960a,b,c) of superconductivity in evaporated thin-film tunnel sandwiches. This thin-film technique was based upon the observation (Fisher and Giaever 1961) that Al and several other metals form suitable (~ 20 Å) oxides upon exposure to air that allow electrons to tunnel through into a subsequently evaporated counter-electrode.

Giaever (1960a) made the important experimental discovery that if one of the metals became superconducting the *differential conductance* $\mathrm{d}I/\mathrm{d}V \equiv \sigma(v)$ of the normal-metal–insulator–superconductor (NIS) sandwich measured in the millivolt bias range showed the energy gap and density-of-states peak structure predicted by the BCS theory (Bardeen *et al* 1957) of superconductivity. The vigorous experimental and theoretical activity (in particular, the work reported by McMillan and Rowell (1969)) that soon followed this discovery has established electron tunnelling as the most sensitive probe of the superconducting state. It is a primary purpose of the present article to review these tunnelling studies of superconductivity from 1960 to the present, which requires us to spend some time initially introducing the concepts of superconductivity which are central to this work.

One may think of electron tunnelling spectroscopy in analogy to a particle scattering experiment. That is, it is a non-equilibrium method in which one measures the response of a quantum-mechanical system, typically a superconductor electrode in its ground state, when excited by a well-defined probe (electrons injected in a controlled energy range from zero to eV) by tunnelling from the opposing electrode through the thin insulating barrier. The response to this excitation by 'hot electrons' of maximum bias energy eV is simply measured as the current I flowing through an external ammeter. In practice, however, it is often of advantage to measure the derivatives $\mathrm{d}I/\mathrm{d}V = \sigma$ or $\mathrm{d}^2I/\mathrm{d}V^2$, to make contact more directly with the underlying physical processes. Thus, σ_S/σ_N in an NIS junction measures, at $T=0$, the normalised *excitation spectrum* $N_T(E)$ (tunnelling density of states):

$$\frac{\sigma_S(eV)}{\sigma_N(eV)} = \mathrm{Re}\,(|E|/\sqrt{(E^2-\Delta^2)}) \equiv N_T(E) \qquad E=eV \tag{1.1}$$

of the superconducting state, with 2Δ the characteristic energy gap (see figure 1(*a*)), while $\mathrm{d}^2I/\mathrm{d}V^2$ is of direct significance in connection with inelastic electron tunnelling spectroscopy (IETS) revealing, for example, phonon energies (figure 1(*b*)). Further, in an NIN junction with organic molecules adsorbed to the insulating barrier $\mathrm{d}^2I/\mathrm{d}V^2$ may reveal the spectrum of vibrational excitations of the molecules. This information is also obtainable from infrared and Raman spectroscopy but, as we shall see, these

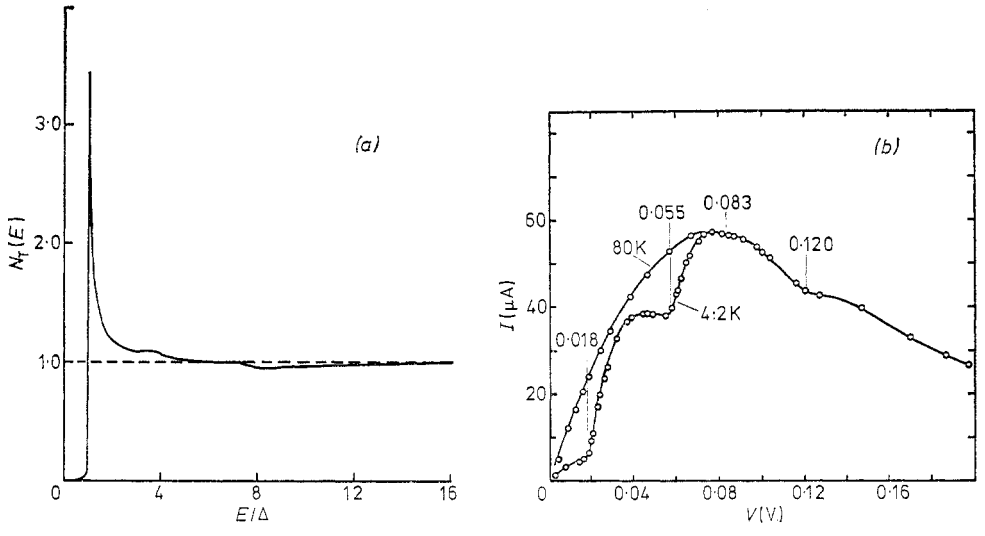

Figure 1. (*a*) The normalised excitation spectrum $N_T(E)$ of Pb measured at 0·3 K. The superconducting energy gap and small deviations from the BCS prediction near $eV = k_B\theta_D$ are shown here (from Giaever *et al* 1962). $\Delta = 1{\cdot}34 \times 10^{-3}$ eV. (*b*) The forward current–voltage relation of a silicon tunnel diode at 4·2 K and at 80 K. The points of current onset correspond to zone boundary phonon energies in the semiconductor (from Esaki 1958). Si: $3{\cdot}4 \times 10^{19}$ cm^{-3} donors.

techniques in general require larger samples than the tunnelling method which can detect as few as 10^{10} molecules.

While the greatest power of the tunnelling method lies in the detailed study of superconductivity in metals, alloys and compounds, a great variety of normal-state phenomena have also been studied, especially in the past 10 years, by tunnelling. Large portions of this work in semiconductors have built upon the pioneering work of Esaki (1958), while new approaches in the NIN category have also been productive.

One might cite as examples the study of phonons in semiconductors, magnetic moments and Kondo scattering, two-dimensional electron systems, Landau levels, and plasmons, in addition to the study of adsorbed molecules, which we have mentioned.

Some measure of the importance of the several forms of tunnelling is indicated by the award of the 1973 Nobel Prize in Physics to Leo Esaki, Ivar Giaever and Brian Josephson. Particularly recommended are the lucid personal accounts of the early work in the areas of superconductive tunnelling (Giaever 1974, Josephson 1974) and semiconductor tunnelling (Esaki 1974) contained in the respective Nobel lectures.

We shall largely restrict our present review to *single-particle tunnelling* as a spectroscopic tool in the study of matter. The important phenomena of *pair* or *Josephson tunnelling* are a separate subject which has recently been reviewed in this journal (Waldram 1976). In our discussion of single-particle tunnelling we have intended to cover the *main* topics in tunnelling since 1958. This is not to say that our coverage is complete either in references or, indeed, in topics discussed; this is simply not possible. For further detail and some additional topics in normal-metal tunnelling the reader is referred to an earlier full length review of this subject (Wolf 1975). For many tabulations and a more extensive set of references (before 1972) see Solymar (1972); experimental techniques are reviewed by Coleman *et al* (1974). The book

by Duke (1969) is recommended for a more complete and historical treatment of the theory of tunnelling using the transfer Hamiltonian. Other specialised review articles are mentioned at appropriate points in the text.

2. Theory of superconductive tunnelling

2.1. Introduction

The theory of tunnelling most appropriate to introduce the spectroscopic study of superconductivity is that based on the transfer Hamiltonian, which we describe after a discussion of basic concepts of tunnelling. We then discuss in some detail the microscopic origins of superconductivity: the concepts necessary are largely those introduced by BCS for the weak coupling case. This prepares the way for the necessary generalisations to describe *strong coupling superconductors* which are, as we have said, the materials most satisfactorily studied by tunnelling spectroscopy.

2.2. Basic concepts of tunnelling

The essential features of a tunnel junction are two electrodes of high electrical conductivity (and thus negligible voltage drop under bias), separated by an insulator layer whose thickness t and barrier height U_B (see figure 2) are such as to withstand

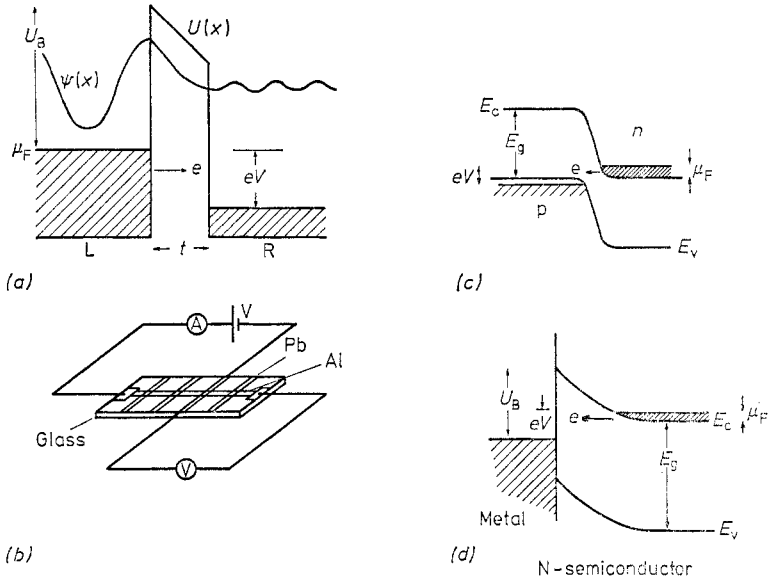

Figure 2. (*a*) Schematic diagram of a stationary electron wave tunnelling from L to R across forbidden potential barrier $U(x)$. V is the bias voltage applied; eV is the range of energies over which tunnelling transitions may occur at $T=0$. (*b*) The elementary measuring circuit shown in connection with a typical thin evaporated film Pb–Al_2O_3–Al tunnel sandwich. (*c*) The narrow (tunnelling) pn junction between degenerately doped (metallic) regions of a semiconductor of band gap E_g. (*d*) The Schottky barrier contact which occurs between a metal and a degenerate semiconductor. A positive uniform space charge leads to a quadratic variation of $U(x)$, i.e. the band edge E_c with x.

an applied bias voltage V of up to several volts and yet permit a measurable flow of electrons by tunnelling. If we represent the barrier as a one-dimensional potential $U(x)$ in the interval $0 \leqslant x \leqslant t$ and the electron wave incident from the left by $\exp(+i\boldsymbol{k}.\boldsymbol{r})$, $\boldsymbol{k}=(k_x, k_y, k_z)$, having energy $E=E_x+E_t$ with $E_x=\hbar^2 k_x^2/2m$, $E_t=E-E_x$, then the amplitude T of the transmitted wave for $x>t$ can be found by solving Schrödinger's equation:

$$\frac{-\hbar^2}{2m}\frac{\partial^2}{\partial x^2}\psi+U(x)\,\psi=E\psi \tag{2.1}$$

in the three regions ($x<0$; $0\leqslant x\leqslant t$; $x>t$) and requiring the wavefunction ψ and its derivative to be continuous at the boundaries $x=0$, t. In the case $U(x)=U_0$, the wavefunction inside the barrier ($0\leqslant x<t$) is $\exp[i(k_y y+k_z z)]$ $[B\exp(-\kappa x)+B\exp(+\kappa x)]$ (we assume specular reflection so that the transverse y, z motion is unaffected), with real decay constant κ obtained by taking $U(x)=U_0$ in:

$$\kappa=\left(\frac{2m}{\hbar^2}[U(x)-(E-E_t)]\right)^{1/2}. \tag{2.2}$$

In the limit $\kappa t\gg 1$ the resulting transmission probability is $T^2=\beta^2\exp(-2\kappa t)$, with $\beta=\kappa k_x(\kappa^2+k_x^2)^{-1}$.

In the more realistic case that the local wavevector x components (and local x-kinetic energies) differ on the opposing sides (corresponding to different bandwidths on the two sides) the transmission probability is of the same form:

$$T^2=\beta^2\exp(-2\kappa t) \qquad \beta^2=16k_1k_2\kappa^2[(k_1^2+\kappa^2)(k_2^2+\kappa^2)]^{-1}. \tag{2.3}$$

In the case of a sloping barrier profile $U(x)$ the WKB approximation may be used, namely:

$$T=\exp(-2K) \qquad K=\int_{x_1(E_x)}^{x_2(E_x)}\kappa(x, E_x)\,dx \tag{2.4}$$

with x_1 and x_2 the classical turning points. In this case the pre-factor β^2 is unity: this difference has a bearing on the band structure information available from tunnelling in the *normal state* case, and illustrates an extreme sensitivity to the details of the interface.

In any case T^2 is to be regarded as the fraction of the probability current $\hbar k_x/m$ in the incident wave that is passed, which can be verified by evaluating the probability current operator:

$$j=\frac{i\hbar}{2m}\left(\psi\frac{\partial\psi^*}{\partial x}-\psi^*\frac{\partial\psi}{\partial x}\right) \tag{2.5}$$

at any point in the barrier or the right-hand region.

As a numerical example, if one takes $m=m_e$, $t=20$ Å, $U_0-E_x=1$ eV, $\beta=1$, one finds $T^2\sim 10^{-9}$, indicating that the two electrodes are indeed only weakly coupled by the barrier. An important feature of the transmission factor is its strong peaking for transmission at normal incidence, $\theta=0$. This can be estimated for small angles $\theta\simeq\sin\theta$ as leading to an angular dependence:

$$|T(\theta)|^2\simeq|T(0)|^2\exp\left(\frac{-\kappa tE}{U_0-E}\theta^2\right). \tag{2.6}$$

In our example, if we specify $U_0=6$ eV and $E=5$ eV, then T^2 is reduced to $1/e$ of its value at 8°. In a real tunnel junction the barrier may be of trapezoidal shape, and,

in fact, its shape must change as the bias voltage V varies. This inherent voltage distortion of the barrier leads, in typical NIS junctions used in superconductive tunnelling, to a weak and approximately parabolic increase in conductance $\mathrm{d}I/\mathrm{d}V$ centred close to $V=0$. Over the small bias voltage range of interest in superconductive tunnelling this effect can be neglected. The implicit voltage or explicit E_x dependencies of T^2 can, however, in other circumstances be very important and these possibilities must always be kept in mind. We will return to the development of the theory of tunnelling in this stationary-state point of view in §5.

2.3. The transfer Hamiltonian method

The experimental measurements of $\sigma(V)$ by Giaever (figure 1(*a*)) suggested that the final density of states (or of excitations of the superconductor) was being directly measured. The stationary-state approach above appeared unsuitable to understand either this experimental result or the phonon threshold observations of Esaki (figure 1(*b*)). The first theoretical explanation of Giaever's experimental result was by Bardeen (1961), whose work was extended and confirmed by Cohen *et al* (1962). The approach (Oppenheimer 1928, Duke 1969) is to seek a perturbing operator $\mathscr{H}^{\mathrm{T}}$, the transfer Hamiltonian, which can be regarded as driving electron transitions across the tunnelling barrier according to the familiar golden rule:

$$W_{\mathrm{LR}}=\frac{2\pi}{\hbar}\,|\langle\psi_{\mathrm{R}}|\,\mathscr{H}^{\mathrm{T}}|\,\psi_{\mathrm{L}}\rangle|^2\,N_{\mathrm{f}}(E_{\mathrm{R}})\,\delta(E_{\mathrm{L}}-E_{\mathrm{R}}) \tag{2.7}$$

of perturbation theory, and to identify the final density of states $N_{\mathrm{f}}(E)$ with the excitation spectrum of the superconductor. One regards the two electrodes as nearly isolated systems with complete Hamiltonians $\mathscr{H}_{\mathrm{L}}$, $\mathscr{H}_{\mathrm{R}}$, and eigenstates ψ_{L}, ψ_{R}, which are weakly coupled by the perturbing barrier term $\mathscr{H}^{\mathrm{T}}$: the total Hamiltonian is thus

$$\mathscr{H}=\mathscr{H}^{\mathrm{L}}+\mathscr{H}^{\mathrm{R}}+\mathscr{H}^{\mathrm{T}}. \tag{2.8}$$

In the language of second quantisation $\mathscr{H}^{\mathrm{T}}$ is expressed as:

$$\mathscr{H}^{\mathrm{T}}=\sum_{k_{\mathrm{L}},\,k_{\mathrm{R}}}(T_{k\mathrm{R},\,k\mathrm{L}}c_{k\mathrm{L}}c_{k\mathrm{R}}{}^{*}+\mathrm{HC}) \tag{2.9}$$

where T is the indicated matrix element of $\mathscr{H}^{\mathrm{T}}$, $c_{k\mathrm{R}}{}^{*}$ creates an electron of wavevector $k\mathrm{R}$ on the right and $c_{k\mathrm{L}}$ destroys an electron of wavevector $k\mathrm{L}$ on the left.

We illustrate the appropriate wavefunctions ψ_{L}, ψ_{R} in the case of a sharp boundary and $U(x)=U_0$; for the corresponding WKB wavefunctions see Bardeen (1961) or Harrison (1961). The approximation consists in neglecting the tail of the wavefunction ψ_{L} in the right electrode, and vice versa. Supposing the electrode thickness to be t, and taking the junction area as unity, one has:

$$\psi_{\mathrm{L}}=\begin{cases} t^{-1/2}\exp\left[\mathrm{i}(k_y y+k_z z)\right]\sin\left(k_x x+\gamma\right) & x<0 \\ \tfrac{1}{2}t^{-1/2}\exp\left[\mathrm{i}(k_y y+k_z z)\right]\beta\exp\left(-\kappa x\right) & 0<x<t \\ 0 & t<x \end{cases} \tag{2.10}$$

with a similar expression for ψ_{R}, which decays oppositely in the barrier. The states ψ_{L}, ψ_{R} are standing waves in the two electrodes, with weak overlapping exponential tails in the barrier. Bardeen (1961) showed that the matrix element T could be

obtained by evaluating the probability current operator *between* the oppositely decaying functions ψ_L, ψ_R at any point in the barrier $0<x<t$:

$$T_{k\mathrm{R},k\mathrm{L}} = -i\hbar\langle\psi_R|j|\psi_L\rangle. \tag{2.11}$$

This expression was evaluated by Harrison (1961) as:

$$|T_{k\mathrm{R},k\mathrm{L}}|^2 = \delta(k_{t\mathrm{R}}, k_{t\mathrm{L}})\,\beta^2 \exp(-2K)(4\pi^2\rho_{x\mathrm{L}}\rho_{x\mathrm{R}})^{-1}. \tag{2.12}$$

Here the δ function requires conservation of the transverse wavevector k_t; $\rho_{x\mathrm{L}}$ and $\rho_{x\mathrm{R}}$ are one-dimensional densities of states:

$$\frac{w}{\pi}\left(\frac{\partial E}{\partial k_x}\right)^{-1} \tag{2.13}$$

on the two sides and the WKB case is obtained by setting $\beta^2=1$; otherwise, $U(x)=U_0$ and $K=\kappa t$ for the sharp boundary. The current density J is obtained by summing all possible transitions at rate W_{LR} between filled initial and empty final states:

$$J = 2e\sum_{k\mathrm{L},\,k\mathrm{R}}\frac{2\pi}{\hbar}|T_{\mathrm{RL}}|^2[f_L(1-f_R)-f_R(1-f_L)] = \frac{4\pi e}{\hbar}\sum_{k\mathrm{L},\,k\mathrm{R}}|T_{\mathrm{RL}}|^2[f(E)-f(E+eV)]. \tag{2.14}$$

Here $f(E)=\{1+\exp[(E-\mu_F)(k_BT)^{-1}]\}$ and $e=-1{\cdot}6\times10^{-19}$ C; we have specified positive bias V as lowering the electron energies on the right, corresponding to electron flow to the right and positive current to the left.

The next step in the reduction of the current J is to change the summations on k_L, k_R to integrals over energy. In performing the change of variable $\Sigma_{k_x}\to\int dk_x\to\int(\partial E/\partial k_x)^{-1}\,dE$; note that the $(\partial E/\partial k_x)^{-1}$ thus introduced will cancel against the same factor in the squared matrix element. As we shall see below, in the case of the weak coupling superconductor the real energy E of a quasiparticle of wavevector k differs from the ('bare') energy ϵ_k which would occur without the pairing interaction: $E=(\epsilon_k^2+\Delta^2)^{1/2}$, where we now measure ϵ and E from the Fermi surface. In this situation a further change of variable is necessary:

$$\sum_{k_x}\to\int\left(\frac{\partial\epsilon}{\partial k_x}\right)^{-1}\frac{\partial\epsilon}{\partial E}\,dE = \int\left(\frac{\partial\epsilon}{\partial k_x}\right)^{-1}\frac{E}{(E^2-\Delta^2)^{1/2}}\,dE \tag{2.15}$$

which indicates the origin of the normalised excitation spectrum $N_T(E)$ in the weak superconductor tunnelling characteristic. The result in the case of an NIS configuration is (WKB approximation):

$$J = \frac{2e}{h}\int\frac{d^2k_t}{(2\pi)^2}\exp(-2K)\int_{-\infty}^{\infty}\mathrm{Re}\left(\frac{|E|}{(E^2-\Delta^2)^{1/2}}\right)[f(E)-f(E+eV)]\,dE \tag{2.16}$$

where the sum over transverse k_t has been replaced by an integral which as we have noted in connection with (2.6) heavily weighs $\theta\simeq0$; $(2\pi)^2$ is the two-dimensional phase space per state. The specification of the real part in (2.16) for a *weak coupling* BCS superconductor is merely a way of stating that $N_T(E)$ is zero for $E<\Delta$.

The integral over transverse wavevector k_t in (2.16) has its main contribution at small k_t corresponding to small tunnelling angle θ (2.6). For superconducting tunnelling at bias voltages less than 0·1 V this integral can often be replaced by an effective $|T|^2\propto\exp[-2t(2mU_B/\hbar^2)^{1/2}]$ where $U_B=\overline{U(x)}-\mu_F$ (Scalapino *et al* 1966); in other cases the voltage dependence of $|T|^2$ through $U(x, V)$ is important.

Numerical integration may be necessary if one wants an accurate comparison to the measured currents, which has been done in the case of metal–semiconductor (Schottky barrier) contacts (Conley *et al* 1966, Conley and Mahan 1967, Steinrisser *et al* 1968), a case unusual in that one has detailed knowledge of $U(x)$. Numerical agreement has also been reported for GaSe barriers by Kurtin *et al* (1971). Numerical integration over k_t in modelling typical oxide barriers has been carried out by Brinkman *et al* (1970), and for oxide barriers containing organic molecules by Walmsley *et al* (1977). The angular dependence $T(\theta)$ permits in favourable cases on single crystals the determination of anisotropy in the energy gap (Blackford and March 1969). The beauty of superconductive tunnelling is that all of these details drop out in forming the ratio $\sigma_S/\sigma_N = N_T(E)$.

Finally, one obtains the useful derivative:

$$\frac{dJ}{dV} = \sigma_S(V) = -\frac{2e}{h}\int \frac{d^2k_t}{(2\pi)^2}\exp(-2K)\int_{-\infty}^{\infty} N_T(E)\frac{\partial f}{\partial E}(E+eV)\,dE. \qquad (2.17)$$

The Fermi function derivative is a sharply peaked function whose full width at half-height is $1{\cdot}2k_BT$: this is effectively a δ function, showing that $\sigma(V) \propto N_T(eV)$ at $T=0$, as stated earlier. Since precisely the same expression with the dimensionless $N_T(E)$ replaced by *unity* describes the normal phase, we have:

$$\frac{\sigma_S(V)}{\sigma_N(V)} = \int_{-\infty}^{\infty} N_T(E)\frac{\partial f}{\partial E}(E+eV)\,dE \to N_T(eV) \qquad (T\to 0). \qquad (2.18)$$

If we have independent means of measuring the density of electronic states (per unit energy and volume at μ_F) $N(0)$, then we may determine the total *density of superconducting excitations* as $N_S(E) = N(0)\,N_T(E)$. Before pursuing the extension to strong coupling superconductors, it is appropriate to discuss the nature of a superconducting metal.

2.4. The microscopic origins of superconductivity

An important experimental result stimulating the microscopic theory of superconductivity was the isotope effect: $T_C M^a = \text{constant}$, where T_C is the superconducting transition temperature, M is the isotropic mass of the metal ion, and the exponent a is near 0·5 for many elements. With this evidence, provided in the early 1950s, that the lattice vibrations must be intimately involved in the superconducting phase the stage was set for a theory involving the electron–phonon interaction. The correct role for the interaction was specified in the most striking hypothesis of BCS: that of *exact pairing* of electrons at the Fermi surface. This was an extension of Cooper's discovery (1956) that *any net attractive* interaction between two electrons above a filled normal-metal Fermi surface ($T=0$) would lead to the formation of a stable pair of electrons.

2.4.1. The electron–phonon interaction. To qualitatively understand the origin of the pairing electron–electron attraction which arises from electron–phonon coupling, imagine (Cooper 1960) an electron at the Fermi surface moving ($v_F \sim 10^8$ cm s^{-1}) through the crystalline lattice of positively charged ions. The nearby ions experience an impulsive force during the electron transit which (figure 3(*a*)) will cause them to come closer together after a half lattice period of $\frac{1}{2}\tau \sim 10^{-13}$ s; at this *later* time one expects a local clustering of the ions and possibly a *net positive* (electron + ion) charge

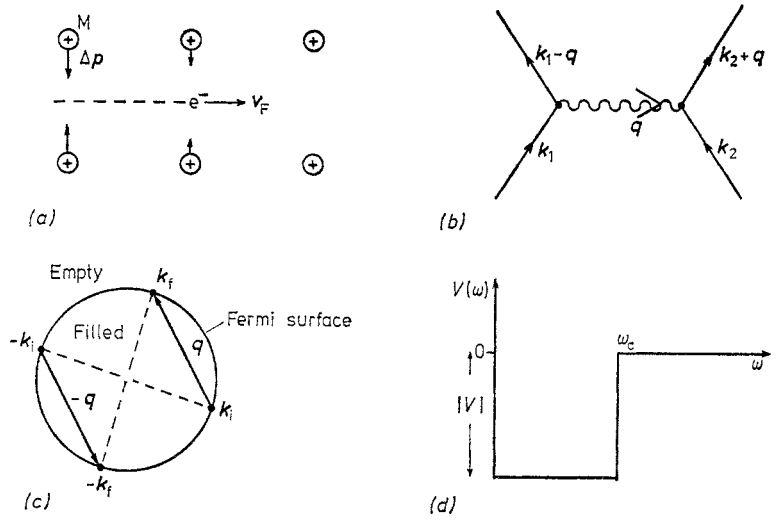

Figure 3. (*a*) The retarded distortion of the metal ion lattice produced by the transit of a Fermi surface electron, $v_F \sim 10^8$ cm s^{-1}. The subsequent positive local charge concentration will favour the passage of a second electron. (*b*) Exchange of a virtual phonon between two Fermi surface electrons, leading to the attractive pairing interaction. (*c*) Typical scattering event undergone by a pair of electrons exchanging a virtual phonon. (*d*) The model pairing potential assumed by Bardeen, Cooper and Schrieffer in 1957. An attractive V, however weak, leads to a paired semiconducting ground state at $T=0$.

density which would make energetically favourable the retarded transit of a *second* electron as a mate to the first. The restrained nature of this electronic mating is indicated by the large optimum spacing between the electrons, $\frac{1}{2}v_{F\tau} \sim \frac{1}{2}(10^8 \times 10^{-13})$ cm $= 500$ Å. This turns out to be the coherence length ξ_0. The very large number of electrons passing between the members of such a pair in a volume of diameter 500 Å implies a great degree of correlation in the motion of adjacent pairs, leading to the remarkable *phase coherence* of the superconducting pair wavefunction, which is the origin of the characteristic *macroscopic quantum effects*: flux quantisation and the Josephson effects.

Quantum mechanically, the first electron $(\boldsymbol{k}, E)$ can emit a (virtual) phonon of energy $\hbar\omega_q$, wavevector $\boldsymbol{q}$, and thus scatter to $(\boldsymbol{k}-\boldsymbol{q}, E-\hbar\omega)$; the second electron $(\boldsymbol{k}', E')$ during a time interval $\Delta t \leqslant \omega^{-1}$ absorbs this phonon to scatter to $(\boldsymbol{k}'+\boldsymbol{q}, E'+\hbar\omega)$ (figure 3(*b*)).

That this process in fact lowers the energy of the two electrons, so long as $|E-E'| < \hbar\omega_q$, follows from second-order perturbation theory, which yields, first:

$$\langle \boldsymbol{k}-\boldsymbol{q}, \boldsymbol{k}'+\boldsymbol{q}|V_1|\,\boldsymbol{k}, \boldsymbol{k}'\rangle = \frac{|M|^2}{E(\boldsymbol{k})-E(\boldsymbol{k}-\boldsymbol{q})-\hbar\omega}. \tag{2.19}$$

Now a second possible process involves *prior* emission of a phonon $-\boldsymbol{q}, \hbar\omega$ by electron $\boldsymbol{k}'$, which is subsequently absorbed by electron $\boldsymbol{k}$; when this process V_2 is added in, taking the matrix element M to be the same, one obtains a total interaction:

$$\langle \boldsymbol{k}-\boldsymbol{q}, \boldsymbol{k}'+\boldsymbol{q}|V|\,\boldsymbol{k}, \boldsymbol{k}'\rangle = \frac{+2\hbar\omega_q|M|^2}{(E_k-E_{k-q})^2-(\hbar\omega_q)^2}. \tag{2.20}$$

Note that this interaction is negative (attractive) for $|E_k - E_{k-q}| < \hbar\omega_q$; in the limit $E_k = E_{k-q}$ (for example, both members of the pair on the Fermi surface) the result is just:

$$V_q \simeq -\frac{2|M|^2}{\hbar\omega_q}. \tag{2.21}$$

Figure 3(*c*) shows the scattering of two Fermi surface electrons $\boldsymbol{k}$, $-\boldsymbol{k}$ by the emission of a virtual phonon of wavevector $\boldsymbol{q}$. This scattering process is possible only if the final states $\boldsymbol{k}-\boldsymbol{q}$, $-\boldsymbol{k}+\boldsymbol{q}$ are *unoccupied*; the maximum rate of such scattering processes, leading to a maximum lowering of energy of the electron system, will thus require many pairs of empty final states. The other important force between electrons is the residual screened Coulomb repulsion U_c. In the same range of $\boldsymbol{q}$ the corresponding Fourier component is:

$$U_q = \frac{4\pi e^2}{q^2 + \lambda^2} \tag{2.22}$$

where λ is the inverse screening length. Bardeen *et al* (1957) take a simple model potential to represent $V_q + U_q$: a constant attractive interaction $-|V|$ between any two electrons with ϵ_k, $\epsilon_{k'} < \hbar\omega_c \sim k_B\theta_D$, now measuring kinetic energies ϵ_k from the Fermi surface (figure 3(*d*)).

2.4.2. The paired ground state. The ground-state wavefunction of BCS incorporates all electron states as symmetric (spin-reversed) pairs $\boldsymbol{k}$, $-\boldsymbol{k}$, for this choice maximises the electron–phonon scattering rate and hence minimises the energy. The *occupation function* of the *pair states*, h_k (which for isotropic materials is a function only of the energy), is determined variationally to find the lowest electron free energy. Reflecting the need for empty pair states in the scattering events, the value of the resulting h_k at the Fermi surface is just $\frac{1}{2}$.

The function h_k turns out to be:

$$h_k = \tfrac{1}{2}\left(1 - \frac{\epsilon_k}{(\epsilon_k^2 + \Delta^2(T))^{1/2}}\right) = \tfrac{1}{2}\left(1 - \frac{\epsilon_k}{E_k}\right) \tag{2.23}$$

where the parameter $\Delta(T)$, the superconducting energy gap, is a measure of the energy range over which electron and hole states are mixed (figure 4(*a*)) by the interaction. The gap parameter Δ is determined by solving the integral equation (2.25), resulting:

$$\Delta(T) = V \sum_{k' < k_c} [h_{k'}(1 - h_{k'})]^{1/2}[1 - 2f(E_{k'})] \tag{2.24}$$

$$= N(0)\, V \int_0^{\hbar\omega_c} \frac{\Delta}{(\epsilon^2 + \Delta^2)^{1/2}} \tanh\left(\frac{(\epsilon^2 + \Delta^2)^{1/2}}{2k_B T}\right) \mathrm{d}\epsilon \tag{2.25}$$

from a combination of (2.23) and (2.24). Equation (2.24) for Δ reveals the self-consistent nature of the superconducting state: Δ depends not only on the existence of a potential V (electron–phonon coupling) but also directly (in the sum on k') upon the number of filled ($\sqrt{h_{k'}}$) and empty ($(1 - h_{k'})^{1/2}$) available pair states. This leads to the concept of the coherence length of the superconducting state and is important, especially in connection with the proximity effect (below). The role of temperature ($f(E_{k'}) \neq 0$) in blocking the scattering states is also evident in (2.24). Equation (2.25) in the $T = 0$ limit determines the gap $\Delta(0)$ as:

$$\Delta(0) = \hbar\omega_c \sinh(1/N(0)\, V) \to \hbar\omega_c \exp(-1/N(0)\, V) \qquad (N(0)\, V \ll 1). \tag{2.26}$$

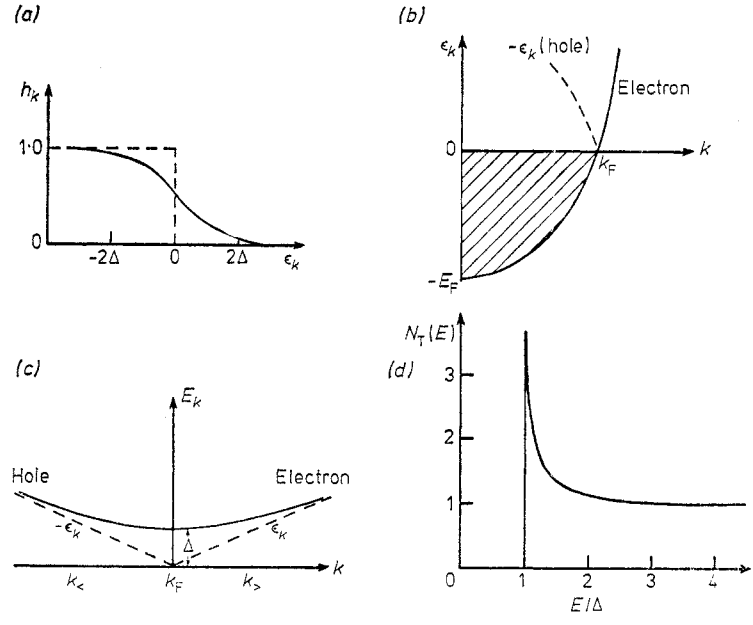

Figure 4. (*a*) Schematic behaviour of the occupation function h_k of the pair states as a function of the bare kinetic energy ϵ_k, measured in units of Δ, at $T=0$. (*b*) Single-particle excitations of the normal phase: electrons of energy ϵ_k, and holes of energy $-\epsilon_k$. (*c*) Single-particle excitations of the superconducting phase lie on the electron-like branch for $k>k_F$ ($k_>$) and on the hole-like branch for $k<k_k$ ($k_<$). The minimum excitation of energy Δ at k_F is an equal admixture of electron and hole. (*d*) The excitation spectrum obtained by BCS.

The transition temperature T_C is determined by solving equation (2.25) for T such that $\Delta=0$; this yields, in the BCS model, $2\Delta(0)=3{\cdot}52k_BT_C$. The function $\Delta(T)$ falls as the temperature rises qualitatively because the empty pair states near k_F, needed as scattering final states, become thermally occupied and thus unavailable. This is described by the term $1-2f(E_k)$, $E_k=(\epsilon_k^2+\Delta^2)^{1/2}$ in equation (2.24).

2.4.3. Quasiparticle excitations. We have thus far discussed the superconducting *ground state*, in which every one-electron state is a member of one, and only one, pair state $\boldsymbol{k}$, $-\boldsymbol{k}$, and these two single-electron states constituting the pair are either simultaneously occupied or simultaneously empty. A *quasiparticle excitation* can occur by destroying a pair and forcing *single occupation* of either $\boldsymbol{k}$ or $-\boldsymbol{k}$. This can arise by *injection* of a single electron (or a single hole) as may occur in a tunnelling experiment, or by *transfer* of a single electron from an occupied pair $\boldsymbol{k}'$ or $-\boldsymbol{k}$ to an unoccupied pair state $\boldsymbol{k}'$, $-\boldsymbol{k}$ as, for example, by photon absorption—in the latter case *two* pair states are disrupted. One must emphasise that an important part of the *excitation energy* E_k is the removal of the pair state in question from the summation in equation (2.24) for Δ, in addition to the direct kinetic energy change, e.g. $\epsilon_{k'}-\epsilon_k$ can be nearly zero in the case of absorption of a photon of energy Δ. BCS thus obtained for the excitation E_k of wavevector k:

$$E_k=(\epsilon_k^2+\Delta^2)^{1/2} \qquad \text{(electron or hole injection)} \qquad (2.27)$$

and

$$E_{k_1,k_2}=(\epsilon_{k_1}{}^2+\Delta^2)^{1/2}+(\epsilon_{k_2}{}^2+\Delta^2)^{1/2} \qquad \text{(thermal or optical excitation)} \quad (2.28)$$

the latter involving two pair states.

In connection with tunnelling it is necessary to examine more closely the processes of electron and hole injection. In figure 4(*b*) the full and broken curves, respectively, are the ϵ_k–k curves representing electron ($k>k_F$) and hole ($k<k_F$) excitations of the normal Fermi gas. The full curve in figure 4(*c*) shows the modification introduced in the superconducting state. We still speak of *hole-like* ($k<k_F$) and *electron-like* ($k>k_F$) branches of the quasiparticle excitation spectrum but at $k=k_F$ we now find a *minimum excitation energy* Δ, corresponding to an excitation which is an equal mixture of electron and hole. This characteristic coupling of electron- and hole-like parts of the quasiparticle excitation at wavevector k is expressed in the (electron and hole) coherence factors u_k and v_k, such that $u_k{}^2+v_k{}^2=1$, $u_k{}^2=1-h_k{}^2$:

$$u_k=\tfrac{1}{2}\left(1+\frac{\epsilon_k}{(\epsilon_k{}^2+\Delta^2)^{1/2}}\right) \qquad v_k=\tfrac{1}{2}\left(1-\frac{\epsilon_k}{(\epsilon_k{}^2+\Delta^2)^{1/2}}\right). \quad (2.29)$$

One says that the excitation at k is an electron with probability $u_k{}^2$ and a hole with probability $v_k{}^2$. Note that for the $k<$ branch one has $\epsilon_k<0$, so the (electron) amplitude u_k becomes small relative to the v_k (hole) amplitude for $E_k>\Delta$, and the opposite situation exists in the $k>$ (electron-like) branch. Finally, if we inject a single electron with specified energy (relative to μ_F) E_k, this is accommodated as a linear combination of quasiparticle excitations of wavevectors $k_{1<}$, $k_{2>}$ such that $u_{k_1<}{}^2+u_{k_2>}{}^2=1$.

The total density of single-particle excitations of energy E_k (figure 4(*d*)) can be obtained from the formula $E_k=(\epsilon_k{}^2+\Delta^2)^{1/2}$ along with the known normal-state density $N(0)\equiv\partial N/\partial\epsilon|_{\epsilon=0}$ as:

$$\frac{\partial N}{\partial E}=\frac{\partial N}{\partial\epsilon}\frac{\partial\epsilon}{\partial E}=N(0)\frac{|E|}{(E^2-\Delta^2)^{1/2}}=N_S(E) \quad (2.30)$$

which is $N(0)$ times the dimensionless quantity directly measured by electron tunnelling, $N_T(E)$, equation (1.1).

2.4.4. The strong coupling case. Extension and generalisation of the BCS theory have been accomplished to allow for strong coupling and for treatment of spatially varying systems, such as proximity sandwiches. One sign of strong coupling is observation of values of the ratio $2\Delta/k_BT_C$ larger than the BCS value 3·52; one also finds deviations in the normalised tunnelling conductance $N_T(eV)$ from (1.1) at bias voltages near the Debye energy, which can be seen in the data of figure 1(*a*). For a historical development of the theoretical advances which have resulted in a satisfactory understanding of these effects the reader is referred to the excellent accounts by McMillan and Rowell (1969) and Schrieffer (1964); we will only summarise the important results.

In the important case when electron–phonon interactions are strong, as in superconductors such as lead or Nb_3Ge, it is no longer possible to assign unequivocally an energy E_k for a state of a given wavevector $\boldsymbol{k}$. In this case the lifetime of state $\boldsymbol{k}$ against emission of a phonon can result in an energy *width* comparable to the energy itself. The resulting distribution of energies is represented by a *spectral function*:

$$A(\boldsymbol{k},E)=\frac{1}{\pi}\,|\operatorname{Im} G(\boldsymbol{k},E)| \quad (2.31)$$

where $G(\boldsymbol{k}, E)$ is the one-electron Green function. Now the density of states per unit energy is given (Mahan 1969) by:

$$N(E)=\int \frac{\mathrm{d}^3\boldsymbol{k}}{(2\pi)^3} A(\boldsymbol{k}, E). \tag{2.32}$$

A treatment of the electron–phonon interaction more realistic than the BCS treatment was developed by Eliashberg (1960), using a Green function approach. This interaction, suitable for strong coupling, is local in position (the BCS assumption is not a local interaction) but retarded in time as suggested by the intuitive argument of figure 3(*a*). The Coulomb repulsion between electrons was more realistically treated by Morel and Anderson (1962) as a pseudopotential:

$$\mu^*=\frac{N(0)\,U_c}{1+N(0)\,U_c \ln (E_F/\omega_0)} \tag{2.33}$$

and the correction arises physically from the more rapid response of the electron system in screening than of the ion system in the attractive interaction.

The strong coupling generalisation of the BCS energy gap parameter is a complex and energy ($E=\omega$) dependent gap function $\Delta(\omega)=\Delta_1(\omega)+\mathrm{i}\Delta_2(\omega)$, whose imaginary part describes the lifetime energy width arising from possible phonon emission if ω is sufficiently large. The gap edge Δ_0 is now the value of the gap function evaluated at energy Δ_0: $\Delta(\Delta_0)=\Delta_0$. In cases where spatial dependence exists the function $\Delta(\omega, \boldsymbol{r})$ is referred to as the *pair potential.* The gap function is related to the *pairing self-energy*:

$$\phi(\omega)=Z(\omega)\,\Delta(\omega) \tag{2.34}$$

with $Z(\omega)$ the *renormalisation function* for the superconducting state. The gap function and renormalisation function for Hg, determined by tunnelling by Hubin and Ginsberg (1969), are shown in figure 5.

The equations for the normal and pairing self-energies $\Sigma(\omega)$, $\phi(\omega)$ (the gap equations), using the Eliashberg form of the electron–phonon interaction, are, for $T=0$ and isotropic materials:

$$\Sigma(\omega)=[1-Z(\omega)]\,\omega=\int_{\Delta_0}^{\omega_c} \mathrm{d}\omega'\ \mathrm{Re}\left(\frac{\omega'}{(\omega'^2-\Delta'^2)^{1/2}}\right) \times \int \alpha^2(\omega_q)\,F(\omega_q)[D_q(\omega'+\omega)-D_q(\omega'-\omega)]\,\mathrm{d}\omega_q \tag{2.35}$$

$$\phi(\omega)=\int_{\Delta_0}^{\omega_c} \mathrm{d}\omega'\ \mathrm{Re}\left(\frac{\Delta'}{(\omega'^2-\Delta'^2)^{1/2}}\right)\{\int \alpha^2(\omega_q)\,F(\omega_q)[D_q(\omega'+\omega)-D_q(\omega'-\omega)]\mathrm{d}\omega_q-\mu^*\} \tag{2.36}$$

where $\Delta_0=\Delta(\Delta_0)$ is the energy gap and $D_q(\omega)=(\omega+\omega_q-\mathrm{i}0^+)^{-1}$. One can identify the integral over the phonon frequency distribution $F(\omega)$, weighted by the averaged electron–phonon interaction strength $\alpha^2(\omega)$, with a sum over intermediate states in the second-order perturbation theory (2.20). The upper limit ω_c corresponds to an energy cutoff.

The superconducting and normal properties of the system are completely described by the complex and energy-dependent functions $\phi(\omega)$ and $Z(\omega)$, given by (2.35) and (2.36). The pairing self-energy $\phi(\omega)$ and the 'pair potential' $\Delta(\omega)$ can be thought of in analogy to the self-consistent Hartree potential as representing the effect of the

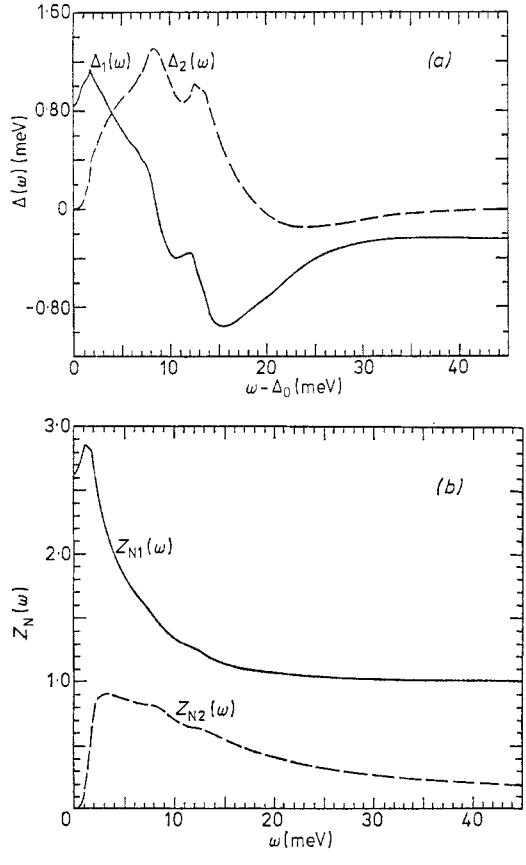

Figure 5. The complex, energy-dependent gap and renormalisation functions $\Delta(E)$ (*a*) and $Z(E)$ (*b*) of mercury as obtained from tunnelling measurements at 0·3 K (from Hubin and Ginsberg 1969).

other particles of the system—but $\Delta(\omega)$ is anomalous in that its action on two electrons in collision is their *removal* to form a Cooper pair or, in effect, to scatter an electron into a hole. The pair potential Δ can be expressed as the product of the *pair amplitude* or pair wavefunction $F(x)$ and a coupling strength λ^* which describe, respectively, the number of pairs per unit volume and the electron–phonon interaction in the local medium. Thus:

$$\Delta = \lambda^* F = \lambda^* \sqrt{\rho} \exp(\mathrm{i}\phi) \tag{2.37}$$

where ρ is the density of pairs and the superconducting phase $\phi(x, t)$ depends on position in the presence of a vector potential $\boldsymbol{A}$, such that

$$\phi_2 - \phi_1 = \frac{2e}{\hbar} \int_1^2 \boldsymbol{A} \, \mathrm{d}\boldsymbol{l}.$$

The prediction of the transition temperature T_C from the Eliashberg equations has been addressed in the basic paper of McMillan (1968a), which has recently been re-examined by Allen and Dynes (1975b). The basis is the set of equations (2.35) and (2.36) extended to include temperature-dependent Fermi and Bose–Einstein

functions governing occupation of the electron and phonon excitation states. In an approximate self-consistent solution of the equations with $T = T_C$ and on the assumption of a phonon spectrum similar to that of Nb, McMillan (1968a) found:

$$T_C = \frac{\theta_D}{1{\cdot}45} \exp\left(\frac{1{\cdot}04(1+\lambda)}{\lambda - \mu^*(1+0{\cdot}62\lambda)}\right) \tag{2.38}$$

a result which has been widely useful, in spite of the fact that it strictly applies only to materials with the phonon spectrum of Nb. Here the important coupling strength parameter:

$$\lambda = 2\int_0^{\omega_0} \frac{\alpha^2(\omega_q)\, F(\omega_q)\, \mathrm{d}\omega}{\omega_q} \tag{2.39}$$

gives the renormalisation function (at $\omega = 0$): $Z(0) = 1 + \lambda$. The BCS T_C formula is recovered in weak coupling with the identification $\lambda - \mu^* \to N(0)\, V$. Here ω_0 is the maximum phonon frequency and $\langle\omega\rangle$ is the average phonon frequency computed using $\alpha^2 F(\omega)/\omega$ as a weighting function:

$$\langle\omega\rangle = \textstyle\int_0^{\omega_0} \mathrm{d}\omega_q \alpha^2(\omega_q)\, F(\omega_q) \left(\int_0^{\omega_0} \mathrm{d}\omega_q \alpha^2(\omega_q)\, F(\omega_q)/\omega_q\right)^{-1}. \tag{2.40}$$

The extent to which the shape of the phonon spectrum of the material in question affects the T_C value in the theory has been re-examined (Allen and Dynes 1975b) who find correction factors to equation (2.38). The most important correction is a change from the pre-factor $\theta_D/1{\cdot}45$ to $\omega_{\log}/1{\cdot}2$ where:

$$\omega_{\log} \equiv \exp\langle \ln \omega\rangle. \tag{2.41}$$

Other correction factors are given by Allen and Dynes. A plot of many T_C values, represented as $T_C/\omega_{\log}$, against coupling strength λ is given in figure 6. The advantage to this particular representation is a minimised sensitivity to the details of the particular phonon spectrum; the disadvantage is the relative inaccessibility of the parameter $\omega_{\log}$, compared, for example, to θ_D, for a given material.

The parameter λ is related to both electronic and lattice properties as:

$$\lambda = \frac{N(0)\langle I^2\rangle}{M\langle\omega^2\rangle}$$

where $\langle I^2\rangle$ is an average over the Fermi surface of the squared electron–phonon matrix element, $N(0)$ is the band density of states of one spin index at the Fermi surface, and M is the atomic mass. It is thought that the $N(0)\langle I^2\rangle \equiv \eta$ product is especially large in certain classes of compounds such as the A15 compounds, which contain linear chains of transition-metal atoms, because of the participation of Fermi surface electrons in metallic covalent bonding.

2.5. Probing the strongly coupled superconducting state by tunnelling

The extension of the tunnelling theory of §2.3 to the strong coupling case, where the one-to-one correspondence between energy and wavevector (presumed in, for example, equation (2.14) for J) is lost, was carried out by Schrieffer *et al* (1963), using the spectral functions (2.31) and (2.32). The required generalisation of (2.14) follows formally directly from the definition of $A(\boldsymbol{k}, E)$ as the probability that an

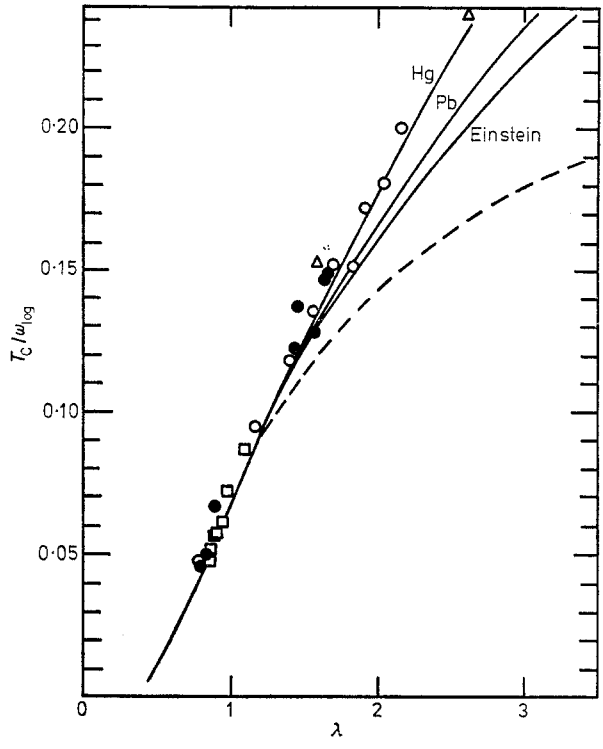

Figure 6. A plot of T_C/ω_{log} against λ for several superconductors (Allen and Dynes 1975b). The broken curve corresponds to the McMillan T_C formula; the full curves are obtained from the theory of Allen and Dynes on differing assumptions for the phonon spectrum. $\mu^*=0{\cdot}1$; ● elements; ○, □ alloys; △ amorphous.

electron of wavevector $\boldsymbol{k}$ has energy E:

$$J=\frac{4\pi e}{h}\sum_{k_L,\,k_R}|T_{k_R,k_L}|^2\int_{-\infty}^{\infty}\frac{dE_L}{2\pi}A_L(k_L,E_L)\int_{-\infty}^{\infty}\frac{dE_R}{2\pi}A_R(k_R,E_R)$$
$$\times\delta(E_L-E_R-eV)[f(E_L)-f(E_R)]. \qquad (2.42)$$

The spectral function A of the superconductor, following Schrieffer *et al* (1963) and Scalapino *et al* (1966), is obtained from the imaginary part (see (2.31)) of the off-diagonal component of the Nambu Green function G_{11}, as:

$$A(k,E)=\frac{1}{\pi}\,\mathrm{Im}\left|\frac{Z(k,E)\,E+\epsilon_k}{Z^2(k,E)[E^2-\Delta^2(k,E)]-\epsilon_k{}^2}\right|. \qquad (2.43)$$

The corresponding density of states (2.32) is evaluated, using the fact that Z and Δ are only weakly k-dependent, as:

$$N(E)=\mathrm{Re}\left(\frac{|E|}{[E^2-\Delta^2(E)]^{1/2}}\right)=N_T(E). \qquad (2.44)$$

The resulting tunnel conductance σ_S in the case of an NIS junction is thus just that found previously in equation (2.20), with the new understanding that the strong coupling aspects are correctly accounted for by allowing $\Delta(E)$ in $N_T(E)$ to be a complex energy-dependent function. Thus, measurements of σ_S/σ_N can be expected to

reveal the energy dependence of Δ: one of the first observations of this is contained in figure 1(*a*) (Giaever *et al* 1962) in the deviations noticeable between 3 mV and 10 mV bias. The extraction of such information from $N_T(E)$ to obtain $\Delta(E)$, $Z(E)$ and $\alpha^2F(\omega)$ (see figure 5) was first accomplished by McMillan and Rowell (1965) and extended by Galkin *et al* (1974) and will be taken up in §3.5.

2.6. Theoretical alternatives to the transfer Hamiltonian

In measuring the tunnelling conductance of NIS junctions to obtain the superconducting gap and phonon structure the bias voltage range, typically ± 50 mV, is small compared with a typical barrier height V_B; furthermore, in taking the ratio σ_S/σ_N one effectively removes from the data the voltage variation due to the transmission factor. The pairing self-energies in superconductors are also always negligibly small on the scale of the barrier height U_B or the Fermi energy E_F. For these reasons, as we have stated, the transfer Hamiltonian approach of Bardeen (1961) and Cohen *et al* (1962) has been wholly adequate to a quantitative understanding of the properties of superconductors from tunnelling spectra.

Nevertheless, the formulation has been shown to have several conceptual weaknesses. The first conceptual question is one of mathematical completeness in the description of the two electrodes' wavefunctions, while at the same time maintaining coupling between the two. This issue was discussed originally by Prange (1963) without a satisfactory resolution; this and several other mathematical points have been recently discussed in an illuminating fashion by Caroli *et al* (1975). In practice it is difficult to treat cases with interacting species within the barrier; as discussed by Duke (1969) the decomposition of the system into $\mathscr{H} = \mathscr{H}_L + \mathscr{H}_R + \mathscr{H}_T$ is rather arbitrary.

But the most serious problem with the transfer Hamiltonian is probably its error in treating *strong* self-energy effects in the electrode (Appelbaum and Brinkman 1969a,b). In some cases an appreciable electron self-energy $\Sigma(k, E)$ arises from interaction, e.g. with phonons to lower the real electron energy E from its 'bare' value $\hbar^2k^2/2m^*$. It has been pointed out by Appelbaum and Brinkman (1969a) that turning on such an interaction Σ must strongly affect the amplitude of a given electron state, say $x = 2$ Å, into the vacuum outside the metal. If the state k_x has non-interacting ('bare') x-kinetic energy ϵ_{kx} and the interaction leads to a real self-energy Σ_x, then certainly the wavefunction tail will vary proportionally to $\exp(-\kappa x)$ with $\kappa = [(\hbar^2/2m^*)(V_B - \epsilon_x - \Sigma_x)]^{1/2}$, and thus be exponentially reduced with a (negative) self-energy Σ_x. In the transfer Hamiltonian model, however, the exponent is constructed with the *non-interacting* or bare energy and can lead in extreme cases to unphysical results. In resonant circumstances, e.g. Σ_x may become very large (negative), forcing the bare energy and hence the exponent and transmission factor to unreasonably large positive values. As has been nicely verified in an independent calculation (Griffin and Demers 1971), the model must be re-interpreted with the real or excitation energy E inserted in the matrix element, with a consequence that purely frequency-dependent self-energy effects cannot enter the conductance via the transmission factor. The matrix element thus becomes energy-dependent, a feature which also appears in several extensions and alternatives to the transfer Hamiltonian model.

The first of these is the Green function theory of Appelbaum and Brinkman (1969b, 1970), which is similar to a theory earlier proposed by Zawadowski (1967). This theory was successfully applied (Davis 1970a,b) to analysis of tunnelling data

from metal–p-silicon contacts showing evidence of a strong electronic self-energy effect arising from coupling to optical phonons (Wolf 1968).

A theory based on stationary current-carrying states across the tunnel junction, and also capable of treating many-body interactions, was put forward by Davis (1970a,b) and was also applied to the observed optical-mode phonon interaction in metal–semiconductor contacts. A theoretical treatment which can incorporate interactions and which does not require weak coupling (i.e. a thick barrier) has first been given by Caroli, Combescot, and collaborators (Caroli *et al* 1971a,b, 1972, Combescot 1971, Combescot and Schreder 1973, 1974) in application of a method developed by Keldysh (1964). The method is able to correctly treat interaction effects, as the authors have demonstrated. The original paper uses a Wannier representation to clarify the question of completeness and the decomposition of the system into parts (electrodes plus barrier); in the second paper a limiting procedure is used to establish continuous wavefunctions and a boundary condition at the interface.

A subsequent and closely related series of papers of Feuchtwang (1974a,b, 1975, 1976) has confirmed and slightly generalised the results of Caroli *et al* and offers some further light on the range of validity of the transfer Hamiltonian approach and on the close relation of the latter two theories to that of Appelbaum and Brinkman (1969a,b, 1970).

3. Experimental techniques

3.1. The tunnelling barrier

A tunnel junction can be regarded as simply a capacitor with a 20–100 Å dielectric spacing, a configuration which can be arrived at experimentally in several different ways.

In all cases, of course, a (possibly amorphous) solid separates the two electrodes, so that the idealised one-dimensional potential barrier is in reality a band-gap region which allows only exponentially decaying electron states. The role of the barrier height U_B is played by the energy (relative to the metal Fermi level) of the lowest conduction band of the insulator, or the Mott mobility edge if the material is amorphous. It is useful to think of the variation of the decay constant κ with energy in this realistic case of an insulating solid with conduction and valence bands as shown in figure 7.

In the real material the decay constant, κ (2.2), must be modified by the effective mass m^* in the insulator and by the presence of both conduction and valence band edges in the insulator (Kurtin *et al* 1971). The dependence of κ on energy in the gap region of GaSe has been determined from J–V measurements and an equation similar to (2.14) and is shown in figure 7.

3.2. Thin-film methods

The most familiar approach to junction fabrication entails successive evaporations of crossing film strips delineated by masks, allowing exposure of the first metal surface to air or to pure oxygen, possibly in a plasma discharge (Miles and Smith 1963), to produce the oxide barrier. The crossed strips are then contacted with separate current and voltage leads to make measurements of the voltage V and the current I which flows through the junction, excluding voltage drops along the lead

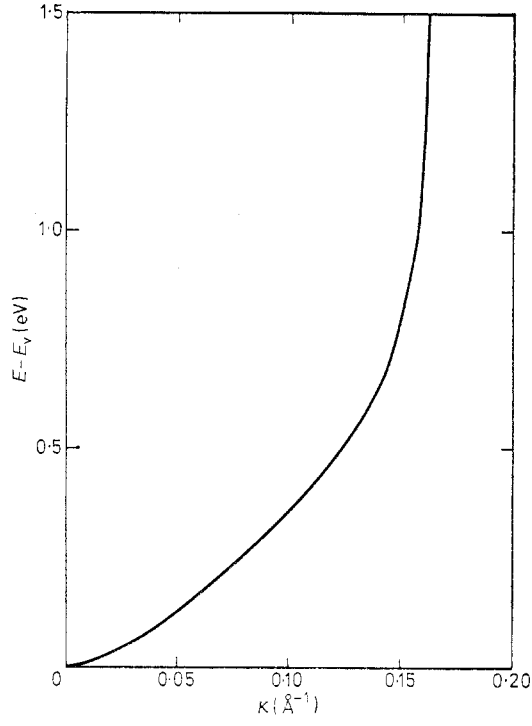

Figure 7. The variation of the electronic decay constant $\kappa(E)$ with energy in the band gap of GaSe, determined from the J–V measurements of Kurtin *et al* (1971) on single-crystal barriers of GaSe. $m_h^* = 0{\cdot}07$.

wires or connecting film strips. The sample must be mounted on a holder which can reach temperatures below the superconducting transition of the metals of interest; this is often simply achieved by immersing the sample in liquid helium. It is desirable to evaporate several junctions onto the same glass slide to confirm reproducibility and proportionality of conductance to junction area. Such a straightforward technique with oxidation of polycrystalline evaporated films by exposure to laboratory air was successfully used by Giaever (1960a,b,c) in his pioneering experiments, and by many other workers studying the 'soft' superconductors, including Al, Sn, Pb and Hg.

The self-limiting oxide which grows on aluminium is particularly reliable and uniform in thickness (Knorr and Leslie 1973), because the growth depends on transport of metal ions through the oxide already present (Mott 1947), thus correcting non-uniformity in thickness. The uniformity of Sn and Pb oxide barriers has been studied by Dynes and Fulton (1971) using the Josephson current. The best metal oxide tunnelling barriers are probably those grown in a plasma (glow) discharge of pure oxygen (Vrba and Woods 1972, Magno and Adler 1976) on metal films which have been made unusually smooth by deposition onto a 77 K substrate. Such layers, less than 30 Å in thickness, can support bias voltages of several volts (Jaklevic and Lambe 1975), corresponding to peak electric fields of several times 10^7 V cm^{-1}.

3.2.1. Epitaxially grown films. Special thin-film techniques have been used for growth of epitaxial single-crystal metal films for studying anisotropy in the energy gap or of the Fermi velocity from the spacing of the Tomasch oscillations. To grow

single-crystal films of Pb in the [100], [110], [111] and [211] orientations (Lykken *et al* 1970) one can proceed by first depositing 0·05–0·15 μm of Ag on an oriented and polished KBr substrate, and then depositing the Pb. Similar methods are applicable to In and several other metals.

3.2.2. Co-evaporation and getter sputtering. Growth of metallic *compound* films such as Nb_3Ge or Nb_3Sn, which are high T_C superconductors, requires special methods. *Co-evaporation* of the two constituents onto temperature-controlled substrates (up to 1000°C) followed by thermal oxidation has been used in preparation of films in a tunnelling study of the gap of Nb_3Sn (Moore *et al* 1976). An alternative thin-film method known as *getter sputtering* (Theuerer and Hauser 1964) uses an argon glow discharge inside a cooled sputtering chamber (inside the basic vacuum bell jar) to deposit the compound from a bulk target onto the temperature-controlled substrate. This is capable of producing films of Nb_3Ge with T_C of 23 K and has been used by Rowell and Schmidt (1976) in measuring the energy gap of Nb_3Ge by tunnelling through a thermally grown oxide from a Pb counterelectrode.

3.2.3. Quench-condensing onto Al–Al_2O_3 substrates. Some metals simply do not form oxides suitable for tunnel barriers—among those listed as impossible by Giaever (1969) are Ag, Au and In, while Cu, La, Co, V and Bi were regarded as difficult. In such cases, it may be possible to form an oxidised aluminium counterelectrode beforehand, and then to deposit the material of interest. It is sometimes necessary to cool the prepared substrate to 4·2 K or even 1·5 K before evaporation to reduce leakage in the resulting junctions. This technique has recently been applied to Nb and V by Robinson *et al* (1976).

3.2.4. Deposited barrier layers (artificial barriers). A different scheme to provide a barrier on an arbitrary (non-oxidising) metal is to deposit a 20–30 Å layer of Al, which is then allowed to fully oxidise (Adkins and Kington 1966). Pinholes, which may occur if the initial surface is not smooth or as a result of dust particles, etc, tend to be filled in with the subsequent expansion in the oxidation step.

Alternatively, one may attempt to deposit the barrier directly as an insulating film of amorphous C, In_2O_3, Bi_2O_3 or various semiconductors. While it has been stated (Giaever 1969) that such films always contain pinholes, leading to short circuits if deposited on a non-oxidising electrode such as gold; it appears that by using small band-gap insulators such as In_2O_3, requiring a relatively large thickness (up to 200 Å for In_2O_3), the pinhole problem can be reduced (Aspen and Goldman 1976). In this case, as in the case of amorphous carbon (MacVicar 1970), however, the relatively low barrier height causes a more rapid variation of background conductance with bias. While these methods have been successful in determining superconducting gaps (a few millivolts bias) they usually do not succeed if the goal is observation of the superconducting phonons (5–40 mV).

3.2.5. Single-crystal barriers. Some compounds of an essentially two-dimensional character can be peeled away layer by layer to leave a single crystal of thickness (< 100 Å) suitable for tunnelling. This has been accomplished in Cu–GaSe–Au junctions in a study which permitted from the tunnel current against voltage relation quantitative extraction of the E–k dispersion relation in the band gap of GaSe (Kurtin *et al* 1971). A similar experiment has been reported using single-crystal films of the

layered semimetal $Bi_8Te_7S_5 = X$ in proximity junctions of the form PbX/I/Pb. Here the objective was to study the manner in which the Pb proximity layer induces a large superconducting gap into the $Bi_8Te_7S_5$ (Lykken and Soonpaa 1973).

3.3. Single-crystal electrodes

We have already mentioned in §3.2.1 epitaxial films of Pb, based on KBr. The epitaxy of Ag and Au on alkali-halide crystal surfaces is well known and such films can be used as the basis for further epitaxial growths of a variety of FCC metals. It is reported that BCC transition metals including Nb and V can be grown epitaxially on MgO surfaces at elevated temperatures.

3.3.1. Single-crystal metal electrodes. Bulk single crystals of several metals have been employed as tunnel electrodes. These include Ga (Gregory *et al* 1971), Pb (Blackford and March 1969), Nb (Bostock *et al* 1976), Sn (Zavaritskii 1965) and Re (Ochiai *et al* 1971).

3.3.2. Single-crystal semiconductor electrodes. Extensive tunnelling studies have been carried out on degenerate (metallic) semiconductor single-crystal tunnel junctions. Historically the first, of course, was the tunnelling pn or Esaki diode junction, which can be generated by diffusing a high concentration of p-type impurities into degenerate n-type semiconducting material, or vice versa. For purposes of tunnelling spectroscopy, both thermally grown oxide barriers and direct metal–semiconductor (Schottky barrier) contacts have also been used. In the Schottky barrier the transfer of electrons (n-type material) from donor impurities to the metal–semiconductor interface leaves behind a distributed positive space charge, which leads to the familiar quadratic variation of band-edge position with space coordinate (Conley and Mahan 1967, Conley *et al* 1966, Steinrisser *et al* 1968). Schottky barriers of a variety of metals deposited onto vacuum-cleaved Si containing 5×10^{18} to 2×10^{19} donors cm^{-3} provide a well-understood tunnelling system in which the Si acts as a single-crystal electrode and also as a single-crystal barrier (Wolf and Losee 1970).

Oxidised barriers on degenerate InAs and several other semiconductors have been employed in elegant tunnelling studies of two-dimensional electron systems (Tsui 1971).

3.4. Data acquisition and reduction

The simplest possible, yet very useful, measurement is directly of the I–V characteristic leading to determination of the energy gap in SIS or NIS junctions (figure 8). This is usually done directly on an x–y recorder, with large x-scale expansion. In such measurements it is important to use a four-terminal technique (to avoid measuring possibly significant voltage drops along current-carrying sample holder wires or evaporated films), and to ensure that the input impedance of the x amplifier is sufficiently high.

The most accurate determination of the superconductor energy gap Δ is made possible in the SIS configuration with identical superconductors. A particularly nice example of the behaviour as a function of temperature (Blackford and March 1968) is shown in figure 9(*a*). The minimised effect of thermal broadening in this case in

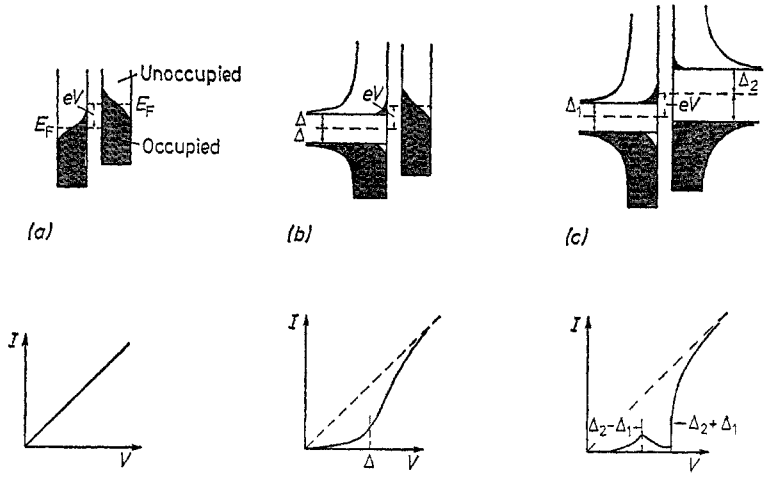

Figure 8. The current–voltage characteristics and their origins in the semiconductor representation for the NIN, NIS and SIS cases.

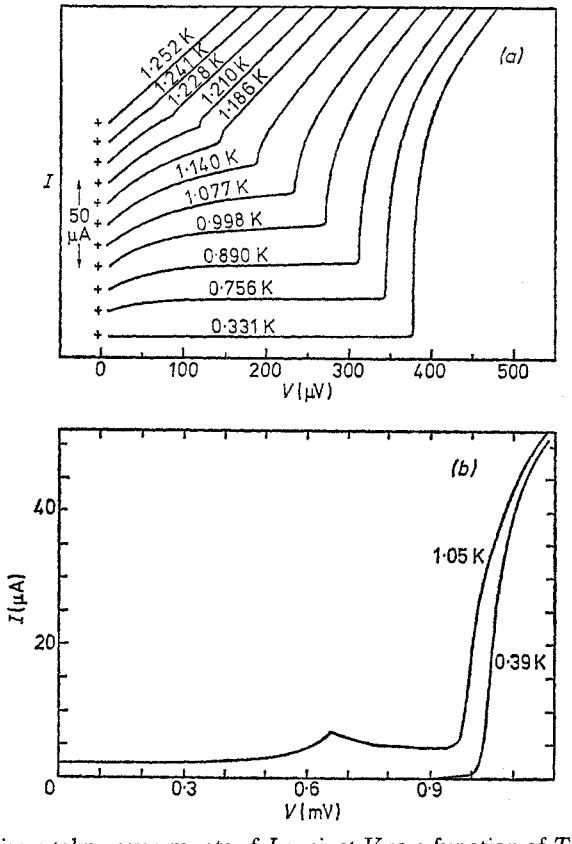

Figure 9. (*a*) Experimental measurements of I against V as a function of T for an Al insulator/Al junction (after Blackford and March 1968). $T_C = 1{\cdot}25$, $2\Delta(0) = 379$ μV. (*b*) Carefully measured I–V curves for an Al/I/Hg junction at 1·05 K and 0·39 K, the former revealing the cusp at $\Delta_{Hg} - \Delta_{Al}$ resulting from thermal quasiparticles in the Al. The leakage current in this junction did not exceed 10^{-6} of the normal current, at 0·37 K (from Hubin and Ginsberg 1969).

comparison to the NIS case is a considerable advantage in determining the gap value as a function of temperature.

The S_1IS_2 case shows structures at $\Delta_1 \pm \Delta_2$ and a negative resistance region occurs for $\Delta_1 - \Delta_2 < eV < \Delta_1 + \Delta_2$. To observe this, it is necessary to use a voltage source rather than a current source. An example which clearly reveals the cusp in the current at $\Delta_1 - \Delta_2$ is shown in figure 9(*b*). The leakage current in this junction is 10^{-6} of the normal current; values up to 10^{-3} are probably acceptable. The temperature-dependent cusp at $\Delta_1 - \Delta_2$ depends upon a measurable population of thermally excited quasiparticles in the superconductor of smaller gap, which varies as $\exp(-2\Delta_2/kT)$; the current near the cusp is of the form $I \propto \ln|eV-(\Delta_1-\Delta_2)|$. At $eV = \Delta_1 + \Delta_2$, current shows a discontinuity of magnitude:

$$\frac{\delta I}{I_{\text{normal}}} = \frac{1}{4}\frac{\pi(\Delta_1\Delta_2)^{1/2}}{(\Delta_1+\Delta_2)}\frac{\sinh(\Delta_1+\Delta_2/2kT)}{\cosh(\Delta_1/2kT)\cosh(\Delta_2/2kT)}. \tag{3.1}$$

The $T=0$ current behaviour of the NIS junction has the form:

$$I_{SN} = \begin{cases} \dfrac{[(eV)^2-\Delta^2]^{1/2}}{R} & eV \geqslant \Delta \\ 0 & eV < \Delta \end{cases} \tag{3.2}$$

where R is the junction resistance at high bias. The value of Δ can be directly measured from such an ideal curve. In the NIS case at finite temperature the current is, from (2.16):

$$I_{SN} = C\int_{-\infty}^{\infty} dE N_T(E)[f(E)-f(E+eV)] \tag{3.3}$$

with $N_T(E)$ from (1.1). A rapidly converging series approximation (Giaever and Megerle 1961) to this integral is:

$$I_{SN} = 2C\Delta\sum_{m=1}^{\infty}(-1)^{m-1}K_1\left(\frac{m\Delta}{k_BT}\right)\sinh\left(\frac{meV}{k_BT}\right) \qquad eV<\Delta \tag{3.4}$$

where K_1 is a modified Bessel function of the second kind. In the finite-temperature case the points on the NIS I–V characteristic at which the slope dI/dV equals that at large bias, i.e. where $\sigma = (dI/dV)_S/(dI/dV)_N = 1$, can be determined graphically (McMillan and Rowell 1969). It is then necessary to consult the tabulation of Bermon (1964) of $\sigma(eV/\Delta, k_BT/\Delta)$ (based on the BCS density of states, thus limiting the applicability of this method).

In practice, the cusp and current discontinuity at $\Delta_1 \pm \Delta_2$ in the S_1IS_2 characteristic are often smeared. Acceptable origins for smearing in a clean polycrystalline or single-crystal film are anisotropy of Δ, or a multiple gap structure as shown for Pb in figure 10(*a*). Note that this does not apply to isotropic 'dirty' superconductors where scattering around the Fermi surface averages out any anisotropy of the energy gap. Broadening of the features at $\Delta_1 \pm \Delta_2$ in a junction composed of two dirty superconductors is thus evidence for a defective junction. It may reflect gaplessness (as may be produced by magnetic impurities), or a metallic short.

The most directly physical information in the current–voltage response of an NIS tunnel junction is contained in the normalised derivative σ_S/σ_N which, in fact, measures the ($T=0$) excitation spectrum of the superconductor. Normally the experimenter

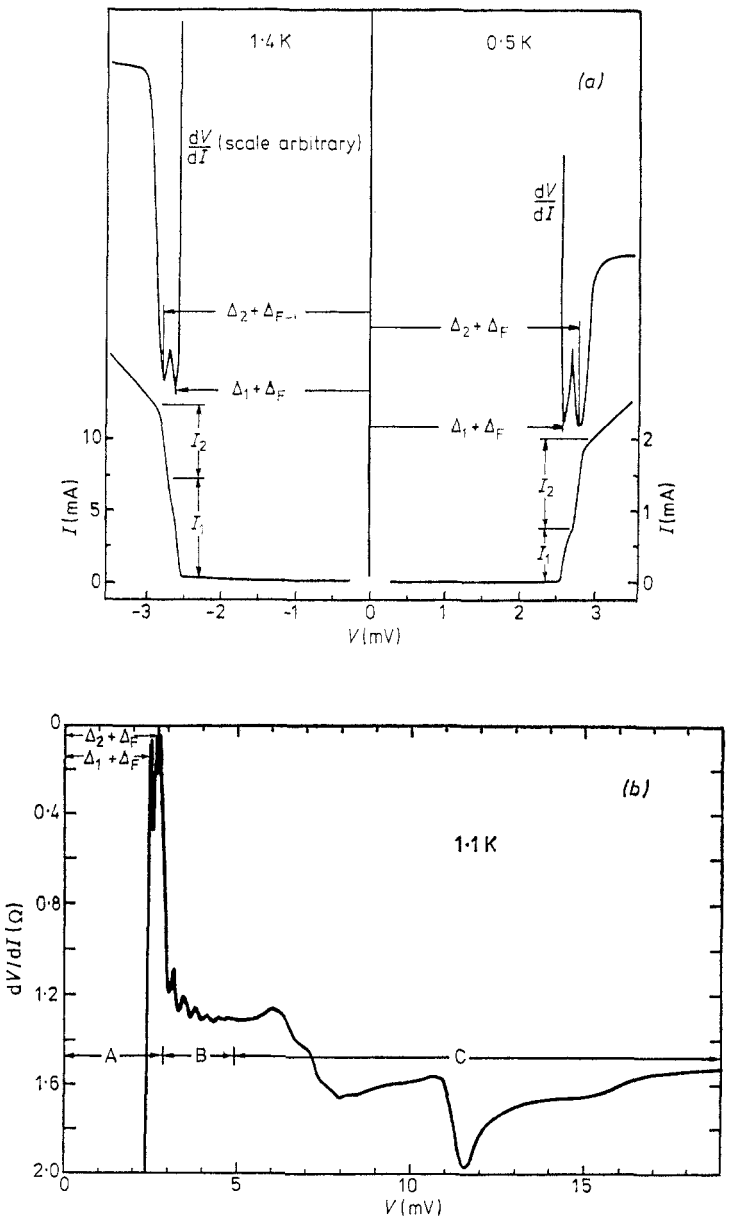

Figure 10. (*a*) I–V and dV/dI curves for tunnelling from dirty (isotropic) Pb into the [001] and [111] directions of Pb single crystals. The multiple gap structure reflects the participation of electrons from different parts of the Fermi surface in forming the ground state (from Blackford and March 1969). (*b*) dV/dI structure at 1·1 K for a Pb/I/Pb junction in which the bottom electrode was a 6·1 μm thick [111] single-crystal epitaxial film. The structure in range B arises from geometrical Tomasch oscillations, while that in ranges A and C, respectively, comes from the multiple gaps and the Pb phonons (from Lykken *et al* 1970).

arranges to sweep the bias voltage V slowly and records the derivatives $(\mathrm{d}I/\mathrm{d}V)_{S,N}$ (or their inverses) directly on an x–y recorder, depending upon later analysis to calculate the normalised $\sigma = \sigma_S/\sigma_N$. The familiar technique of synchronous detection of the derivative signal $(\mathrm{d}I/\mathrm{d}V)\,\delta_0 \cos \omega t$ is universally used and is sometimes extended to the second derivative $\mathrm{d}^2I/\mathrm{d}V^2$, obtained from the second harmonic generated by the junction, as described by the Taylor series expansion:

$$I(V_0+\delta V) = I(V_0) + \left(\frac{\mathrm{d}I}{\mathrm{d}V}\right)_{V_0} \delta_0 \cos \omega t + \tfrac{1}{2}\left(\frac{\mathrm{d}^2I}{\mathrm{d}V^2}\right)_{V_0} \tfrac{1}{2}\delta_0^2(1+\cos 2\omega t) + \ldots . \quad (3.5)$$

Frequently it is more convenient to measure the voltage derivatives $\mathrm{d}V/\mathrm{d}I$ and $\mathrm{d}^2V/\mathrm{d}I^2$ by using a current modulation, and then to calculate $\mathrm{d}I/\mathrm{d}V$ and $\mathrm{d}^2I/\mathrm{d}V^2$ from the identities:

$$\frac{\mathrm{d}I}{\mathrm{d}V} = (\mathrm{d}V/\mathrm{d}I)^{-1} \qquad \frac{\mathrm{d}^2I}{\mathrm{d}V^2} = -\frac{\mathrm{d}^2V}{\mathrm{d}I^2}\frac{1}{(\mathrm{d}V/\mathrm{d}I)^3}. \quad (3.6)$$

Some workers even arrange for a minicomputer to do such numerical chores during the measurements. Careful measurements of σ over the whole gap region $0 \leqslant eV \leqslant 5\Delta$, with suitable attention to a small modulation voltage δ, of an NIS junction permit detailed comparison with the (thermally smeared) prediction of the BCS theory. It is sometimes adequate to measure only the most sensitive portion of the characteristic for determining Δ, which is the $(\mathrm{d}I/\mathrm{d}V)_S$ peak region $eV \sim 1{\cdot}1\,\Delta$. Indeed, even a measurement of $\sigma(0)$ at a known temperature $T \lesssim T_C$ may give a useful estimate of Δ by use of the Bermon tabulation. This method usually does not work at low temperature $T \ll T_C$ because the slightest spurious leakage in this case can dominate the measurement of $\sigma(0)$.

Derivative measurements must be done with considerably more care if the objective is to fully characterise a strong coupling superconductor in an NIS junction. A bridge circuit is generally necessary to attain the stability of one part in 10^5 needed for accurate measurement of the small deviations of σ/σ_{BCS} from unity in the phonon energy range, from which the energy dependence of the gap function $\Delta(\omega)$ is extracted. Such bridge circuits (Rogers *et al* 1964, Christopher *et al* 1968) are also useful in high-gain second-derivative measurements of inelastic tunnelling effects, to null out, before amplification, the undesired first harmonic signal; of course, filters may alternatively be used for this purpose.

An example of a full $\mathrm{d}V/\mathrm{d}I$ spectrum for a Pb/I/Pb junction (Lykken *et al* 1970) is shown in figure 10(*b*); the multiple gap and the geometrical Tomasch oscillations evident, respectively, in regions A and B of the bias range are consequences of the epitaxial single-crystal nature of one of the Pb films. In most superconductors the structure in the phonon region is relatively weak, $\sim \Delta\sigma/\sigma \leqslant 10^{-2}$, and a change in vertical expansion (i.e. the gain in measurement of $\mathrm{d}V/\mathrm{d}I$) will be necessary to put both the phonon range and the strongly varying σ in the BCS peak region on the chart. Weaker phonon structure thus puts more stringent demands on the gain stability of the circuitry. If the deviation $\sigma/\sigma_{BCS} - 1$ is 10^{-3}, and is measured with 1% accuracy, then in order to perform the gap inversion (below) stability in measurement of the derivatives $(\mathrm{d}I/\mathrm{d}V)_{S,N}$ of $1/10^5$ is clearly required. If a bridge circuit is balanced to $1/10^2$ at the biases of interest, then $1/10^3$ stability of the oscillator and tuned amplifier would suffice.

3.5. Numerical inversion of the gap equations

The measured quantities in superconducting tunnelling are the tunnelling density of states $N_T(\omega)=\sigma(\omega)=\mathrm{Re}\,[\omega/(\omega^2-\Delta^2(\omega))^{1/2}]$ (equation (1.1)) and the gap energy $\Delta_0=\Delta(\Delta_0)$. The basic problem is to get from $\sigma(\omega)$ to the underlying spectral function $\alpha^2F(\omega)$ (and its integral, λ) by *inversion* of the coupled integral equations (2.35) and (2.36). Once this is done, these equations can be used to calculate the complex functions $\Delta(\omega)$ and $Z(\omega)$.

There are two approaches to this problem: the variational method of McMillan and Rowell (1969) and the recent solution of Galkin *et al* (1974) and Svistunov *et al* (1978).

The former method has been most widely used; indeed, most data are reduced using McMillan's original computer program (Hubin 1970). As explained by McMillan and Rowell (1969), the doubly iterated variational solution starts by *assuming* a form for $\alpha^2F(\omega)$ and a value for μ^* for which a first solution of (2.35) and (2.36) for $\Delta^1(\omega)$ is obtained in the inner iterative loop starting with an arbitrary $\Delta^0(\omega)$. An improved value of μ^* is then obtained by requiring that $\Delta^1(\Delta_0)$ equal the measured gap. The next step is to compute $\sigma_c'(\omega)=\mathrm{Re}\,[\omega/(\omega^2-\Delta^1(\omega)^2)^{1/2}]$ from $\Delta^1(\omega)$, and also the difference $\delta\sigma'(\omega)=\sigma(\omega)-\sigma_c'(\omega)$. The derivative $\delta\sigma(\omega)/\delta\alpha^2F(\omega)$ is calculated and used with $\delta\sigma'(\omega)$ to obtain a first improved $\alpha^2F(\omega)$. Once again the iterative solution for $\Delta^2(\omega)$ is carried out using the first improved $\alpha^2F(\omega)$ and μ^*; this outer iteration loop is continued until μ^* and $\alpha^2F(\omega)$ have converged.

Galkin *et al* (1974) have solved the posed problem without the need for iterations by proving a further identity:

$$\mathrm{Im}\,[\omega/(\omega^2-\Delta^2(\omega))^{1/2}]=\frac{2}{\pi}\int_{\Delta_0}^{\infty}\frac{[\sigma(\omega')-\sigma_{\mathrm{BCS}}(\omega')]}{\omega^2-\omega'^2}\,\omega\,\mathrm{d}\omega'.$$

Taken together with (1.1) $\sigma(\omega)=\mathrm{Re}\,[\omega/(\omega^2-\Delta^2(\omega))^{1/2}]$, this provides two equations from which the two unknowns, Re $\Delta(\omega)$ and Im $\Delta(\omega)$, can be determined directly. Once $\Delta(\omega)$ is thus determined, the inversion of the gap equation is simplified and in fact reduced to a linear integral equation for $\alpha^2F(\omega)$ in which μ^* does not appear. Iterations are not needed to solve for $\alpha^2F(\omega)$. It appears that this scheme is more direct and economical of computer time, and it certainly deserves wider appreciation and application than it has thus far received. Further discussion of the method is given by Svistunov *et al* (1978).

4. Studies of the superconducting state

Having described the theoretical background and the experimental techniques involved in tunnelling spectroscopy, we will now summarise the properties of superconducting elements and alloys as revealed by tunnelling, comparing the results, where possible, to those obtained by other techniques, such as neutron scattering.

4.1. Energy gaps, phonons and T_C

We have, somewhat arbitrarily, organised the materials according to the atomic origin of the conduction electrons, i.e. s–p, d-band or f-band materials.

In this section we draw on a useful compilation by Rowell *et al* (1978) of the

Table 1. Superconducting materials.

Material	T_C (K)†	θ_D (K)†	ω_{log} (meV)‡	$\langle\omega\rangle$ (meV)	$\sqrt{\langle\omega^2\rangle}$ (meV)	λ	$2\Delta/k_BT_C$	Reference
(a) s, p elements								
Be	0·026	1390				0·23	—	
Al	1·18	420				0·38§	3·53, 3·50	Blackford and March (1968), Hubin and Ginsberg (1969)
Cd	0·52	209				0·38§	3·2	Kumbhare *et al* (1969)
Zn	0·85	310				0·38§	—	
Ga	1·08	325				0·40§	3·63	Yoshihiro and Sasaki (1968), Wühl *et al* (1968)
Sn	3·72	195	8·53	9·48	10·43	0·72	3·7, 3	Rowell *et al* (1969), Zavaritskii (1965)
In	3·41	109	5·86	6·81	7·67	0·805	3·68, 2	Dynes (1970)
Tl	2·38	79	4·48	5·0	5·51	0·795	3·6, 2	Dynes (1970), Clark (1968)
Pb	7·196	105	4·83	5·20	5·55	1·55	4·67, 4·30	Townsend and Sutton (1962), McMillan and Rowell (1965, 1969), Dynes and Rowell (1975)
Hg(α)	4·15	72	2·5	3·27	4·22	1·6	4·61	Hubin and Ginsberg (1969), Rowell *et al* (1978)
(b) Alloys and unusual phases—s, p elements								
$Tl_{0.9}Bi_{0.1}$	2·3		4·14	4·74	5·34	0·78	3·58	Dynes (1970), Allen and Dynes (1975a,b)
$In_{0.5}Tl_{0.5}$	2·52		4·57	5·51	6·29	0·83	—	Dynes (1970), Allen and Dynes (1975a,b)
$In_{0.9}Tl_{0.1}$	3·28		5·43	6·46	7·41	0·85	—	Dynes (1970), Allen and Dynes (1975a,b)
$In_{0.57}Tl_{0.43}$	2·60		4·57	5·51	6·38	0·85	—	Dynes (1970), Allen and Dynes (1975a,b)
$In_{0.67}Tl_{0.33}$	3·26		4·91	5·86	6·81	0·90	—	Dynes (1970), Allen and Dynes (1975a,b)
$In_{0.07}Tl_{0.93}$	2·77		4·22	4·83	5·43	0·89	—	Dynes (1970), Allen and Dynes (1975a,b)
$In_{0.73}Tl_{0.27}$	3·36		4·74	5·77	6·63	0·93	—	Dynes (1970), Allen and Dynes (1975a,b)
β Ga	5·90		7·5	9·31	11·1	0·97	—	Allen and Dynes (1975a,b)
$In_{0.17}Tl_{0.83}$	3·19		3·88	4·74	5·43	0·98	—	Dynes (1970), Allen and Dynes (1975a,b)
$In_{0.27}Tl_{0.73}$	3·64		3·62	4·57	5·43	1·09	—	Dynes (1970), Allen and Dynes (1975a,b)
$Pb_{0.4}Tl_{0.6}$	4·60		4·14	4·79	5·31	1·15	4·06	Dynes and Rowell (1975)
$Pb_{0.6}Tl_{0.4}$	5·90		4·31	4·87	5·34	1·38	4·25	Dynes and Rowell (1975)
In_2Bi	5·6		3·96	4·91	5·77	1·40	—	Rowell *et al* (1978)
Sb_2Tl_7	5·2		3·19	4·14	5·00	1·43	—	Rowell *et al* (1978)
$Pb_{0.8}Tl_{0.2}$	6·8		4·31	4·84	5·27	1·53	4·37	Dynes and Rowell (1975)
Am–Ga	8·56		4·74	6·63	8·70	1·62	4·5	Chen *et al* (1969), Leslie *et al* (1970)
Bi_2Tl	6·4		4·05	4·57	5·08	1·63	—	Rowell *et al* (1978)
$Pb_{0.9}B_{0.1}$	7·65		4·31	4·80	5·20	1·66	4·67	Dynes and Rowell (1975)
$Pb_{0.6}Tl_{0.2}Bi_{0.2}$	7·26		4·14	4·57	4·96	1·81	4·80	Dynes and Rowell (1969)
$Pb_{0.8}Bi_{0.2}$	7·95		3·96	4·44	4·88	1·88	4·70	Allen and Dynes (1975a,b)
$Pb_{0.7}Bi_{0.3}$	8·45		4·05	4·48	4·87	2·01	4·86	Dynes and Rowell (1975)
$Pb_{0.65}Bi_{0.35}$	8·95		3·88	4·31	4·74	2·13	4·78	Dynes and Rowell (1975)
Am–$Pb_{0.45}Bi_{0.55}$	7·0		2·50	3·27	4·05	2·59	—	Allen and Dynes (1975a,b)
Bi III	7·19	126					4·35	Nedellec *et al* (1974)

(c) d-band elements								
W	0·015	390				0·28§		
Ir	0·1125	420				0·34§		
Ti	0·40	425				0·38§		
Zr	0·61	290				0·41§		
Ru	0·49	550				0·38§		
Os	0·66	500				0·39§		
Mo	0·92	460				0·41§		
Re	1·70	415				0·46§	3·59	Ochiai *et al* (1971)
Ta	4·47	258	11·37	12·06	12·75	0·69	3·66	Shen (1970), Townsend and Sutton (1962)
V	5·40	383				0·60§	3·5	Noer (1975), Robinson and Rowell (1978)
Tc	7·77							
Nb	9·25	276				0·82§	3·89	Townsend and Sutton (1962), Bostock *et al* (1976), Robinson *et al* (1976), Wolf and Zasadzinski (1978)
(d) d-band alloys and compounds								
$Nb_{0·6}Ti_{0·4}$	9·8							Hulm and Blaugher (1961)
$Nb_{0·80}Zr_{0·20}$	11·0							Hulm and Blaugher (1961), Dietrich (1964)
$Mo_{0·6}Re_{0·4}$	12·2							Hulm and Blaugher (1961)
NbN	15							Horn and Saur (1968), Komenou *et al* (1968)
V_3Ga	15·9	310						Flükiger and Jorda (1977)
V_3Si	17·0	530					3·8	Blaugher *et al* (1969), Hauser *et al* (1966)
$NbN_{0·65}C_{0·35}$	17·5							Pessall and Hulm (1966)
Nb_3Sn	18·3	290				~1·67	4·3	Hanak *et al* (1964), Shen (1972a,b), Moore *et al* (1976), Allen and Dynes (1975a,b)
Nb_3Al	18·9							Sahm and Pruss (1969)
Nb_3Ga	20·7							Flükiger and Jorda (1977)
$Nb_3Al_{0·8}Ge_{0·2}$	21							Matthias *et al* (1967), Dew-Hughes (1975), Gregory *et al* (1973)
Nb_3Ge	23	378					4·2	Gavaler (1973), Testardi *et al* (1974), Rowell and Schmidt (1976)
(e) f-band elements								
Hf	0·128							
U(α)	0·68							
Th	1·38	165					3·47	Haskell *et al* (1972)
La(α)	4·88	151					3·8	Lou and Tomasch (1972)
La(β)	6·00	139						

† Many of these values are taken from Roberts (1976).
‡ Values obtained by use of McMillan's formula (McMillan 1968a), equation (2.38).
§ From Allen and Dynes (1975a,b): see also Rowell *et al* (1978).

detailed superconducting parameters for several materials to which the full spectroscopic tunnelling investigation has successfully been applied.

Table 1 is divided into three main parts containing properties of superconducting elements, alloys and compounds, in which the superfluid electrons may be regarded, respectively, as deriving from s–p, d-, and f-like states. The energy gap parameter Δ as determined by tunnelling is given and referenced. In each category the elements are arranged, at least approximately, in the order of increasing electron–phonon coupling parameter λ. This essential quantity is derived from the tunnelling data as $\lambda = 2\int \alpha^2(\omega)\, F(\omega)\, \mathrm{d}\omega/\omega$. In cases of weak coupling where deviations from σ_{BCS} are too small to permit accurate tunnelling determinations of α^2F we have, following McMillan, estimated λ from θ_{D} and T_{C} using equation (2.38). In those cases where the full tunnelling analysis has been possible we also list $\omega_{\log}$ (2.41), used in plotting T_{C} against λ in figure 6.

4.1.1. s- and p-band metals. As an example of the detailed information that is available for an interesting case (the most strong coupling crystalline element, mercury), we review in figure 11 the beautiful results of Hubin and Ginsberg (1969). The I–V curves for the $Al/Al_2O_3/Hg$ junction at 1·05 K and 0·39 K have been shown in figure 8(*b*), leading to the values $\Delta_{\mathrm{Hg}} = 0{\cdot}833 \pm 0{\cdot}004$ mV and $\Delta_{\mathrm{Al}} = 0{\cdot}211 \pm 0{\cdot}004$ mV. The conductance $\sigma/\sigma_{\mathrm{BCS}}$ at 0·35 K is shown in figure 11(*a*) and the α^2F corresponding to these data and the quoted Δ are shown as dashes in figure 11(*b*). The prominence and clarity of the van Hove singularities is striking. This α^2F leads to $\lambda = 1{\cdot}6$ and corresponds to $\mu^* = 0{\cdot}11$. The associated superconducting gap function $\Delta(\omega)$ and normal-state renormalisation function $Z_{\mathrm{N}}(\omega)$ for Hg have been shown in figure 5. Note that $Z_{\mathrm{N}}(0) = 1 + \lambda$ is the factor by which the electron cyclotron mass and the specific heat in the normal state are increased by the electron–phonon coupling. A comparison between $\alpha^2F(\omega)$ for Hg obtained by tunnelling (dashes) and the $F(\omega)$ from neutron data is shown in figure 11(*b*). The neutron $F(\omega)$ (full curve) has been calculated using an eight-neighbour Born–von Karman model from inelastic neutron ω–k dispersion measurements at 80 K along five particular directions in reciprocal space. The comparison of the two curves in figure 11(*b*) shows two major points of difference: first, the $F(\omega)$ is higher at high energy than the tunnelling data, $\alpha^2F(\omega)$, i.e. $\alpha^2(\omega)$ is thus determined to be a decreasing function of energy; and second, small shifts of up to 0·5 meV are observed between the positions of the measured and predicted critical points. A direct calculation of $\alpha^2(\omega)\, F(\omega)$, also based on the Born–von Karman fit to the neutron dispersion data (in a one-OPW approximation for the electron–phonon matrix element evaluated using a local Heine–Abarenkov pseudopotential) clearly confirms that $\alpha^2(\omega)$ is a decreasing function of energy ω in this case, although the calculated value λ comes out rather too high, 2·0 as compared to the measured 1·6. (This would displace the point for Hg quite noticeably from the line of $T_{\mathrm{C}}/\omega_{\log}$ against λ plotted in figure 6; such overestimations in theoretical calculations of λ may be attributed to a neglect in the calculation of screening of the electron–phonon interaction by the other electrons.) Returning to the question of the small shifts, in the past such shifts have been shown to arise from the inadequacy of the Born–von Karman model (Roy and Brockhouse 1970) in prediction from measurements along a few directions of the energy of a van Hove singularity which may lie elsewhere in reciprocal space. The tunnelling measurement, in which the critical energies are directly revealed as peaks in $\mathrm{d}^2V/\mathrm{d}I^2$ plotted on the x–y recorder, inherently integrates (2.36) over all phonon wavevectors. We thus expect the tunnel-

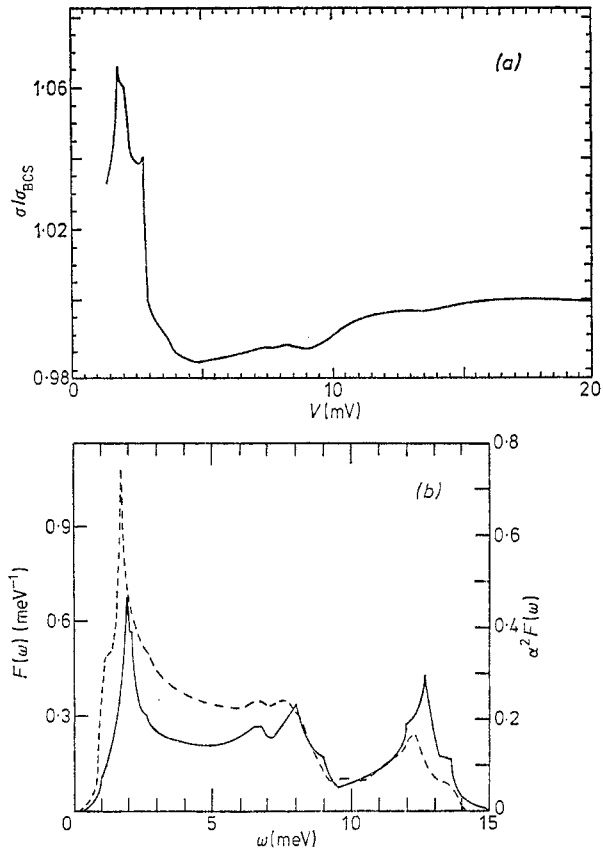

Figure 11. (*a*) Normalised conductance σ/σ_{BCS} for Hg at 0·35 K (from Hubin and Ginsberg 1969). $T=0{\cdot}35$ K. (*b*) A comparison of the tunnelling $\alpha^2F(\omega)$ with an α^2F calculated from neutron scattering measurements (from Kamitakahara *et al* 1977). ———, $F(\omega)$ neutron; - - - - - - -, $\alpha^2F(\omega)$ tunnelling.

ling experiment to provide the more reliable energies for the van Hove singularities. Careful extension of neutron measurements to more widely spaced k values (and, as well, use of incoherent scattering techniques) have brought into close agreement the corresponding neutron and tunnelling values for the van Hove singularity energies in Pb, which were similarly initially in disagreement.

A similarly complete description of the superconducting state exists in the literature for the s–p elements Pb, In, Sn and Tl in the crystalline state. We will also discuss alloys and amorphous phases of these materials below. The effect of pressure on the gap of In and Tl has been measured by Galkin *et al* (1969).

We close by mentioning that the analysis leading to figure 6 of T_C/ω_{log} against λ was made possible by the tunnelling results, and shows that T_C is a rising function of λ for values up at least to 2·5, with the implication that higher T_C values may be achieved by raising λ. This replaces an earlier prediction (McMillan 1968a) that T_C should saturate at about $\lambda=2$; this is an optimistic change from the point of view of high T_C.

4.1.2. d- and f-band elements and compounds. For several reasons the experimental

picture is not as satisfactory in d- and f-band materials, although some progress is being made. Speaking first of transition elements, principally Nb, V and Ta; only Ta (Shen 1970) had until recently been satisfactorily studied by conventional methods (i.e. the Ta–Ta oxide–M junction). It is clear that the thermal oxides of V make poor tunnelling barriers (Noer 1975) and the same tendency is more subtly present in Nb. As pointed out by Shen (1972a), the cleanliness of the metal electrode surface layers adjacent to the barrier is of greater importance in transition metals because the sampling depth of the tunnelling electron is smaller than in s–p materials. The results thus more heavily weight the contribution from a possibly contaminated surface. The sampling depth at low bias is the coherence length $\xi = \hbar v_F/\pi\Delta$, which is reduced in transition metals by generally smaller values of v_F. At higher bias ω the injected electron can emit phonons (more rapidly for a stronger coupling material); the mean free path then determines the sampling depth as $l \sim \hbar v_F/2\omega$ Im $[Z_N(\omega)]$. Shen estimates the sampling depth as falling to about 60 Å at the higher energy longitudinal phonon peak, 18 meV in Ta. This effect, with an imperfect surface, may possibly contribute to the appearance of a falling $\alpha^2(\omega)$. A further difficulty in Nb and V is that dissolved oxygen produces about a 1 K per atomic per cent reduction in T_C, with a corresponding effect on Δ. In view of these difficulties with traditional junctions (Bostock *et al* 1976)†, improved tunnelling results for Nb and V are now being sought from two alternative junction types, the quench-condensed film on a prepared Al–Al_2O_3 substrate (Robinson *et al* 1976), and those produced by oxidation of a thin Al layer deposited *in situ* onto an ultra-high-vacuum outgassed Nb or V foil (Wolf and Zasadzinski 1977, Wolf *et al* 1978).

As might be expected from the preceding discussion, good tunnelling results from alloys or compounds of transition elements are scarce, but once again, improved results are being actively pursued. The two alternative methods mentioned in connection with Nb and V are applicable to at least some of the alloys which are of considerable interest from both fundamental and practical points of view. The fundamental question relates to the connection between T_C and $N(E_F)$, both of which go through a minimum between Nb and Mo in the 4d series or, alternatively, to the Matthias empirical rule correlating high T_C to particularly favoured electron/atom ratios of 4·8 and 6·4. Of the high T_C transition compounds in the A15 crystal structure, such as V_3Si, Nb_3Sn and Nb_3Ge (T_C values of 17, 18 and 23 K, respectively), only Nb_3Sn has been reasonably thoroughly studied by electron tunnelling. (High T_C films of these materials must be prepared at substrate temperatures between 500 and 1000 °C, and the quench-condensing method is thus not applicable.) We show in figure 12 the $\alpha^2(\omega)\,F(\omega)$ obtained by Shen (1972b); the corresponding λ of Nb_3Sn was estimated to be between 1·55 and 1·69. The overall structure and peak positions of the tunnelling α^2F for Nb_3Sn have been confirmed on polycrystalline Nb_3Sn by a time-of-flight neutron scattering technique. Shen's method was an extension of his earlier fabrication procedure for Ta–Ta oxide–Pb junctions by outgassing a pure foil to its melting point in a 10^{-9} Torr vacuum. In this case the outgassed Nb foil in ultra-high vacuum was coated with 300 Å of Sn and heated to 700 °C to form a surface layer of Nb_3Sn on the Nb substrate. Upon opening the vacuum chamber the Nb_3Sn layer was found to form a satisfactory thermal oxide tunnel barrier. The I–V characteristic of the Pb/oxide/Nb_3Sn/Nb junction was complicated by structure

† Very recently Arnold *et al* (1978) have shown that the anomalous inversion parameters from thermally oxidised Nb can be accounted for by the presence of a thin proximity layer, probably NbO.

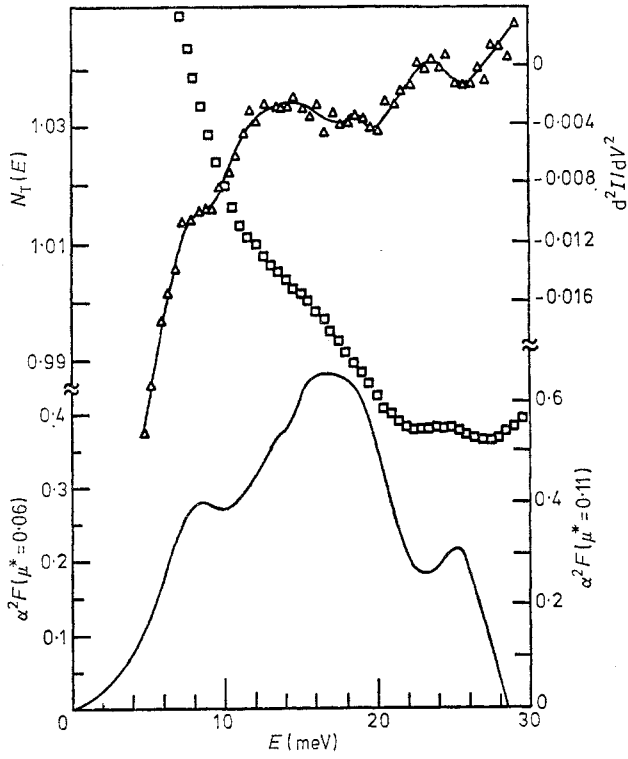

Figure 12. The electron–phonon spectral function $\alpha^2F(\omega)$ for Nb_3Sn (Shen 1972b). The upper curves in the figure are the normalised conductance (squares) and the second derivative d^2I/dV^2 (triangles).

attributed to the proximity effect from the Nb substrate, but which was removed by a parallel magnetic field of 0·5–1·5 T. The remaining phonon structure was independent of H in the range 0·5–1·5 T and is thus attributed to the Nb_3Sn layer (the critical field H_{c2} of Nb_3Sn is 23·5 T, which of course is one reason for its practical importance in fabrication of high-field magnets). Preliminary results on films of Nb_3Ge prepared by getter sputtering have been reported (Schmidt *et al* 1976); the $\alpha^2(\omega)\,F(\omega)$ is generally similar to that of Nb_3Sn.

The carbide (Geerk *et al* 1975) and nitride (Komenou *et al* 1968) compounds of Nb are also strong superconductors for which some tunnelling results have been obtained. A similar study of TaC (Zeller 1972) also showed strong coupling phonon responses, but did not permit the determination of λ. Of the rare-earth metals, La has received the most attention, culminating in the determination of a detailed $\alpha^2F(\omega)$ by Lou and Tomasch (1972) for the HCP phase, with $\lambda = 0{\cdot}77$. While the authors feel that they cannot rule out completely the presence of peculiar f-band effects in the superconductivity of La, no strong evidence for such effects is present.

4.1.3. Alloys, amorphous and granular metals and implantations. We consider first the crystalline but disordered alloys of the elements Bi, In, Pb and Tl, several of which have been studied by tunnelling and by neutron scattering. (Some of these same alloys have also been studied in the amorphous state, to which we return below.) Alloys under hydrostatic pressure have been studied by Wright and Franck (1977).

Two types of systematic alloying variation are of particular interest: basically shifting the phonon spectrum at a fixed electron/atom ratio, as in the In–Tl system (Dynes 1970), or, alternatively, varying the electron/atom ratio with elements of nearly the same mass, as in binary and ternary combinations of Tl, Pb and Bi (Dynes and Rowell 1975). The resulting sequence of $\alpha^2(\omega)\,F(\omega)$ functions in a study of the latter type is shown in figure 13, spanning the electron/atom range from 3·0 to 4·35, and representing ranges in T_C from 2·36 K to 8·95 K and in λ from 0·795 to 2·13. The gross effects here may be regarded as an increase in $\alpha^2(\omega)$ resulting from the increase in the rate of electron–phonon scattering possible with a larger Fermi surface. To be sure, the disorder in masses and in local force constants does lead to a smearing effect on the α^2F function, revealed in the comparison of the two isoelectronic members of the series: Pb and $Pb_{0\cdot9}Tl_{0\cdot05}Bi_{0\cdot05}$, both at 4 electrons per atom. Such smearing has also been observed directly in neutron scattering work and described as energy smearing arising from the finite lifetimes of the phonons caused by force constant disorder in the alloy (Roy and Brockhouse 1970). In the case of $Pb_{0\cdot4}Tl_{0\cdot6}$ in particular, close agreement was found between $F(\omega)$ determined by neutron scattering and $\alpha^2F(\omega)$ determined by tunnelling.

In general, the behaviour in crystalline alloys is not greatly different from that seen in elemental superconductors and this favourable circumstance has enabled researchers to use a wider selection of superconductors for studying, for example, the relation between the phonon spectrum, the electronic structure, and T_C. The Tl–Pb–Bi alloy system results shown in figure 13, for example, have been analysed by

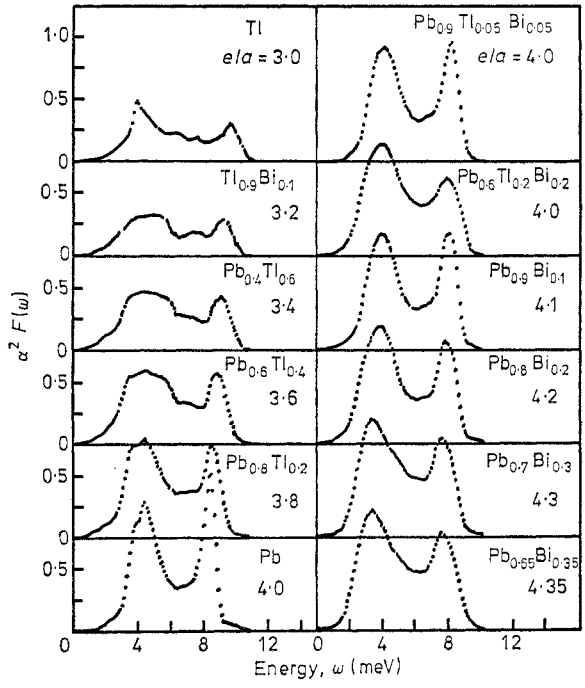

Figure 13. The change of the effective phonon spectrum $\alpha^2F(\omega)$ with concentration in the PbTlBi (crystalline) alloy system (Dynes and Rowell 1975). The broadening of the spectrum for $Pb_{0.9}Tl_{0.05}Bi_{0.05}$ relative to that for pure Pb, which is isoelectronic, is attributed to phonon lifetime broadening arising from the random variations in mass and force constants in the alloy.

Allen and Dynes (1975a,b) in an investigation of an alternative basis for predicting T_C from the observed phonon spectrum. The idea is that in a perfect crystal with no electron–phonon coupling the phonon frequencies Ω_q would be arbitrarily sharp, while an increasing electron–phonon coupling would introduce a lifetime and consequent energy smearing $\delta\Omega_q$ and also lower (soften) the phonon frequencies. If it is possible to calculate the phonon spectrum Ω_q in the *absence* of electron–phonon coupling, then comparison to the real spectrum ω_q can be shown to offer a means of calculating λ *without* such detailed knowledge of the electronic properties as is required to calculate matrix elements. According to Allen and Cohen (1972), the alternative relation for λ is:

$$\lambda = \sum_q \frac{2\gamma_q}{\pi N(E_F)\,\hbar\omega_q^2} \tag{4.1}$$

where $2\gamma_q$ is the rate of a phonon decay by electron–hole pair creation and can be related to the difference between the 'bare' and electron-renormalised phonon frequencies $\Omega_q^2 - \omega_q^2$.

In contrast to the reasonably well-understood situation with *crystalline* alloys, *amorphous* elements and alloys have offered many surprises and puzzles, the resolution of which are still being sought. The results when some elements are condensed from the vapour onto a cryogenic substrate at 4·2 K or even 1·5 K are often very different from conventional condensation at room temperature. As extreme examples, quench-condensed bismuth and gallium form phases with larger Fermi surfaces and thus become strong coupling superconductors with T_C values of 6·11 K and 8·56 K, respectively, and ratios $2\Delta/k_B T_C$ of 4·6 and 4·5. These amorphous materials, in beautiful tunnelling data from several authors (Leslie *et al* 1970, Jackson *et al* 1971), do show very clearly the characteristic enhancement and shift of the $\alpha^2(\omega)\,F(\omega)$ function to low energies. An example is shown in figure 14 for the α^2F amorphous gallium (Chen *et al* 1969). Similar shifts of α^2F are observed in amorphous films of Pb, Sn, In, and in PbBi alloys (Chen *et al* 1971). In these cases, however, the T_C is not enhanced, although higher values of λ are produced.

Contrary to some of the literature, particularly concerning granular aluminium, it is now doubted (Dayan and Deutscher 1975) that the change in α^2F (and the T_C enhancement of Al) is due primarily to a shift in $F(\omega)$, the true phonon spectrum. Indeed, recent tunnelling and lattice heat capacity measurements (Ewert *et al* 1975) on amorphous In, and an elegant Mössbauer effect study of amorphous and crystalline Sn (Bolz and Pobell 1975), support little if any net shift (softening) of the phonon spectrum $F(\omega)$ in the amorphous state, implying that the strong effect in $\alpha^2F(\omega)$ comes largely from $\alpha^2(\omega)$ and is thus presumably related to the density of electronic states and/or the electron–phonon matrix elements. The details of this seem an open question, and possibly of some practical importance, as we shall see below.

Another interesting case is Be, which in the crystalline form has $T_C = 0{\cdot}026$ K but when quench-condensed superconducts at 9·5 K (Léger *et al* 1975). This material is intriguing in that it should have an exceptionally high $\theta_D = 1400$ K so that if λ could in some way be enhanced, an unusually large increase in T_C might be expected from the pre-factor ($\langle\omega\rangle$, θ_D or ω_{log}) in the McMillan formula.

These questions become of some technological interest when one learns that in several cases the high T_C amorphous phase can be *stabilised* against high-temperature anneals by addition of an impurity or by an unusually damaging preparation scheme. For example, amorphous Mo (crystalline $T_C = 0{\cdot}92$ K), which becomes super-

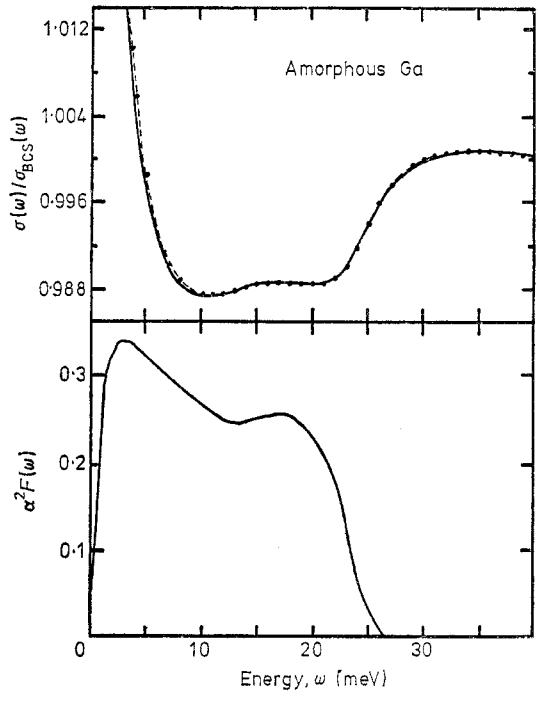

Figure 14. The $\alpha^2F(\omega)$ for an *amorphous* superconductor, quench-condensed gallium (Chen *et al* 1969). In the upper panel is shown the experimental tunnelling conductance normalised to BCS (full curve) in comparison with the same quantity calculated via the gap equations from the deduced $\alpha^2F(\omega)$ (broken curve and points).

conducting at 8 K when quench-condensed (Collver and Hammond 1973), can also be formed by a high-energy sputter deposition process (Schmidt *et al* 1973) to yield an amorphous phase of $T_C = 7{\cdot}2$ K, which, interestingly, is stable upon storage of the film at room temperature. It has further been reported (Meyer 1975, see Buckel (1975)) that Mo which is ion-implanted at helium temperature with a few atomic per cent of Cu, Au, Ag or Ge attains $T_C = 8$ K, and this amorphous phase is thus stabilised up to nearly 400 °C! The nature of the superconducting T_C enhancement of Mo and its relation to the other amorphous enhancement cases would seem an interesting and useful tunnelling study for the future.

Finally we mention the unusual cases of PdH_x and PdD_x which are superconductors of $T_C \sim 10$ K with x near 1·0. The PdH and PdD have been fabricated into tunnel junctions by several schemes; $\alpha^2F(\omega)$ data for $PdD_{0{\cdot}9}$ ($T_C = 5{\cdot}5$ K) have been obtained (Eichler *et al* 1975) from a junction made by exposing a prefabricated $Al/Al_2O_3/Pd$ structure to about 1900 atm of D_2 in a temperature cycle, up from 77 K. A peak in $\alpha^2F(\omega)$ at 35 meV is clear evidence of the participation in the superconducting state of a localised mode vibration of the deuterium.

Extensions of this line of research using ion implantation show for example (Stritzker 1974) that $Pd_{0{\cdot}55}Cu_{0{\cdot}45}+H$ can achieve a T_C of nearly 17 K.

4.1.4. Gapless superconductivity. The remaining case is that of superconductivity with zero gap, a condition which was predicted theoretically (Abrikosov and Gor'kov 1960) and substantiated in tunnelling measurements (Woolf and Reif 1965). Magnetic

scattering acts to break up superconducting pairs as it, unlike potential scattering, acts asymmetrically on the two oppositely projected spins. Consequently, the pair states in the presence of a magnetic impurity concentration c will have a lifetime energy broadening Γ which, qualitatively, will fill in the energy gap when $\Gamma = \Delta$: according to Abrikosov and Gor'kov (1960) this occurs at $c = 0{\cdot}91\,c_{Cr}$, with c_{Cr} the concentration at which superconductivity disappears. Experiments on Pb:Gd (Reif and Woolf 1962) indeed showed that as a function of c, Δ extrapolated to 0 before T_C. In figure 15(a) is shown the comparison of the normalised conductance measured for two concentrations of Gd in Pb with the AG theory as elaborated by Skalski *et al* (1964). The qualitative trend to fill in the energy gap is evident.

4.2. *Effects of magnetic field and included flux quanta*

4.2.1. Homogeneous field penetration. A parallel magnetic field $H < H_c$ (or $H < H_{c1}$ in the type II case) penetrates a superconductor to a depth λ according to the law:

$$H(x) = H(0) \exp(-x/\lambda). \tag{4.2}$$

The diamagnetic screening of the field from the interior is accomplished by sheet current flow, perpendicular to H, in the same surface layer. Tunnelling studies on the effects of the magnetic field and associated screening current can then be carried out by applying a parallel magnetic field to a junction: the use of a tunnelling electrode

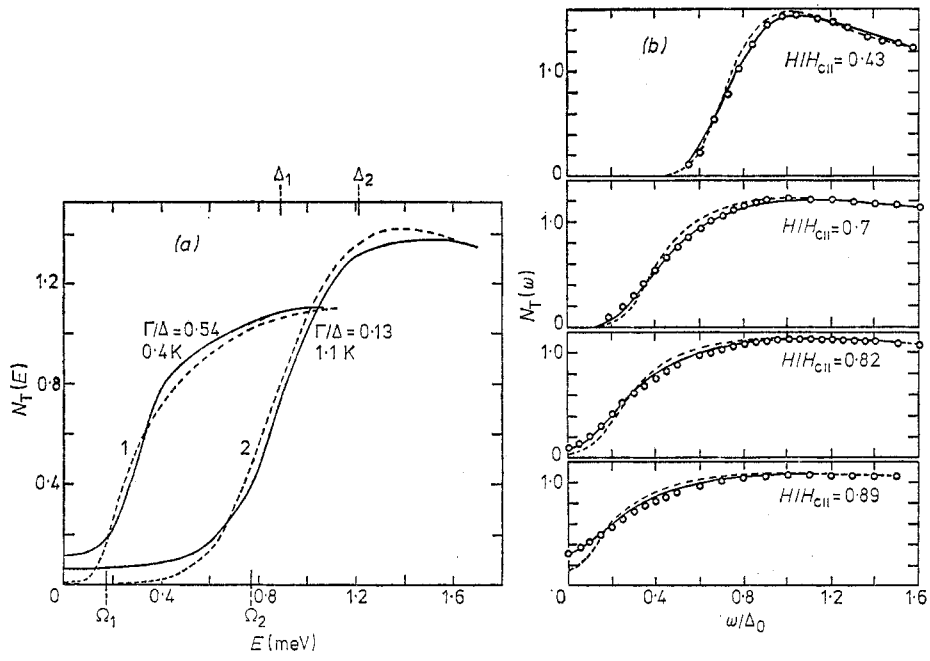

Figure 15. (a) The normalised conductance for Pb:Gd showing pair breaking by the magnetic impurity (Reif and Woolf 1962). The comparison theory curves were calculated by Skalski *et al* (1964). ———, experiment; — — —, theory. (b) The effect of a homogeneous magnetic field on the density of states in a superconductor. Data of Millstein and Tinkham (1967) on $Sn_{0.95}In_{0.05}$ films compared to the Abrikosov and Gorkov theory (1960) as elaborated by Strässler and Wyder (1967). ○, experiment; ———, theory, $l/\epsilon_0 = \pi/10$; — — —, theory, $l = 0$; $T = 0{\cdot}361$ K.

of thickness $d \ll \lambda$ will minimise the diamagnetic screening and variation of H with x in the sampled region and enable study of a superconductor in a nearly uniform magnetic field $H(0)$. In a strong type II superconductor (defined by $K \equiv \lambda/\xi\sqrt{2} \gg 1/\sqrt{2}$) the penetration depth λ may be so much larger than the sampling depth λ of the tunnelling measurement that, again, an approximately constant H can exist over the sampled region, even for a thick electrode.

The homogeneous magnetic field affects the superconductor through two different pair-breaking mechanisms, associated with the cyclotron orbital motion of the electrons (screening currents) and with the electron spin moments. The first effect can be shown (Fulde 1969) to lead to a possibly gapless density of states similar to that discussed in connection with paramagnetic impurities, but with the pair-breaking parameter now identified (Fulde 1969) as:

$$\Gamma/\Delta = \tau(v_F edH)^2/18\,\Delta_0. \tag{4.3}$$

Here τ is the transport mean free time, and a is film thickness. Tunnelling measurements of a $Sn_{0.95}In_{0.05}$ film, with l/ξ_0 measured as 0·14, at 0·36 K in indicated parallel fields H (Millstein and Tinkham 1967) are shown in figure 15(*b*). The points are experimental while the full curve is theory (Abrikosov and Gor'kov 1960, Maki 1964) adapted to the magnetic-field case and including a finite mean free path (Strässler and Wyder 1967). Note the similarity of these curves to those of Woolf and Reif in figure 15(*a*) for the paramagnetic case.

Because of the presence of d^2 in the orbital pair-breaking parameter, in a very thin film this term can be sufficiently reduced so that the spin-polarising effect of the magnetic field (independent of d) will dominate the cyclotron orbital effect. This has been demonstrated in a beautiful series of experiments by Meservey and Tedrow (Meservey *et al* 1970, Tedrow and Meservey 1971, 1973) and the relation of these results to theory has been thoroughly discussed by Fulde (1973). These results depend upon a successful technique (Meservey and Tedrow 1971) for making ultrathin Al tunnelling electrode films with $d \sim 50$ Å for which the critical magnetic fields are of the order of 40 kOe: in figure 16 is shown the spin-split quasiparticle spectrum in the dI/dV characteristic of an $Al/Al_2O_3/Ag$ junction. The splitting of the quasiparticle peaks is simply $2\mu_B H$, while the breadth of the individual peaks is governed by the spin–orbit scattering time which is unusually long in Al. Theoretical curves given by Fulde (1973) agree closely with the data as a source of spin-polarised tunnelling electrons (below).

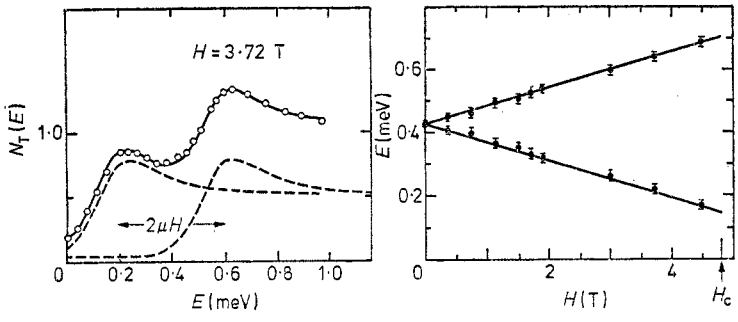

Figure 16. Magnetic splitting by $2\mu_B H$ of the quasiparticle excitation spectrum in an ultrathin Al film in a parallel magnetic field of 3·72 T at 0·4 K (from Meservey *et al* 1970).

4.2.2. Inhomogeneous flux penetration. In type II materials and films of type I materials with $d \leqslant \xi$ a perpendicular magnetic field of magnitude $H_{c1} < H < H_{2c}$ penetrates inhomogeneously in separated vortex lines which form a triangular lattice array as observed directly by decoration with ferromagnetic dust or by neutron diffraction. An individual vortex consists, qualitatively, of a normal core of radius $r_c \sim \xi$ surrounded by a circulating screening current distribution of radius $\sim \lambda$.

In thin-film tunnel junctions of the SIS and S_1IS_2 types in perpendicular fields chosen to produce non-overlapping vortices, measurements of field-dependent excess conductances at bias below the quasiparticle tunnelling threshold $eV < \Delta_1 + \Delta_2$ have been interpreted in terms of NIN tunnelling contributions between opposing normal vortex core regions at least partially aligned across the insulating tunnel barrier (Band and Donaldson 1973, Gray 1974).

In one report (Fulton *et al* 1977) very small junctions (area $\leqslant 25$ μm^2) have made possible measurements of discrete increments in conductance associated with single flux quanta. The results, however, were reported to indicate flux quanta misaligned by more than ξ and a density of states below that predicted by accepted models of the normal core.

If a parallel field is applied to a thin type II superconductor film one again expects to find a critical field H_e for entry of vortices into the film. It is found that the vortex parallel to a nearby free surface interacts with the surface (Clem 1974), leading to a surface barrier to entry and exit of flux. Because the fluxlines interact with each other and also feel the presence of the boundary, intrinsic size effects are implied, corresponding to integral numbers of fluxlines (parallel to the surface) across a thin film of type II material. These effects have been observed by microwave measurements (Joseph *et al* 1967), and by electron tunnelling (Guyon *et al* 1967, Tomasch 1965a,b, Sutton 1966, Moore and Beasley 1977). In the tunnelling observation of the entry of a fluxline, following Moore and Beasley, one sets the bias to be sensitive in dV/dI to the closing of the gap at the surface consequent to the onset of screening current flow for $H < H_e$, with H_e the critical entry field. As H_e is approached the vortex nucleates at the surface, yielding a minimum gap; for small increases beyond this the observed gap recovers quickly as the fluxline moves to the centre of the slab. The gap behaviour with the field, which up to H_e is reversible, now becomes hysteretic, indicating that the fluxlines, once injected into the film, are trapped by the surface barrier effect. The tunnelling data of Sutton on PbIn films showing these effects have been analysed by numerical solution of the Ginzburg–Landau equations in the slab geometry by Ballay (1977), which beautifully depicts the vortex nucleation process. The work of Moore and Beasley (1977) is notable in the observation of surface barrier fields of the order of 0·1 T in high-quality co-evaporated films of Nb_3Sn.

4.3. Non-equilibrium effects: branch imbalance, quasiparticle lifetimes and fluctuations

4.3.1. Non-equilibrium states. Important progress using tunnelling techniques is being made in understanding in homogeneous superconductors the details of non-equilibrium states generated by irradiation with light, microwaves, and phonon fluxes, and by tunnel injection of quasiparticles. Recall from §2.4 that the superconductor in thermal equilibrium contains three coupled subsystems: the pairs, which may be described by a semiclassical wavefunction (pair amplitude) $F(\boldsymbol{r}, t) = \sqrt{\rho(\boldsymbol{r}, t)} \exp [i\phi(\boldsymbol{r}, t)]$, with the pair density $\rho(r, t)$ and described by the optimum pair

state occupation function $h_k(\epsilon_k)$ (equation (2.23)) in BCS theory; the phonons, described by Bose–Einstein statistics; and the two branches of quasiparticle excitations $k > k_F$ and $k < k_F$, whose populations ($n_>$ and $n_<$) in thermal equilibrium described by Fermi statistics $f(E_k)$, $E_k = (\epsilon_k^2 + \Delta^2)^{1/2}$, with $\mu_F = 0$, i.e.:

$$n_> = N(0) \int_\Delta^\infty \frac{E}{(E^2 - \Delta^2)^{1/2}} f_{k>}(E)\, dE \tag{4.4}$$

and similarly for $n_<$.

The non-equilibrium steady state produced, e.g. by a flux of injected electrons, will result in distribution functions $f_{k>}$, $f_{k<}$ and phonons $n(\Omega)$ altered from their thermal equilibrium values, brought about by a balance between the flux and the relaxation mechanisms in the superconductor. The nature of the departure of these altered distributions from the thermal case is a central question, and one which can be directly probed by electron tunnelling. For example, a clear experimental demonstration of *branch imbalance*, i.e. unequal population $Q \equiv n_> - n_<$ of the electron-($k_>$) and hole-($k_<$) like branches of the quasiparticle excitation spectrum, produced by tunnelling injection is shown in figure 17 (after Kaplan *et al* 1977). These data are d^2I/dV^2 spectra measured by the 'detector' tunnel junction (between films 2 and 3) under three different bias settings of the 'generator' junction (between films 1 and 2). The asymmetric responses for hole-like and electron-like injection across the generator junction into the middle aluminium film directly measure the non-equal distributions $n_{k>}(E)$, $n_{k<}(E)$ under injection and are clear evidence for a branch imbalance Q in the central Al film. For electron-like injection, for example, it is necessary to bias the generator film negative, exceeding -2Δ by several multiples of the Al gap at the temperature under study.

The details of the lineshapes here contain information about the non-equilibrium distributions $f_k(E)$ and show that these are non-thermal in nature (i.e. cannot be generated simply by an altered μ^*, or by altering μ^* and T^*).

There are several questions of interest which we will discuss in turn: the means by which the superconductor seeks to restore equilibrium; the nature of the non-equilibrium quasiparticle distribution resulting from, for example, injection, laser

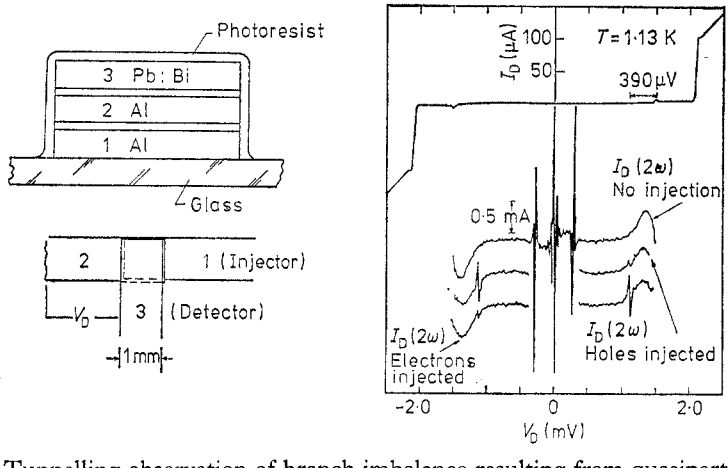

Figure 17. Tunnelling observation of branch imbalance resulting from quasiparticle injection (Kaplan *et al* 1977). The lineshapes imply that the non-equilibrium distributions cannot be satisfactorily described by an effective chemical potential μ^*.

illumination, and microwave irradiation at frequency $\nu < 2\Delta/h$; and the effect that these flux-driven departures from equilibrium will have on the superconducting properties Δ and T_C. Interestingly, the microwave irradiation can lead to an *enhancement* of T_C and Δ and this has been observed by tunnelling.

The resulting non-equilibrium quasiparticle population, e.g. $n_>$, will decay upon the removal of injection with characteristic rates τ_Q^{-1} (the branch-mixing rate) for transitions at constant energy between the $k_>$, $k_<$ branches, and the excess populations of the two branches will decay at a rate τ_R^{-1}, first by inelastic quasiparticles scattering and finally by recombination to bring the quasiparticles into equilibrium with the pairs. During both stages of the recombination process, the emission of phonons must occur and a complication arises in analysis of the results because the excess phonons in a pair-breaking time τ_B may in turn generate quasiparticles. In simple cases the effect is to lengthen the observed recombination times τ_R by a factor $(1+\tau_\gamma/\tau_B)$, where τ_γ characterises the length of time the phonons remain in the active volume. For a detailed discussion of this situation the reader is referred to a recent review of non-equilibrium superconductivity (Langenberg 1975).

Clever experiments have been devised to measure the various characteristic lifetimes, usually based on a three film tunnelling geometry, but with variation, e.g. in the nature of the detection junction, depending upon the experiment. For example, Clarke and Paterson (1974) used a *normal*-metal film as the detector in their measurement of the potential difference $V=(\mu_>-\mu_<)/e$ generated, as a consequence of the branch imbalance $Q=n_>-n_<$ and consequent quasiparticle current density, between the injected and non-injected portions of the central film in a device similar to that of figure 17. In this experimental method the potential V was used to infer the branch-mixing time τ_Q from the theory of Tinkham and Clarke (1972).

4.3.2. Gap changes. The importance of such non-equilibrium states arises in part because of the possibilities, several of which have been demonstrated, of increasing Δ and T_C. An increase of Δ measured directly by tunnelling at reduced temperatures $t=T/T_C=0{\cdot}99$ in Al has been accomplished by microwave irradiation such that $h\nu < 2\Delta(T)$ (Kommers and Clarke 1977). This effect, and an analogous effect involving irradiation with *phonons* $\hbar\omega < 2\Delta(T)$, is implicit in equation (2.24) (Parmenter 1961, Eliashberg 1970) because of the term $[1-2f(E_k)]$ in the integral expression for Δ. The largest gap $\Delta(0)$ at $T=0$ requires $f(E_k)=0$, corresponding to no quasiparticle excitations, so that the maximum number of quasiparticle states will be available for the attractive scattering processes. The role of thermal excitations in lowering Δ to 0 at T_C is to block the scattering paths. Conversely, in cases of substantial occupation of quasiparticle states just above the gap edge Δ, the application of $h\nu \lesssim 2\Delta$ will again *reduce* the occupation which blocks the attractive interaction, and will tend to artificially restore the $T=0$ quasiparticle occupation for those states near the gap edge. So long as $h\nu < 2\Delta$, pair breaking is not possible.

The opposite effect, also implicit in equation (2.24), of *reducing* Δ by artificially *filling* the low-lying quasiparticle states by tunnelling quasiparticle injection, has also been observed by tunnelling, again using a structure similar to that of figure 17. In this case (Fuchs *et al* 1977) a Sn–Sn generator junction biased at several multiples of $2\Delta_{Sn}$ provided primary injected quasiparticles in the centre 1000 Å Sn film which, by phonon emission and subsequent phonon-induced pair-breaking processes, were effectively multiplied in number as they more nearly approached thermal equilibrium. The Pb–Sn detector junction is then used to measure the gap of the injected film, the

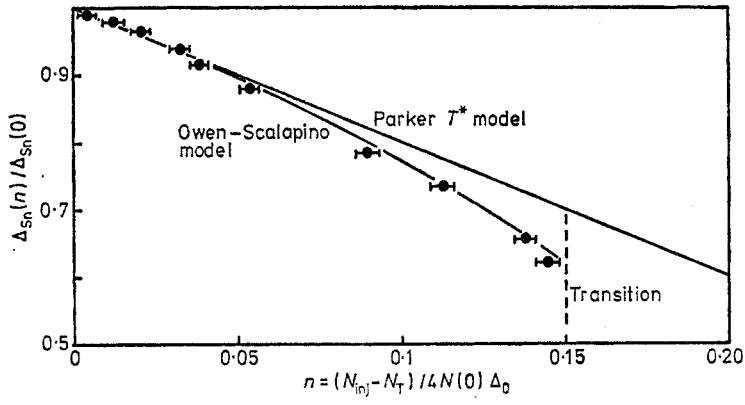

Figure 18. Reduction of the superconducting gap by high tunnelling injection of quasiparticles, after Fuchs *et al* (1977). The theory curve is based on the Owen and Scalapino model (1972).

data being shown in figure 18. The abscissa here is the excess quasiparticle density n (above the thermal value), measured in units of $4N(0)\,\Delta_0$, where $N(0)$ is the single-spin density of states at the Fermi surface. The data points for Δ/Δ_0 fall linearly with n (for small n) as suggested by equation (2.24) and in fact agree closely over the whole measured range with the prediction of a model introduced by Owen and Scalapino (1972) in which the non-equilibrium injected quasiparticle distribution is characterised by a single parameter, an effective chemical potential μ^*. The apparent agreement here is somewhat surprising as the model assumes the non-equilibrium quasiparticles to be nevertheless thermalised to the lattice temperature, while other experiments (to be sure, the conditions differ in detail) have indicated clearly non-thermal quasiparticle distributions. An instability of the Sn gap is also observed at the point $\Delta/\Delta_0 = 0{\cdot}62$, $n = 0{\cdot}15$, at which the Owen–Scalapino model actually predicts transition to the normal state. Similar experiments have been performed by Dynes *et al* (1977) and K E Gray (1978, private communication).

4.3.3. Superconducting fluctuations. While the equilibrium superconducting state disappears at $T = T_C$ in a macroscopic specimen, it is possible in small specimens to have fluctuations into the superconducting state (i.e. pairs form momentarily during fluctuations) even for $T > T_C$. The effect of such fluctuations on the electrical conductivity σ of a thin film above T_C (Glover 1967) is well described by the fluctuation pairing model of Aslamazov and Larkin (1968):

$$\sigma = \sigma_{res} + \frac{e^2(T - T_C)}{16d\hbar T_C} \tag{4.5}$$

where σ_{res} is the residual conductivity of the film of thickness d; the added term is referred to as the paraconductivity. The corresponding tunnelling density of states for $T > T_C$ in the cases of two- and three-dimensional fluctuations has been measured by Cohen *et al* (1969) in granular Al films produced by evaporation of Al in an oxygen atmosphere and by co-sputtering Al and SiO_2. The data for $\xi < d$ (the second derivative d^2I/dV^2) reveal structure due to three-dimensional fluctuations up to $T/T_C \sim 1{\cdot}4$. From the energy width of the structure it is possible to estimate the decay rate of the fluctuations to be of the order of $0{\cdot}2\Delta_{Al}(0)/\hbar$.

4.4. Inhomogeneous superconductors: interference effects and bound states

4.4.1. Andreev scattering. We recall from our discussion of quasiparticle excitations (equation (2.27)) that electron-like and hole-like excitations of the same energy E occur at different wavevectors $k_> = k_F + (E^2 - \Delta^2)^{1/2}\,\hbar v_F$, $k_< = k_F - (E^2 - \Delta^2)^{1/2}\,\hbar v_F$ (see figure 4(*c*)). A discontinuity in the pair potential Δ generally occurs (as we shall see in the next section) at the interface between different metals and leads to scattering of quasiparticles of one branch into the other (Andreev 1964). Consider first an ideal normal–superconductor boundary between metals of the same Fermi wavevector, and suppose that an electron of energy $E > \Delta_S$ in the N region ($\Delta_N = 0$) reaches the NS interface: while it can propagate into the region of larger gap, there is also a small probability that it will be reflected. The unusual nature of the pair potential Δ requires that the reflection occur by *pairing* with an electron *below* the Fermi sea in the S region, leaving a *hole*-like excitation propagating back into the N region. This scattering process was first discussed by Andreev (1964).

4.4.2. Tomasch and Rowell–McMillan oscillations. The possibility of interference arises because the wavevector of the scattered hole differs by $-2E/\hbar v_F$ from that of the incoming electron. In the case at hand, the Andreev-reflected hole must propagate back to the opposite side of the normal metal, be reflected normally as a hole, return and again suffer Andreev reflection at the NS interface, to become once more an electron, but now shifted in phase by $2d(k_> - k_<) = 2d\Delta k$. The difference $\Delta k = 2E/\hbar v_F$ is small compared to k_F (for E in the millivolt range), so that oscillations can be observed for d of the order of 1 μm, presuming that other scattering events do not destroy the coherence. The energy spacing ΔE of the oscillations is determined (from the condition $2d\Delta k = 2\pi$) as $\Delta E = 2\pi\hbar v_F/4d$. These '4$d$' oscillations were first observed and explained by Rowell and McMillan (1966) in tunnelling measurements into Ag films backed by Pb.

The oscillations observed earlier by Tomasch (1965a,b, 1966) arose in tunnelling into a thick superconductor *backed* by a normal metal. In this case interference can occur with only one traversal of the superconductor film: an electron-like quasiparticle in the superconductor is reflected into a hole at the normal back interface, which propagates back across the film and interferes with the hole-like part of the initial wave. The energies of the Tomasch oscillations were thus shown (McMillan and Anderson 1966) to be, for integer n:

$$E_n = \left[\Delta^2 + n^2\left(\frac{\pi\hbar v_F}{d}\right)^2\right]^{1/2}. \tag{4.6}$$

Measurements of these oscillations (see, for example, figure 19) have been used to determine the Fermi velocity v_F as *renormalised* by the electron–phonon interaction. These topics have recently been reviewed by Nedellec *et al* (1976).

4.4.3. Bound states. Again looking at an electron in the N region of a perfect NS sandwich, and considering the case $E < \Delta_S$, we see that this quasiparticle must be totally reflected by the pair potential step Δ_S; in fact it can be shown (de Gennes and Saint-James 1963, Saint-James 1964) that at least one bound state of energy $E < \Delta_S$ will occur in the slab of normal material. (The same conclusions apply for quasiparticles of energy $\Delta_1 \leqslant E < \Delta_2$ in an S_1S_2 sandwich.) Such bound states have been observed directly in the I–V characteristic by Rowell (1973) in PbZn/ZnO/Pb

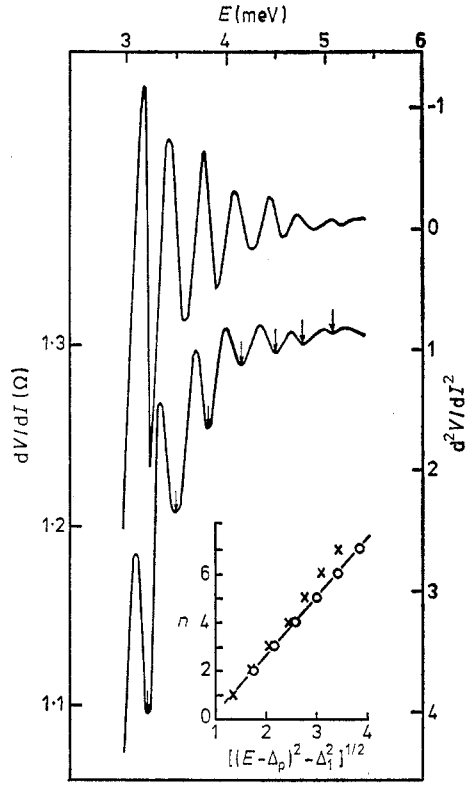

Figure 19. Tomasch oscillations in the thick Pb film (6·1 μm) of figure 10(*b*) (Lykken *et al* 1970). The spacing of the oscillations is governed by the renormalised Fermi velocity.

proximity sandwich tunnel junctions with Zn thicknesses of 1–5 μm. As the Zn is actually induced into the superconducting state with a small gap Δ_1 by its proximity to the Pb, the bound states observed by Rowell are in the range $\Delta_1 < E < \Delta_2$. The single bound state which occurs in a *thin* normal or $\Delta_1 (\ll \Delta_2)$ layer approaches the energy Δ_2 in the limit of zero thickness.

4.5. Inhomogeneous superconductors: the proximity effect

In the previous section we have discussed oscillatory phenomena and bound states observed in tunnelling into NS sandwiches. The effects have been explained in terms of an assumed discontinuity in the pair potential Δ at the NS boundary, without probing the origin of such a discontinuity or the other basic properties of N and S films in close metallic contact. As the use of the proximity effect is now at a frontier in extension of tunnelling research both to study phonon interactions in very weak coupling metals, and in the study of otherwise intractable superconducting compounds and alloys, we shall discuss this topic in some depth.

4.5.1. Experimental background. It has long been known (Meissner 1960) that SNS structures can allow supercurrent flow in the usual sense, even if the N region is Au or Cu several tenths of a micron in thickness. The critical temperature of the structure

is reduced from that of the pure S metal as the N thickness increases and as the S thickness decreases. It is found that the critical current of the SNS structure increases with decreasing temperature and decreases (exponentially, for $l \ll \xi$) with the thickness of the N layer.

Such experimental results are understood on the assumption that the probability amplitude for finding pairs (the pair wavefunction) $F(\boldsymbol{r}) = [\rho \exp(i\phi(\boldsymbol{r}))]^{1/2}$ does not vanish in N but rather decays smoothly into N from the NS interfaces. The details of the decay depend on the ratio of the coherence length ξ_N to the mean free path l; for $l \ll \xi_N$, $F(r) \propto \exp(-Kr)$ with $K^{-1} = (\hbar v_F l/6\pi k_B T)^{1/2}$. In the clean case the length scale of the associated decrease of the pair wavefunction F in N is set by ξ_S (McMillan 1968a), but the decay of F in the N region can be slower than exponential (Falk 1963) at $T=0$, while at $T \sim T_C$ it is again exponential, with $K^{-1} = \hbar v_F/2\pi k_B T$. If we exclude the special case of the *weak link*, for which the critical current is an oscillatory function (Josephson 1962, Waldram 1976) of a phase difference $\Delta\phi$ (produced, for example, by a magnetic field), and suppose the supercurrent to be given in the usual way by

$$\boldsymbol{J} = -\frac{e\hbar}{2im}(F^*\nabla F - F\nabla F^*) = -\frac{e\rho\hbar}{m}\nabla\phi$$

evaluated at the middle of the N region, then this region of non-zero F is, for finite coupling λ_N^*, evidently induced into the superconducting state with a pair potential $\Delta_N = \lambda_N^* F$. Consideration of the NS boundary condition, taking into account the continuity of J across the interface, requires a discontinuity in F (Falk 1963) and the continuity, at least for $T \sim T_C$, of $F/N(0) = \Delta/N(0)\,V$ across the interface (de Gennes 1964).

Tunnelling measurements into the N side of NS sandwiches at low temperatures indeed show a well-defined gap-like structure, qualitatively similar to that predicted by BCS, for N layer thicknesses up to typically 100–300 Å, but showing more prominent positive peaks in dI/dV just above the apparent gap. It was clear, in addition, even from early work (Adkins and Kington 1966, Hauser 1966) that the observed width of the apparent gap Ω_N induced into the N metal approached in magnitude the pair potential Δ_S of the superconducting electrode as the thickness of the normal metal d_N approached zero; this in apparent disagreement with the pair potential:

$$\Delta_N = \frac{(N(0)\,V)_N}{(N(0)\,V)_S}\,\Delta_S \tag{4.7}$$

required by the de Gennes (1964) boundary condition, which is typically much less than Δ_S. Further, in a study of 500 Å Ag films backed by Pb, Rowell and McMillan (1966) observed (in the Ag electrode) an image in dI/dV of the Pb phonon structure, which systematically changed in shape with increasing Ag film thickness and eventually became inverted. It was observed that the induced gap and phonon structures decreased with increasing normal layer thickness and, quite reasonably, with variations in the preparation scheme which allowed more oxide or other impurities to accumulate at the NS interface. Further, for thick N layers more than a few hundred Å thick, the dI/dV peak structure above the apparent gap became broader and more complicated, showing in some cases a second, *negative* dI/dV peak at an energy close to Δ_S, the pair potential of the underlying superconductor (Freake 1971). Measurements from the S side of NS sandwiches showed qualitatively a progressive reduction in the dI/dV

peak height, sharpness, and apparent gap as the ratio d_N/d_S increased and as the coupling strength between the N and S members was increased.

4.5.2. States in the N *region.* The tunnelling experimental results summarised above thus do *not* confirm in any simple way the presence of BCS-like superconductivity of gap Δ_N in the N layer, but rather suggest a more complicated situation. The most obvious discrepancy, the observation of an apparent gap Ω_N *larger* than Δ_N, and approaching Δ_S in the limit $d_N \to 0$, has been theoretically discussed in two different ways. In one approach (Arnold 1978) it is associated with a quasiparticle *bound state* (or states) in the N layer, trapped by the pair potential step $\Delta_S - \Delta_N$. These states, predicted by de Gennes and Saint-James (1963), were observed by Rowell (1973) in thick layers of Zn backed by Pb: but in the limit $d_N \to 0$ only one state is possible and its energy becomes arbitrarily close to Δ_S. An alternative explanation is found in the McMillan (1968b) tunnelling model, in which Ω_N is associated with $\Delta_N{}^{ph} + \hbar/\tau_N$, where τ_N is the time the carrier remains in the N region before returning to the S region. Both treatments agree that the induced pair potential in the normal layer does not have associated with it a peak at Δ_N in the density of excitations, consistent with the tunnelling experiments.

Treatments of the NS problem detailed enough to compare with the N side tunnelling results have thus far been limited to the case $d_N \ll \xi$, so that the superconducting properties, e.g. Δ_N, may be assumed constant across the layer. The bound state, which is a fundamental feature of the situation, was quantitatively treated in this thin N case by de Gennes and Saint-James (1963) (and later extended by Saint-James (1964) and Bar-Sagi and Entin-Wohlmann (1977)) by solution of the coupled Gor'kov–Bogoliubov equations, taking Δ_S to be constant in the semi-infinite clean superconductor:

$$\begin{aligned} Eu &= -\frac{\hbar^2}{2m}\nabla^2 u + \Delta_S v \\ Ev &= \frac{\hbar^2}{2m}\nabla^2 v + \Delta_S u \end{aligned} \tag{4.8}$$

subject to the appropriate boundary conditions and no scattering for quasiparticle amplitudes u and v and the excitation energies E. The excitations (de Gennes and Saint-James 1963) are equal mixtures of electron and hole; the excitation spectrum has a sharp bound-state peak (multiple peaks for larger d_N) with a spectrum falling sharply toward lower energy; the highest energy corresponds physically to propagation normal to the film and the lowest energy, zero, corresponds to quasiparticle motion parallel to the film. One expects that the low-energy excitations, which are relatively fewer as d_N is decreased, are not sampled by tunnelling injection which favours final states normal to the tunnelling barrier. Figure 20(a) shows the bound-state energy relative to Δ_S as a function of d_N for several values of a reflection parameter arising from an assumed δ-function repulsive potential at the NS interface, after Bar-Sagi and Entin-Wohlmann (1977). The relatively minor effect on the bound-state energy arising from $\lambda_N{}^*$ (neglected in figure 20(a)) was calculated by Saint-James (1964).

4.5.3. The McMillan tunnelling model. McMillan (1968b) published a very useful tunnelling Hamiltonian model calculation capable of estimating the energy density of excitations in both members of the NS sandwich, and which can be extended (Chaikin *et al* 1976, 1977) to discuss the energy-dependent pair potentials arising from

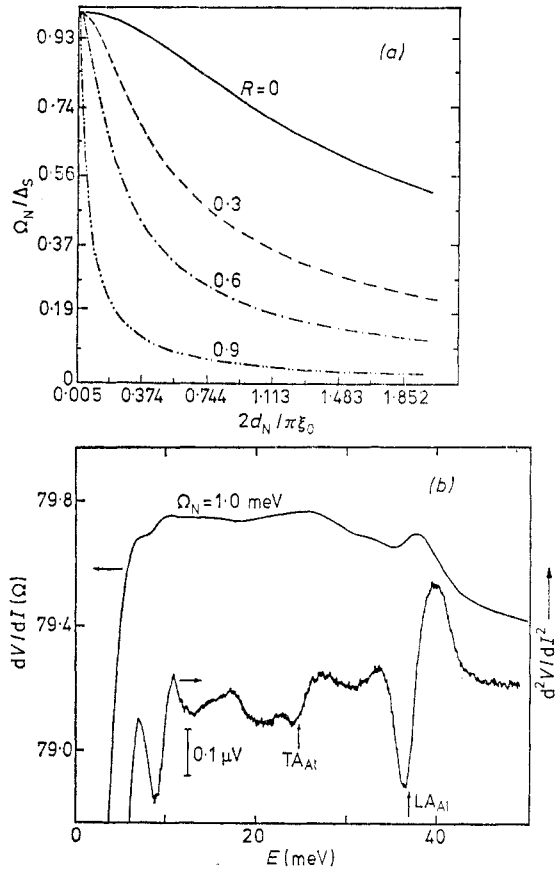

Figure 20. (*a*) The energy of the bound state in the N side of the NS sandwich as a function of d_N and of the reflection produced at the NS interface by an assumed repulsive δ function potential. The bound-state energy approaches the superconducting energy gap as d_N approaches zero (from Bar-Sagi and Entin-Wohlman 1977). (*b*) Proof of the proximity-induced superconductivity of Al backed by Pb in the observation (Chaikin *et al* 1977) of a strong response at the Al phonon energy. $t_{Al}=200$ Å, 1·4 K.

the strong electron–phonon interaction. In this model the N and S layers are both thin compared with the coherence lengths and are coupled to each other via the transfer Hamiltonian of an assumed tunnelling barrier of transmission coefficient $\sigma \ll 1$. The latter condition provides a fundamental restriction of the model, as is an assumption that there are no selection rules relating the initial and final wavevectors. Further, since Andreev reflection does not occur in the model it cannot predict the $2d$ or $4d$ oscillations or the bound states. The tunnelling Hamiltonian produces transitions, for example, from a state in N to any of those in S at a total rate:

$$\Gamma_N = \frac{\hbar}{2\tau_N} = \pi T^2 A d_S N_S(0) \tag{4.9}$$

with τ_N the lifetime of an electron in N, $\tau_N \sim L_N/v_{FN}\sigma$, with L_N the path length between collisions with the barrier, and an analogous rate Γ_S from S to N. If $\Delta_{N,S}^{ph}$ are the phonon-induced pair potentials in the bulk N, S materials, then in proximity

$\Delta_{N,S}$ are given by McMillan's equations:

$$\Delta_N(E)=\left(\Delta_N^{ph}+\frac{\Gamma_N\Delta_S(E)}{[\Delta_S^2(E)-E^2]^{1/2}}\right)\left(1+\frac{\Gamma_N}{[\Delta_S^2(E)-E^2]^{1/2}}\right)^{-1} \tag{4.10}$$

$$\Delta_S(E)=\left(\Delta_S^{ph}+\frac{\Gamma_N\Delta_S(E)}{[\Delta_N^2(E)-E^2]^{1/2}}\right)\left(1+\frac{\Gamma_S}{[\Delta_N^2(E)-E^2]^{1/2}}\right)^{-1}. \tag{4.11}$$

The corresponding densities of excitations can be computed via:

$$N_{S,N}(E)=\mathrm{Re}\left(\frac{E}{[E^2-\Delta_{S,N}^2(E)]^{1/2}}\right). \tag{4.12}$$

One recognises from the first equation that a basic prediction of the model for the N side is for an enhanced energy-dependent pair potential, which for low energy, $E\ll\Delta_S$, becomes a constant: $\Delta_N^{ph}+\Gamma_N=\Delta_N^{ph}+\hbar/2\tau_N=\Omega_N$ with which is associated (from (4.12)) a gap $\Delta_N^{ph}+\Gamma_N$ and a roughly BCS-like peak in $N_N(E)$. Quantitatively, however, the peak in $N_N(E)$ at Ω_N is sharper and taller than the equivalent BCS peak and also the peak in $N_S(E)$ at Δ_S is reduced below the BCS value. An improved energy-dependent pair potential $\Delta_N^{ph}(E)$ can be calculated for N from the Eliashberg gap equation (2.36), by putting the enhanced energy-dependent pair potential (4.10) into the equation along with the $\alpha^2F(\omega)$ appropriate to the bulk N metals (Chaikin *et al* 1977). The improved $\Delta_N^{ph}(\omega)$ now contains more prominent deviations at the phonon frequencies of the N metal, and the correspondingly improved $N_N(E)$ can now again be calculated from equation (4.12). Strongly enhanced strong coupling Al phonon structure in 200 Å Al films backed by Pb (Chaikin *et al* 1976, 1977) is shown in figure 20(*b*).

Of course Ω_N, which depends on τ_N, must be understood in the McMillan model as an average value so that one would expect experimentally a broader gap-like structure than described above with a single value of Ω_N. Although McMillan loosely identifies the response at $\Omega_N=\Delta_N^{ph}+\hbar/2\tau_N$ with the bound-state contribution at angle θ in the de Gennes–Saint-James model which would be associated with the same lifetime $\tau_N=d_N/v_F\cos\theta$, clearly there is no structure in McMillan's result corresponding to the $\theta=0$ bound state which, as we have said, approaches Δ_S in energy as d_N approaches zero. Still, in the limit of large Γ_N and Γ_S, with rapid transfer across the barrier one expects the self-energies and densities of states on the two sides to become the same, and McMillan points out that the solution of the coupled equations for $E\ll\Gamma_S$, Γ_N is $\Delta_N(E)=\Delta_S(E)=(\Gamma_S\Delta_N^{ph}+\Gamma_N\Delta_S^{ph})/(\Gamma_S+\Gamma_N)$ which reduces to $\Delta_N(E)=\Delta_S^{ph}$ for $\Gamma_N\gg\Gamma_S\gg E$. Curves for $N_N(E)$ numerically obtained from the coupled equations which correspond to the approach to the above limit of a BCS peak at Δ_S for Γ_N large (d_N small) are plotted by Wyatt *et al* (1972); experimental values of the apparent gap against d_N for several NS systems have been successfully fitted to the McMillan model by Adkins and Kington (1969). The quality of fit of experimental dI/dV data to the model, which is generally at best semi-quantitative, has been demonstrated and discussed by Adkins and Kington (1969), Freake (1971), Vrba and Woods (1971a,b), Wyatt *et al* (1972), Prothero (1974) and Toplicar and Finnemore (1977).

4.5.4. Induced superconductivity of Kondo alloys. An interesting use of proximity effect tunnelling which can be discussed in terms of the McMillan model and its extensions is the study of dilute magnetic alloys, inherently non-superconducting,

as they are induced into the superconducting state by proximity, for example, to Pb (Dumoulin *et al* 1977). The magnetic exchange interaction $-J\boldsymbol{S}.\boldsymbol{\sigma}$ between a magnetic moment $\boldsymbol{S}$ (produced, for example, by Cr in Cu) and the host conduction electron of spin $\boldsymbol{\sigma}$ can lead (Kondo 1964) to the anomalous resistivity minimum as a function of T, and to the formation of a type of spin-compensating bound state at very low temperatures. The theoretical treatment of Abrikosov and Gor'kov (1960) examined the effect of dilute magnetic impurities in pair breaking via a parameter $\Gamma=\frac{1}{2}cN(0)\,J^2S(S+1)$ leading to a gapless density of states as discussed above in §4.1.4. The theory of Zittartz *et al* (1972) predicted the presence and energy density of a localised band of excited states in the superconducting gap. The beauty of the proximity effect technique is that the well-studied (non-superconducting) Kondo alloy systems can be induced into the superconducting state where their excitation densities can be measured and compared to the above theory. Experimentally this technique is more reliable than methods in which magnetic moments remain in a normal-metal matrix, because of the relatively larger superconducting coherence length. Such measurements of Cu:Cr/Pb tunnel junctions by Dumoulin *et al* (1977) have indeed revealed the predicted localised band and rather closely resemble the predictions of the theory of Zittartz *et al* (1972), as shown in figure 21; similarly close resemblance is obtained by the recent theory of Machida (1977) (see below).

This line of research was stimulated initially by the extension of the McMillan model to include the $-J\boldsymbol{S}.\boldsymbol{\sigma}$ interaction in the Hamiltonian of the N metal (to the level of the Born approximation) by Kaiser and Zuckermann (1970). This theory shows the onset of gaplessness with impurity concentration in the tunnelling density of states from the N side but does not give the bound states. A further extension of this theory to incorporate the bound states has been made by Machida (1977) and Machida and Dumoulin (1978) whose results also closely resemble the experimental data of figure 21. Machida's analysis is, in fact, more appropriate to the experiment as it includes the proximity effect with the Pb electrode.

We have already mentioned one of the uses of the proximity effect in boosting the pair potential in a very weak coupling metal like Al, Cu or Ag (Chaikin *et al* 1977) to observability in tunnelling in the N side of an NS sandwich. The second main interest in this situation is in studying strong coupling materials which, for example, do not oxidise easily by making a thin NS junction with an N metal such as Al which is easily oxidisable. We have already had a suggestion from the McMillan model that in the limit $d_N\to 0$ the self-energies and densities of states should become identical and be weighted by the thicker S material. To pursue this type of experiment one wants to avoid contamination at the NS interface and thus is led to very tightly coupled NS layers, to which the McMillan model does not apply.

4.5.5. The Arnold model. A new Green function calculation for the N side of NS sandwiches by Arnold (1978) assumes no bulk scattering, $d_N \ll \xi$, and a perfect or highly transparent NS interface. The theory includes the bound state whose position in energy is shown in figure 20(*a*) in the N layer and the oscillatory geometrical resonance effects. The logical predecessors of this work are those of McMillan (1968c) and Wolfram (1968).

A narrow gap between the bound state and Δ_S is predicted by this calculation which probably corresponds to the negative dI/dV peak observed by Freake (1971) and Prothero (1974) at $eV\sim\Delta_S$ with thicker N layers; this gap becomes unmeasurably small as $d_N\to 0$. In this limit the bound state disappears and the calculated density

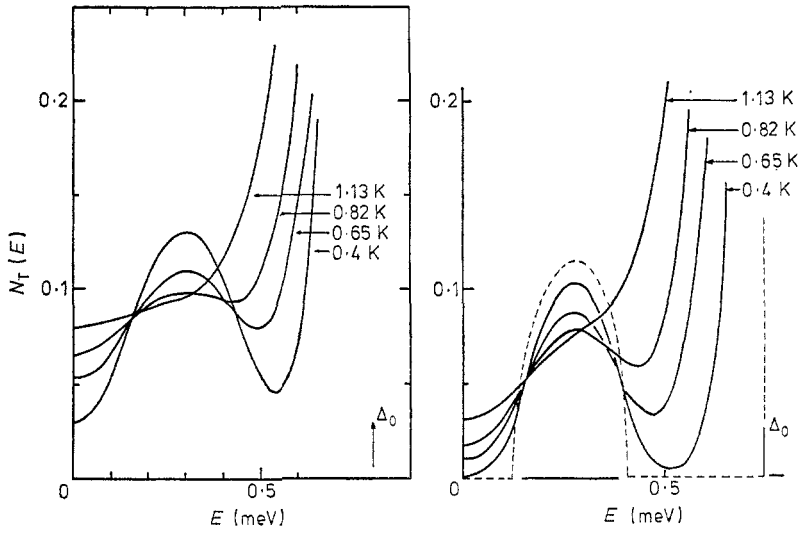

Figure 21. (*a*) Observation of localised states in the energy gap produced by magnetic impurities in a Kondo alloy (**Cu**:Cr) induced by proximity into the superconducting state (from Dumoulin *et al* 1977). $d_N = 250$ Å. (*b*) Theoretical matching of the data (figure 2(*a*)) by use of the theory of Zittartz *et al* (1972) (from Dumoulin *et al* 1977).

of states becomes that of (1.1) with $\Delta_N(E) = \Delta_S(E)$. For $E \gg \Delta_S$ and finite d_N the normalised density of states is:

$$N_T(E) \simeq 1 + \tfrac{1}{2}\,\mathrm{Re}\left(\frac{\Delta_N^2}{E^2}\right) + \tfrac{1}{2}\,\mathrm{Re}\left(\frac{(\Delta_S - \Delta_N)^2}{E^2}\, I(2R\Omega_N)\right) + \mathrm{Re}\left(\frac{\Delta_N(\Delta_S - \Delta_N)}{E^2}\, I(R\Omega_N)\right) \tag{4.13}$$

with $R = 2Z_N d/\hbar v_F$, $\Omega_N = (E^2 - \Delta_N^2)^{1/2}$, and $I(y) = \int_1^\infty (\mathrm{d}x/x^2)\, D(1/x) \exp(\mathrm{i}yx)$ where $x = 1/\cos\theta$, θ being the angle of transmission relative to the normal, and $D(1/x) = \beta \exp[\beta(1-x)]$ (McMillan 1968c). The terms involving I are the '$2d$' and '$4d$' oscillations discussed earlier; $I(y)$ is qualitatively like a damped $\cos y$, whose decay is hastened if y has an imaginary part. For small values of $d_N \sim 100$ Å and a large N metal Fermi velocity v_F, the R parameter (which is an inverse energy) becomes small, (100 meV)$^{-1}$ or less, corresponding to slow oscillations in energy whose period is $R^{-1} \gtrsim 100$ meV. It is thus reasonable to approximate the function $I(y)$ by its leading terms or, in the limit $d_N \to 0$, by unity. In such an expansion of the expression for $N_T(E)$, cancellation of the Δ_N terms occurs and the limit $N_T(E) \simeq 1 + \frac{1}{2}\,\mathrm{Re}\,(\Delta_S^2/E^2)$ is obtained, which is the expansion for $E \gg \Delta_S$ of Re $[E/(E^2 - \Delta_S^2(E))^{1/2}]$, the response expected for a single *superconductor* electrode, and contains all of the energy variation in $\Delta_S(E)$ at phonon energies. The other notable feature of the Arnold expression is the presence, for non-zero values of d_N, of the term, $1 + \frac{1}{2}\,\mathrm{Re}\,(\Delta_N^2/E^2)$, which, similarly, is the response (for $E \gg \Delta_N$) expected from the *normal* metal N. One understands that Δ_N in this expression will be increased in magnitude above Δ_N^{bulk} in the absence of the S proximity layer, as discussed in connection with the McMillan model.

Experimental data on ultra-thin AlNb proximity sandwiches prepared at 10^{-9} Torr by ultra-high-vacuum techniques have been obtained by Wolf and Zasadzinski (1977, 1978); an example of the directly obtained $\mathrm{d}V/\mathrm{d}I$ spectrum for such a junction with

$d_N \simeq 75$ Å is shown in figure 22. The notable feature here is that the Nb phonon structure (at 20–25 meV) corresponds to $\Delta\sigma/\sigma \sim 10^{-2}$, close to the strength expected in an ideal N/I/Nb tunnel junction, while the presence of the Al structure at 36 meV makes it clear that one has indeed a proximity junction. The strength of both N and S phonon contributions here greatly exceeds that typically obtained in thin-film NS layers prepared in conventional 10^{-6} Torr evaporation systems (Chaikin *et al* 1977); the increased strength of the S phonon contributions and the availability of Arnold's theory (valid, unlike the McMillan model, in the limit of strong NS coupling) now have made possible, in cases where the $\alpha^2F(\omega)$ of the N metal is known, extraction from N side proximity data the superconducting properties and $\alpha^2F(\omega)$ of the S electrode.

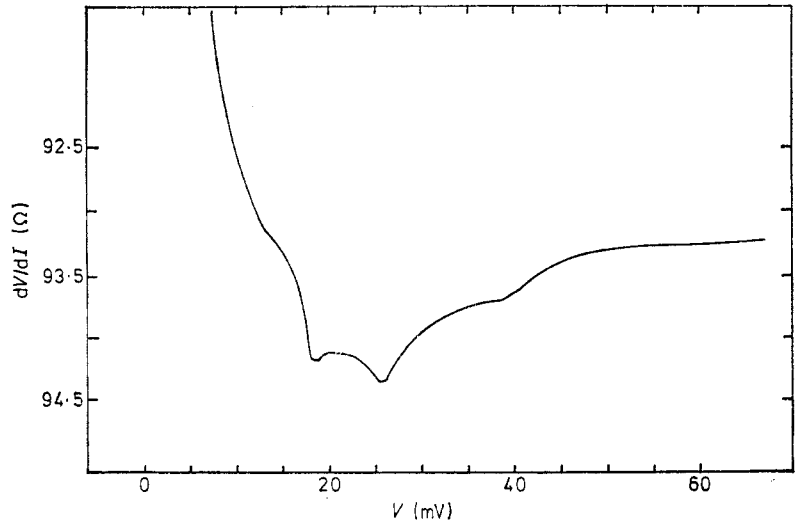

Figure 22. Demonstration of strong superconducting phonon effects in observation on the N side of an NS sandwich. Here in an $In/Al_2O_3/AlNb$ junction (Wolf and Zasadzinski 1977) are shown strong coupling deviations in dV/dI from both the Nb phonons (17 and 25 meV) and the Al phonon (36 meV). With knowledge of the $\alpha^2F(\omega)$ for Al such data can be reduced to determine the $\alpha^2F(\omega)$ for the Nb or other S member of the sandwich (Arnold 1978). $t_{Al} = 75$ Å, 1·37 K, $H_{\parallel} = 30$ mT.

(Wolf *et al* 1978b). This is expected to make possible quantitative study of a variety of interesting superconducting compounds and alloys whose surfaces are difficult to clean and which oxidise poorly in conventional tunnelling methods.

5. Studies of the normal phase: final-state effects

Before describing particular cases of normal-metal or semiconductor tunnelling it is appropriate to reconsider and extend the stationary-state calculation of the current density J across an MIM structure as an alternative to the transfer Hamiltonian method described earlier. Following our discussion at the beginning of §2.2, travelling waves across the (idealised) tunnelling structure can be obtained by matching the wavefunction and its derivative at each boundary. Clearly such waves can be used to

compute directly the current, as:

$$J=\frac{2e}{(2\pi)^3\hbar}\int \mathrm{d}k_x\,\mathrm{d}^2k_t\,\frac{\partial E}{\partial k_x}\,[f(E)-f(E+eV)]\,D(E,k_t) \tag{5.1}$$

where $\hbar^{-1}(\partial E/\partial k_x)$ is the group velocity in the x direction, k_t represents the wave-vector transverse to the x direction, and the barrier transmission probability D is expressed as a function of E and either k_t or E_t and is understood to depend also on the bias voltage V. If the integrations over k are changed to integrations over E, one obtains, for $T=0$:

$$J=\frac{2e}{h}\int_0^{eV}\mathrm{d}E\int_0^{E}\rho_t(E_t)\,D(E,E_t)\,\mathrm{d}E_t. \tag{5.2}$$

Here E_t is the kinetic energy in the transverse (y, z) directions, and $\rho_t(E_t)$ is the density per unit energy of states for the two-dimensional transverse motion. Note that this expression does *not* depend in a direct linear fashion on either the one-dimensional density of states for x motion, $(\partial E/\partial k_x)^{-1}$, or the three-dimensional density of states, as in the superconducting case (Harrison 1961). Recall that bias V corresponds to lowering the Fermi energy in the right-hand electrode, and suppose, for example, that the right-hand electrode is a transition metal with the Fermi level lying in an s band and with an empty d band lying at an energy eV_{D} above the Fermi level. The nature of the current response at the band edge $V=V_{\mathrm{D}}$, assuming the WKB transmission factor $D=\exp(-2\kappa t)$, from equation (5.2) is $J\simeq J_{\mathrm{s}}+c(V-V_D)^2$, for $V-V_D$ small enough to neglect the variation with V of D. Such effects have generally not been observed in metals (see, however, Jaklevic and Lambe 1973) but have clearly been observed in Schottky contacts to the n-type semiconductor Ge in locating a higher $k=0$ conduction band. Here it is believed that the transmission factor D for the $k=0$ band is larger than for the occupied lower conduction band, whose minima lie along the 111 directions in the Brillouin zone, on the basis of a smaller effective mass m^* at Γ. While the case of the oxide barrier on a transition metal is complicated (Dowman *et al* 1969) because the barrier is a different material, and consequently no obvious relation exists between the m^* of the d electrons and that in the oxide, which primarily influences D, one still suspects that the failure to observe d-band edges is associated with a lower transmission factor relative to s electrons, associated with the higher m^* of the d electrons.

5.1. Quantum size effects

A simple relation does exist between the tunnelling conductance $\mathrm{d}J/\mathrm{d}V$ and the density of states $\rho_t(E)$ in cases of size quantisation where the electron system under study is effectively *two-dimensional*. In such a case discrete energy levels E_{nx} $(n=1, 2, \ldots)$ characterise the x motion, corresponding physically to $n-1$ nodes in the wave-function across the x coordinate; for each quantum state E_{nx} the total energy $E=E_{nx}+E_t$ where E_t is the transverse energy $\hbar^2k_t^2/2m_t^*$. As a specific illustration we may consider standing waves $\psi_{nx}=L^{-1/2}\sin(n\pi x/L)$, $(n=1, 2, \ldots)$ across a thin slab of width L; since $k_x=n\pi/L$ the band edges are $E_{nx}=(\hbar^2/2m_x^*)(n\pi/L)^2$. The transverse y, z motion is not affected, and may be described as $\exp[\mathrm{i}(k_yy+k_zz)]$, corresponding to transverse kinetic energy $E-E_{nx}=E_t=\hbar^2k_t^2/2m^*$. In the simplest case the density of states for fixed n for transverse two-dimensional motion is simply a

constant, $\rho_{n,t}=2\pi m_t^*/\hbar^2$, independent of energy for $E>E_{nx}$. The total spectrum would be a 'staircase' with an increment ρ_{nt} at each E_{nx} ($n=1, 2, \ldots$). According to equation (5.2), specified to this case, one finds the current corresponding to the nth $2d$ final state to be (Ben Daniel and Duke 1967):

$$J_n=\frac{2e}{h}\int \gamma_n D(E_{nx})\,\rho_t(E-E_{nx})\,\mathrm{d}E \tag{5.3}$$

and

$$\frac{\mathrm{d}J_n}{\mathrm{d}V}=\frac{2e^2}{h}\,\gamma_n D(E_{nx})\,\rho_t(eV-E_{nx})+\frac{2e}{h}\,\frac{\mathrm{d}D}{\mathrm{d}V}\,\gamma_n\int \rho_t(E-E_{nx})\,\mathrm{d}E. \tag{5.4}$$

The constant γ_n (with units of energy) is such that $\gamma_n D(E_n)=\hbar/\tau_n$ where τ_n is the decay of the state by tunnelling to the metal through the oxide barrier (Ben Daniel and Duke 1967).

Observation of the two-dimensional density of states $\rho_t(E-E_{nx})$ is thus possible (Tsui 1970, 1972) in those cases where the transmission factor is approximately constant against variations in V.

In other cases the V variation of D for $V>V_{nx}$ may obscure the $\rho_t(E-E_{nx})$ structure and reduce the spectroscopy to one of simply locating the band edges E_{nx} (Jaklevic *et al* 1971, Jaklevic and Lambe 1973, 1975).

In a series of experiments on partially oriented small-grained metal films Jaklevic and Lambe have located in special cases the band edges E_{nx} corresponding to electron standing waves in Pb, Mg, Au and Ag in thicknesses between 150–1000 Å, corresponding to observed level spacings varying from about 130 meV to 25 meV.

The observed structure corresponds to peaks in $\mathrm{d}J/\mathrm{d}V$ at E_{nx}, rather than the steps expected from $\rho_t(E-E_{nx})$, which from the above analysis means that the observed lineshape must be dominated by the bias voltage (V) dependence of the barrier transmission factor D, which depends on the properties of the *oxide*, rather than the metal under study. This has been confirmed in an analysis by Davis *et al* (1975). The observed lineshape in this case depends so heavily on the (unknown) properties of the oxide as to obscure the presence or absence of an inherent energy-dependent lifetime effect on the lineshape, predicted (Wolf 1974) on the basis of the peculiarly small-grained mosaic nature of the films.

Despite this weakness, the method, when applicable, is useful for band edge location. A nice example has been shown (Jaklevic and Lambe 1975) for the L_2' and L_1 band edge states of Au (a 150 Å film) plotted against k in the [111] direction.

5.2. Landau levels

In beautiful experiments employing grown-oxide barriers on the n-type degenerate (metallic) semiconductor InAs, Tsui (1970, 1971, 1972) has observed a two-dimensional density of states $\rho_t(E-E_{nx})$ (in a surface accumulation layer, i.e. mobile electrons bound to the surface by positive oxide charge) break up into Landau levels with the application of a magnetic field perpendicular to the surface. The data are shown in figure 23; the two prominent negative peaks in $\mathrm{d}^2I/\mathrm{d}V^2$ marked E_c and E_b correspond, respectively, to the lower edges of the conduction and surface bands. The oscillatory structure represents direct observation of two sets of Landau levels in a 3·5 T perpendicular field. On application of a *parallel* field the set of levels arising from the surface band disappears, but the set above E_c remains, confirming its origin

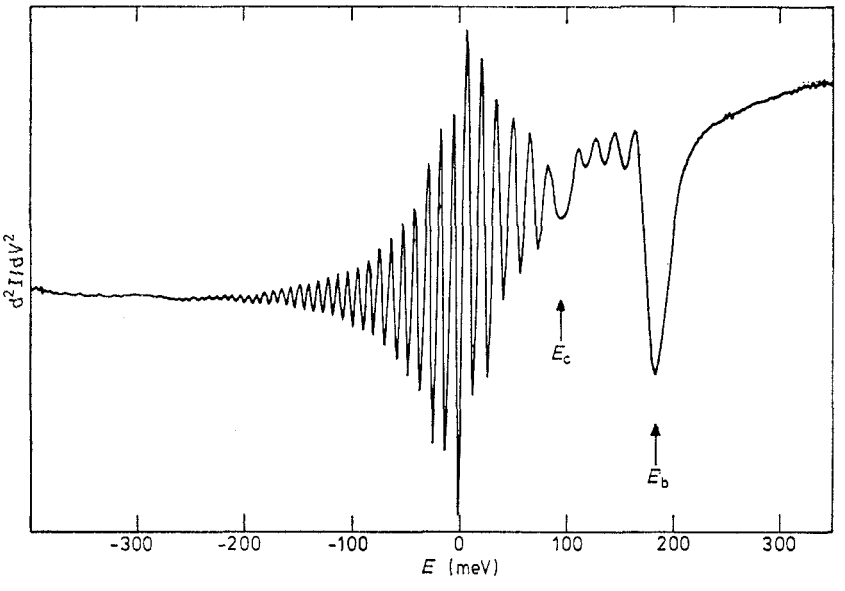

Figure 23. Tunnelling d^2I/dV^2 measurements on degenerate InAs of two-dimensional electron motion in a surface accumulation layer, after Tsui (1970). The oscillations are due to Landau levels in both the surface and the bulk conduction bands induced by a 3·5 T magnetic field applied perpendicular to the tunnelling barrier.

in bulk Landau levels. It is suggested by Tsui that the observation in this latter case may come predominantly from those bulk electrons which lie in 'skimming orbits' and pass by the surface tangentially, thus having some of the attributes of electrons in a two-dimensional band. These observations confirm the theoretical expectation that the conductance in the most favourable two-dimensional case indeed measures $\rho_t(E-E_{nx})$ and thus exhibits steps in dJ/dV at $V=V_{nx}$.

5.3. Spin polarisation in ferromagnets

We have shown in figure 16 the spin splitting into peaks at $eV=\Delta_{Al}\pm\mu_B H$ of the superconducting density of states $N_T(E)$ of a thin ($\sim$50 Å) Al film with an Ag counterelectrode, accurately parallel to a large magnetic field H. In the case of a ferromagnetic electrode, the relative strengths of the two peaks affords a means (Meservey *et al* 1970) for estimating the spin polarisation $P=(N_\uparrow-N_\downarrow)/(N_\uparrow+N_\downarrow)$ of the ferromagnetic electrons at the Fermi surface. It is assumed that the magnetic field aligns the magnetisation of the ferromagnet parallel to that in the Al film, that the tunnelling transitions preserve the spin projection and that the observed differences in N_T can be used directly in the formula for P. The last assumption is basically empirical and presumably arises in the k dependence of the pre-factor β^2 (2.3). This method measures the spin polarisation of the *tunnelling* electrons at the Fermi surface; which are primarily s electrons; the fact that the ferromagnet is evaporated as a 300–1000 Å deposit onto the oxidised 50 Å Al film means that it is polycrystalline and the polarisation P is presumably an average over crystalline directions. (However, in the case of FCC metals it is found (Jaklevic *et al* 1971) that in such deposits the [111] direction tends to lie normal to the substrate; x-ray analysis could perhaps be used to

determine the degree of such orientation in the ferromagnetic films. This appears not to have been reported.)

Extensive results from the tunnelling method have been reported by Tedrow and Meservey (1973) and by Meservey *et al* (1977). The polarisation P (in %) is measured to be positive (i.e. tunnelling electron spin *parallel* to majority ferromagnetic electron spin) with values: Fe, 44; Co, 34; Ni, 11; Gd, 15; Tb, 6·7; Dy, 6·8; Ho, 7·6; Er, 5·3; Tm and Yb, 0.

The uniformly positive numbers for Fe, Co and Ni were at first surprising, for one expects on the Stoner theory of band magnetism that the d electrons of positive P lie in a filled band well below the Fermi energy, so that the d electrons at E_F are fewer in number and fully polarised *antiparallel*. This experimental result for Ni (and presumably Fe and Co also) has been nicely explained by Chazalviel and Yafet (1977) following earlier work (Hertz and Aoi 1973). The explanation requires that the d electrons contribute very little to the tunnel current (Politzer and Cutler 1970) and that the 's' electrons at the Fermi surface be polarised positively. Chazalviel and Yafet (1977) show clearly how such a positive polarisation in the case of Ni arises from hybridisation of s and d wavefunctions. Their calculation also allows a negative P to occur in directions of small hybridisation (e.g. the [100] for Ni, in which angle-resolved field emission (Landolt and Campagna 1977) has yielded $P=-3\%$). On the whole, the several instances in which positive values of P have been observed in both field emission and photoemission (although the latter samples electrons below the Fermi energy) had been until recently the more difficult to understand.

The recent work of Meservey *et al* (1977) extends the tunnelling observations to most of the heavy rare-earth metals, in which the positive P values at the Fermi level are consistent with the results of other experiments relating to the conduction band ($5d^1\,6s^2$) polarisation (Koehler 1972). The method has been applied to 3d ferromagnetic metals and alloys by Paraskevopoulos *et al* (1977).

6. Studies of the normal phase: assisted threshold spectroscopy

6.1. Phonons, magnons and plasmons

The characteristic features of inelastic threshold tunnelling spectra are positive increments in conductance symmetrically observed at $eV=\pm\hbar\omega$, with $\hbar\omega$ the excitation energy of the interacting mode. Such effects are conveniently observed in the second derivative d^2I/dV^2 (or $-d^2V/dI^2$) in which one then observes spectra (*antisymmetric* about $V=0$) which are similar to those observed in infrared absorption spectroscopy. The basic assumption is that beyond threshold, $|eV|>\hbar\omega$, an additional electron transfer process occurs in parallel with direct elastic tunnelling.

6.1.1. Phonons. The first, and one of the clearest observations of this type of effect (Esaki 1958), was in tunnelling pn junctions in degenerate indirect band gap semiconductors such as Si and Ge. In n-type degenerate Ge containing 5×10^{18} Sb atoms cm^{-3} the electron Fermi surface at 4·2 K consists of four equivalent ellipsoids representing conduction bands filled to 36 meV above the minimum at the intersections of the [111] directions and the zone boundary (the point L). (The conduction band at $\Gamma^{(\Gamma_2')}$ is known from tunnelling measurements (Conley and Tiemann 1967) to lie $\simeq0{\cdot}15$ eV higher in energy, and is unoccupied.) In the process for forming a tunnelling pn junction (Esaki 1958) concentrated p-type dopant is diffused into the n-type

material, leaving a p-type Fermi surface about 140 meV below the $k=0$ valence band maximum. The width of the band bending region (barrier) between the p and n material is less than 200 Å, which is thin enough to allow tunnelling. At 4·2 K, however, virtually no current is observed in good diodes for biases $eV \leqslant 7{\cdot}76$ meV, the optically measured value of the TA phonon at L. Very carefully measured d^2I/dV^2 spectra (Payne 1965) are shown in figure 24 (see also figure 1) revealing four zone boundary phonon thresholds; the TA, LA, LO, and TO phonons at L with measured energies 7·766, 27·58, 30·62 and 36·15 meV, respectively. Clearly a conservation rule for wavevectors permits the electron to transfer from L to Γ only with the emission of one of the four zone boundary phonons. This case is unusual, in that virtually *all* the current flows by the phonon-assisted process. In many cases, the

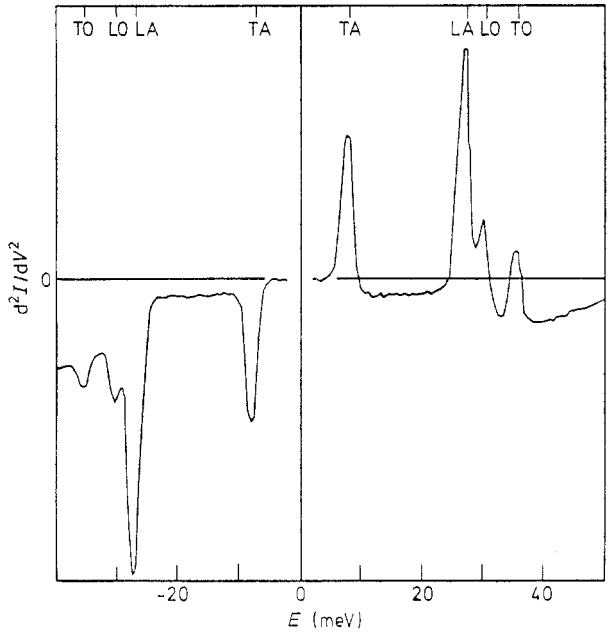

Figure 24. Threshold spectroscopy of phonons in Ge measured as d^2I/dV^2 of Sb-doped pn junction (figure 2(*c*)) at 4·2 K (Payne 1965). Accurate antisymmetry of the structure about $V=0$ is the signature of an assisted tunnelling process.

assisted flow is a very small fraction of the total current and the second derivative technique with synchronous detection is used to increase the sensitivity. In the case of a metal–semiconductor contact, the metal Fermi surface is typically large enough to permit direct transitions from all parts of the semiconductor Brillouin zone.

In contrast, in tunnelling d^2I/dV^2 data obtained from In superconducting electrodes against degenerate p-type silicon containing up to $2{\cdot}3\times10^{20}$ cm^{-3} boron (figure 25), the prominent peaks at 64·2 meV the $k=0$ optical phonon energy have the wrong *symmetry* about $V=0$ to be such a threshold effect. This effect is believed to arise as a modification of the electronic (hole) states at $E\sim64$ meV relative to the Fermi surface in the degenerate silicon by their strong resonant interaction with the $k=0$ optical phonon (Wolf 1968). Theoretical fits to this data, free from the objections of Appelbaum and Brinkman (1969a), have been given by Davis (1970a,b) and Combescot and Schreder (1974). (Incidentally, in this data at $eV\simeq80$ meV the

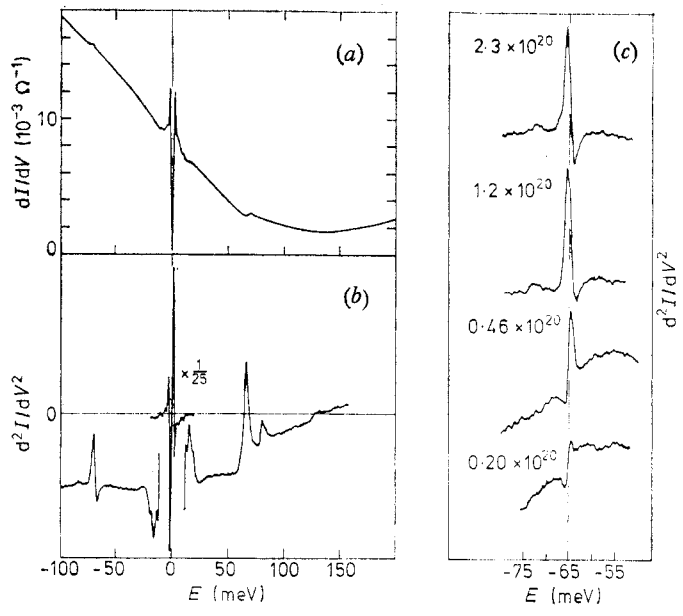

Figure 25. (*a*) dI/dV and (*b*) d^2I/dV^2 data for In–silicon oxide–degenerate silicon tunnel junctions (figure 2(*d*)). The structure at ± 64 meV arises from distortion of the E–k relation of the holes at $k=0$, ± 64 meV by interaction with the $k=0$ optical phonon, i.e. this is a polaron effect. *Symmetry* of structure in d^2I/dV^2 about $V=0$ rules out a simple assisted process. (*c*) Detail of the concentration dependence of the phonon structure at negative bias (from Cullen *et al* 1970).

excitation of the boron local phonon mode in the (heavier) silicon lattice is clearly revealed. Theoretical treatment of this feature is given by von Baltz and Urban (1977). A somewhat different phonon impurity band due to 3% In in Pb had earlier been observed in superconductive tunnelling by Rowell *et al* (1965).)

6.1.2. Magnons. An interesting threshold observation is given in figure 26 for inelastic magnon emission in antiferromagnetic NiO in the form of a barrier grown thermally on a single crystal of Ni (Tsui *et al* 1971). The NiO specimen is thus perhaps 50 Å thick. Nevertheless, the well-resolved peak at 107 meV and cutoff at 122 meV (in measurements at 1 K) in the derivative of the even (in voltage) part of the conductance are in good agreement with the full lower curve, which is the one-magnon density of states computed from the magnon dispersion relation as determined independently from inelastic neutron scattering (Hutchings and Samuelson 1971) and Raman scattering (Dietz *et al* 1971). Further, the broadened higher energy peaks at 190 and 270 meV compare favourably (see arrows) with the two-magnon and (estimated) three-magnon emission densities determined from Raman scattering. From the shift of the observed two- and three-magnon peaks relative to the dashed and dotted curves (representing, respectively, the double and triple convolutions of the single-magnon density) corresponding to multiple emission of *non*-interacting magnons; it is clear that the magnon–magnon interactions are strong. Further, from the roughly equal strength of the one- and two-magnon peaks (unfortunately, the background here is not well known), it is clear that the electron–magnon interaction is strong. One may say, following Tsui, that the electron in NiO is a *magnetic polaron*

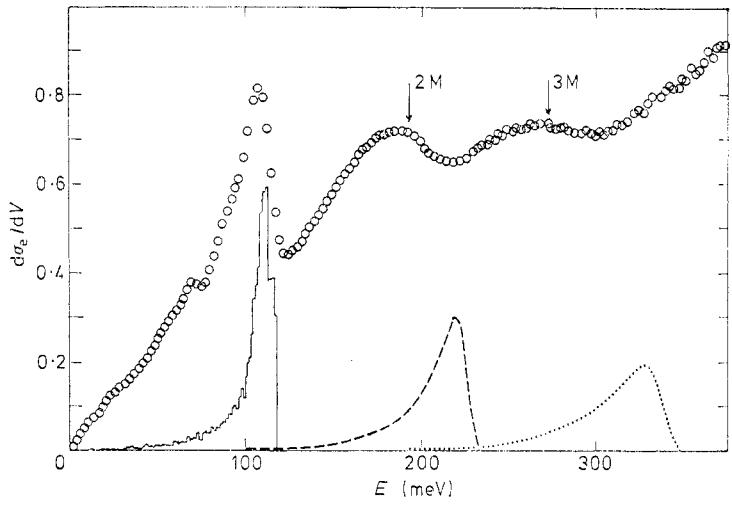

Figure 26. Tunnelling observation of magnon (spin-wave) emission in ferromagnetic NiO grown thermally on a Ni single crystal (from Tsui *et al* 1971). $t_{NiO} = 50$ Å, 1 K.

associated with perhaps two virtual magnons, in contrast to the more familiar case of the lattice polaron.

6.1.3. Plasmons. A third example of inelastic threshold spectroscopy involves surface plasmons, collective motions of the electrons against the positive ionic charge, whose characteristic frequency (in the surface case) is (Duke *et al* 1969):

$$\frac{\omega_p}{\sqrt{2}} = \left(\frac{2\pi N e^2}{m^* \epsilon}\right)^{1/2}. \tag{6.1}$$

The energy $\hbar\omega_p$ is ~ 10 eV in metals, but may be less than 0·1 eV in degenerate semiconductors. In a spectroscopic sense, the surface plasmon emission threshold has been observed in the degenerate semiconductor n-GaAs (Tsui 1969, Duke 1969) at energies between 55 and 80 meV with the predicted theoretical electron concentration dependence between $4{\cdot}2 \times 10^{18}$ and $9{\cdot}5 \times 10^{18}$ cm^{-3}; these data have been analysed by Ngai *et al* (1969) on the basis of the theory of Bennett *et al* (1968). In metals the surface plasmons are well known from optical measurements, but as they generally lie in the 5–10 eV range they have not been observed directly in tunnelling. Recently, however, the light emitted from a tunnel junction by radiative decay of surface plasmons excited by tunnelling electrons has been observed (Lambe and McCarthy 1976) and clearly identified by its high-frequency cutoff $\hbar\omega_{co} = |eV|$. The discoverers of the effect point out that it is a new method for the generation of light and have investigated means of increasing the radiation efficiency.

6.2. Spin-flip and Kondo scattering

Small temperature-dependent conductance peak anomalies at $V = 0$ were simultaneously reported by Wyatt (1964) in tunnel junctions involving oxidised Nb and Ta, and by Logan and Rowell (1964) in narrow Si pn tunnel junctions. The magnetic-field splitting of the conductance peak was demonstrated by Shen and Rowell (1967, 1968), making clear the involvement of magnetic moments. The voltage and tempera-

ture dependences were approximately given by the logarithmic form $F(eV) \propto -\ln(|eV| + nkT)/E_0$, with $n \sim 1{\cdot}3$ and E_0 typically a few meV for the semiconductors and ~ 10 meV for the Nb and Ta junctions. An example of the conductance peak split by varying magnetic fields is shown in figure 27.

6.2.1. Appelbaum's perturbation calculation. In a useful application of the transfer Hamiltonian theory Appelbaum (1967) calculated the conductance assisted by interaction with magnetic moments $\boldsymbol{S}$, in the barrier near one electrode, assumed to be magnetically coupled to the conduction electron spins $\boldsymbol{\sigma}$ (in the electrode) via the exchange interaction $\mathscr{H}^* = -2J\boldsymbol{S}.\boldsymbol{\sigma}$. The moments are assumed not to interact with each other.

The accuracy of this transfer Hamiltonian calculation for the moments *in the barrier* has recently been reconfirmed (Ivesić 1975) in a careful application of the

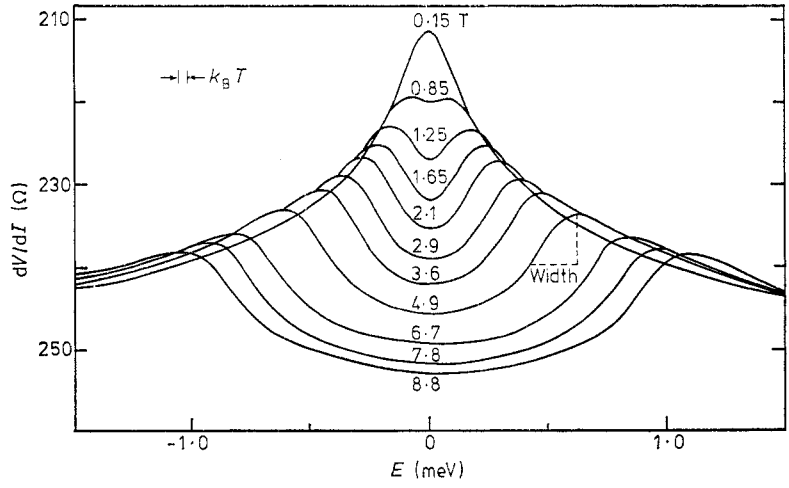

Figure 27. The conductance peak associated with Kondo scattering across a tunnel barrier. Data of Appelbaum and Shen (1972) on a Ta–Ta oxide–Al junction containing Ta moments, at 0·3 K and magnetic fields up to 8·8 T. The smeared well prominent at high field is associated with the spin-flip threshold $g\mu_B H$ which is broadened by the interaction of the moment with conduction electrons in the Ta electrodes.

model of Caroli *et al* (1971a). Indeed, this original calculation of Appelbaum remains to date the only one available to describe the effects of a magnetic field, the application of which is essential to an experimental study of these effects.

In this calculation a direct correspondence exists between terms of second and third order (G_2 and G_3, respectively) in the assisted conductance and terms of the same form derived by Kondo (1964) in his original explanation (in perturbation theory) of the relation between the interaction $\mathscr{H}^*$ in a metal containing magnetic impurities and the anomalous low-temperature resistivity minimum. The two basic scattering processes (leading to scattering *across* the barrier in the tunnelling geometry, and hence of the order of $\sim \exp(-2\kappa t)$) are spin-flip scattering, in which both the conduction electron $\boldsymbol{\sigma}$ and local moment $\boldsymbol{S}$ reverse their spin projections (this becomes inelastic with threshold $g\mu_B H$ in the presence of a magnetic field) and a third-order term in which a *virtual* spin flip takes place and in which the usual energy denominator leads to an unusual Fermi surface divergence because of the non-

commuting nature of the raising and lowering operators S^+, S^- for the spin which leaves the Fermi function in the integral. The resulting term in the scattering rate at energy E (relative to the Fermi surface) is (Kondo 1964, Appelbaum 1967):

$$F(E)=\int_{-E_0}^{E_0}\frac{\tanh(\beta\epsilon/2)\,\mathrm{d}\epsilon}{E-\epsilon}\simeq-\ln\left(\frac{E^2+(k_\mathrm{B}T)^2}{E_0^2}\right) \tag{6.2}$$

with $\beta=1/k_\mathrm{B}T$ and E_0 is an energy cutoff.

The divergence of $F(E)$ at $E=0$, $T=0$ implies the inadequacy of perturbation theory for T comparable to a characteristic Kondo temperature T_K below which a spin compensated bound state is believed to exist. (In the tunnelling geometry the coupling J between the moment and the conduction electrons is somewhat reduced by the decay of the wavefunctions into the oxide. Thus the T_K for a given moment will be expected to be lower than if the moment were in the metal itself.)

The second-order G_2 term is constant in voltage until the spin-flip is made inelastic with threshold $|eV|=g\mu H$ by the application of a field. Appelbaum's result for this case is:

$$G_2(V)=\int_{-\infty}^{\infty}g_2(\epsilon)\frac{\partial f}{\partial\epsilon}(\epsilon-eV)\,\mathrm{d}\epsilon$$

$$g_2=c_2(S(S+1)+\tfrac{1}{2}\langle M\rangle\{\tanh[\beta(\epsilon+\Delta)/2]+\tanh[\beta(\Delta-\epsilon)/2]\}). \tag{6.3}$$

Here $\Delta=g\mu_\mathrm{B}H$, μ_B is the Bohr magneton, f is the Fermi function, and $\langle M\rangle$ is the expectation value of the magnetisation of the moment of spin S. The measurement of G_2 thus determines the Zeeman splitting of the moment as it is coupled to the conduction electrons in the electrode by $-2J\boldsymbol{S}.\boldsymbol{\sigma}$; this interaction is known to produce a g shift $g-g_0=2JN(0)$ (the Knight shift in nuclear magnetic resonance) and a related lifetime broadening of the Zeeman level $\Gamma=\pi(JN(0))^2\,\Delta$, for $\Delta>k_\mathrm{B}T$. These effects arise, in turn, from the magnetisation of the conduction electrons via an assumed Pauli susceptibility $2\mu_\mathrm{B}{}^2N(0)$, and from the decay of the upper energy Zeeman state by spin-flip against a conduction electron of opposite spin in a range Δ below the Fermi energy.

The observed g values of moments have indeed always been less than the free-electron value $g=2$ and some evidence has been given for the lifetime effect and for its effect through broadening of the spin-flipped intermediate state on the $F(E)$ function in a large magnetic field (Appelbaum and Shen 1972, Wolf and Losee 1970, Losee and Wolf 1971, Bermon *et al* 1978).

6.2.2. The origin of moments in barriers. Junctions showing this conductance peak anomaly have been prepared by depositing submonolayer amounts of magnetic 3d atoms onto prepared oxide layers (Nielsen 1970, Cooper and Wyatt 1973, Christopher *et al* 1968). In some cases, such as the Ag–Ta oxide–Ta junction studied by Appelbaum and Shen (1972) the anomaly appears to arise from reduced Ta atoms in the oxide left as a result of the conventional fabrication procedure. In the case of vacuum-cleaved metal–degenerate-semiconductor Schottky barrier junctions the conductance peak is an intrinsic feature and has been shown to arise (Wolf and Losee 1970) from localised occupied donor states at the inner edge of the depletion region (barrier). One can deduce that these local moments will experience an antiferromagnetic exchange coupling:

$$J=-\frac{8}{\pi N(0)}\left(\frac{\Gamma_\mathrm{A}}{U}\right) \tag{6.4}$$

to the delocalised states from application of Anderson's model (1966) using the transformation of Schrieffer and Wolff (1966). From Anderson's estimate (1966) of $\Gamma_A/U \simeq 0{\cdot}1$ for a localised moment one deduced $JN(0) = -0{\cdot}25$, i.e. a g shift of $-0{\cdot}5$: the observed g shifts of $\sim -1{\cdot}0$ would required $\Gamma_A/U = 0{\cdot}2$.

6.2.3. Other tunnelling approaches to the Kondo problem. We have already mentioned another tunnelling approach to the Kondo problem via proximity-effect-induced superconductivity in films of the principal Kondo alloys studied in transport. The advantages of the proximity approach are that the longer superconducting coherence length removes the critical dependence on the position of the moment with respect to the conduction electrons which has been pointed out by Appelbaum and Brinkman (1970). Further, the transport studies carry over directly to the proximity tunnelling case. On the other hand the results in the proximity case are less directly related by theory to the Kondo scattering problem.

A third approach, which has been studied theoretically by Mezei and Zawadowski (1971a,b), considers moments embedded in a planar distribution in the electrode close to its surface. In this case an alteration in the density of states at the electrode–barrier interface is induced and the prediction is of a conductance *minimum*. This geometry is very difficult to establish and to characterise from an experimental standpoint, in that the position of the plane of moments should be well defined on the scale of the Fermi wavelength.

One critical test of such an experiment would be whether or not the predicted (Appelbaum and Brinkman 1970) oscillatory dependence of G_3 on z/λ_F, with z being the distance into the electrode and λ_F being the Fermi wavelength, were observed. On the other hand, the theory of Mezei and Zawadowski does predict also a non-oscillatory z-dependent (conductance minimum) term which has been reported by Bermon and So (1978).

6.3. Vibrational spectroscopy of molecules adsorbed on the barrier surface

It was noticed by Jaklevic and Lambe (1966) that evaporated Al–Al oxide–Pb junctions examined in d^2I/dV^2 with large modulation voltage amplitudes at high gain in the bias range 0–0·5 V revealed rather broad peaks at 120 meV and 450 meV, which coincide, respectively, with the energies of OH 'bending' and 'stretching' modes as observed in infrared spectroscopy applied to Al_2O_3.

Further, if molecules such as water, acetic acid, methyl alcohol, or a hydrocarbon (pump oil) were introduced in approximate monolayer amounts onto the Al oxide barrier (by gentle vapour deposition) *additional* peaks appeared in d^2I/dV^2 which were identified as essentially the vibrational spectrum of the molecule in question. This interpretation was confirmed by demonstration of the expected shift in frequency by $1/\sqrt{2}$ upon deuteration, e.g. replacing a CH by a CD group. Theoretical investigation by Scalapino and Marcus (1967) treated the molecule as an oscillating electric dipole (x component p_x) of characteristic frequencies $h\nu$ which interacted with the tunnelling electron via:

$$\delta U(x) = \frac{2ep_x x}{(x^2 + r_\perp^2)^{3/2}} \tag{6.5}$$

and could thus be excited if a resonance condition $eV = h\nu$ were satisfied. Here x is the coordinate across the barrier and $r_\perp = (y^2 + z^2)^{1/2}$. In the calculation of Scalapino

and Marcus the term $\delta U(x)$ is added to the barrier potential $U(x)$ in the WKB tunnelling exponent. By assuming $\delta U(x)$ is small and expanding the exponential one obtains for the matrix element T in the transfer Hamiltonian:

$$T \simeq \left[1+\left(\frac{2m}{V_B}\right)^{1/2} \frac{ep_x}{\hbar t}\, g\, \frac{r_\perp}{t}\right] \exp\left[-\left(\frac{2mV_B}{\hbar^2}\right)^{1/2} t\right] \tag{6.6}$$

where t is the barrier thickness, V_B is its height relative to the Fermi energy, and $g(x)=1/x-(1+x^2)^{-1/2}$.

From the extra term one can find the assisted conductance $\Delta\sigma$ (normalised to the elastic conductance) expressed as a function of the perpendicular distance $r_\perp$ of the electron to the impurity:

$$\frac{\Delta\sigma}{\sigma} = \frac{2m}{V_B}\left(\frac{e}{\hbar t}\right)^2 |\langle 1|\, p_x\, |0\rangle|^2\, g^2\left(\frac{r_\perp}{t}\right)\theta\left(V-\frac{\hbar\omega_1}{e}\right) \tag{6.7}$$

where the θ function ($\theta(x)$ is 1 for $x \geqslant 1$, and 0 otherwise) expresses the (threshold) condition that the interaction cannot occur unless enough energy $\hbar\omega_1$ is available to excite the vibration; in case $eV=\hbar\omega_1$ the electron appears precisely at the Fermi energy of the opposite electrode after tunnelling. This result yields increments in conductance $\Delta\sigma/\sigma \sim 10^{-2}$ as observed and points to an important feature of this effect, which is its extreme sensitivity in detecting the presence of small numbers of molecules. Quantitative experimental measurements on benzoic acid (Langan and Hansma 1975) show that about 1/30 monolayer can be detected. With a junction area 4×10^{-4} cm^2 this corresponds to about 10^{10} molecules, or 2×10^{-12} g.

It has been found experimentally and theoretically (Lambe and Jaklevic 1968) that Raman-active vibrations can also be observed; the tunnelling electron, which clearly interacts more strongly with the molecule than does a photon, can be regarded as inducing an electric dipole in the molecule. The calculation of the expected intensities in these two cases has recently been generalised by Kirtley *et al* (1976). The possible effects of the metal electrode and oxide layer in shifting the vibrational frequencies of molecules have been examined by Klein *et al* (1973), Walmsley *et al* (1975), McMorris *et al* (1977) and Kirtley and Hansma (1976). For details of these and other technical points the reader is referred to a recent review by Hansma (1977).

The utility of this technique for detecting (and potentially observing reactions among) very small numbers of molecules on an alumina surface has been increased by the discovery of means other than vapour deposition for introducing the molecules. The very convenient method of *liquid doping*, i.e. simply placing a drop of a dilute (1/10 to 1 g litre^{-1}) solution of the desired species in water or benzene onto the Al oxide barrier, and removing the excess by spinning, was demonstrated by Hansma and Coleman (1974). This has allowed the study of rather large organic molecules, including biological molecules. In figure 28 is shown the spectrum of the amino-acid L-phenylalanine (after Hansma and Coleman (1974)); the arrows in the figure identify peaks observed in the IR and Raman spectra of this molecule.

Very recently the introduction (and removal) of organic molecules into *completed* Al–Al oxide–Pb diodes in a humid atmosphere has been demonstrated (Jaklevic and Gaerttner 1977). It is believed that an adsorbed water layer, two or three molecules thick, assists the flow of the molecules through pores in the Pb electrode into the barrier region.

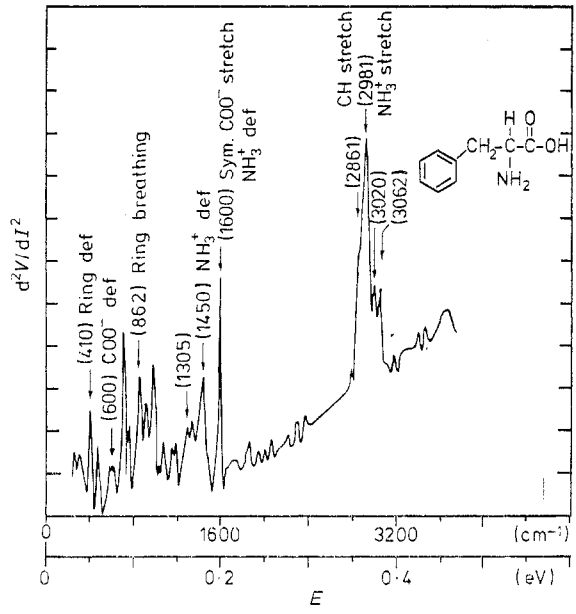

Figure 28. IETS spectrum of the amino-acid L-phenylalanine (Hansma and Coleman 1974) showing identification of peaks observed also in IR and Raman spectroscopy. The molecules are introduced into the Al_2O_3 barrier by *liquid doping* (see text).

A similar introduction of hydrogen into a completed junction has been used (Hansma 1978 and private communication) in a preliminary example of experimental work on *catalysis*. In this case the prepared Al–Al_2O_3 substrate was exposed to a submonolayer evaporation of Rh, believed to exist as small discrete particles on the alumina. The surface thus prepared was then exposed in vacuum to CO, which is known to adsorb to Rh. The junctions, completed by covering with Pb, indeed revealed upon measurement structure corresponding to the vibration of CO against the Rh surface. The introduction of H_2 was subsequently accomplished in a pressure vessel at 100 atm and at increasing temperatures. After exposures up to 420 K, the remeasured spectrum revealed the presence of additional vibrations characteristic of CH modes; these were not present in control junctions (containing Rh but no CO) similarly exposed to the H_2. It was thus tentatively concluded that evidence for the production of methane (CH_4) from the reaction $3\,H_2 + CO \rightarrow CH_4 + H_2O$, catalysed by the Rh, had been observed. This reaction appears in the gasification of coal, and thus its optimum catalysis may be of some importance. It appears that there are many extensions of work of this sort; one important extension will be to barriers other than Al_2O_3.

7. Conclusion

Electron tunnelling has been and remains the definitive technique for determining the energy gap and excitation spectrum (density of states) of a superconductor. Measurements of the tunnelling density of states have made possible the detailed verification of the strong coupling Eliashberg theory (McMillan and Rowell 1965, 1969) and have led to the extensive compilation of the properties (i.e. $\alpha^2(\omega)\,F(\omega)$,

the gap and renormalisation functions, and μ^*) of soft superconductors. The basic changes in tunnelling density of states resulting from pair breaking (e.g. by magnetic impurities) and from proximity of a superconductor to a normal metal (and vice versa) have been observed and compared to appropriate theories. The tunnelling technique has been helpful in continuing studies of superconductors held out of thermal equilibrium in various ways. A major weakness in the conventional tunnelling technique has been its inapplicability to materials which do not readily form insulating barriers of extremely high quality: thus, definitive tunnelling measurements have not yet been obtained on most of the high T_C compound superconductors or alloys.

The technique has provided a variety of useful information when applied to normal metals and degenerate semiconductors, including excitation energies and/or other information on phonons, plasmons, magnetic moments, band edge positions and pressure shifts, Landau levels, polaron effects, and size quantisation effects. Further information has been obtained on the properties of the barrier region; we note particularly the measurement of vibrational frequencies of molecules adsorbed to the barrier (IETS). As a whole, however, these results on normal systems are not subject to as comprehensive a theoretical understanding as are the superconducting results. In fact, in normal systems it is only in the case of final electronic states of a two-dimensional nature, such as electrons confined to a surface potential well (accumulation layer), that one can predict from elementary theory a direct proportionality of the tunnel conductance to the density of states per unit energy. Normal-state measurements are generally more sensitive to conditions in the immediate vicinity of the barrier and electrode surfaces, because the coherence distance characteristic of normal-state effects, generally of the order of the Fermi wavelength, is usually much less than the coherence length $\xi_0 \simeq \hbar v_F/\pi\Delta$ of a superconductor (Appelbaum and Brinkman 1970). In fact, a great deal of information about real *surfaces* and interfaces of normal metals and semiconductors has been obtained, and substantial overlap of questions and answers, if not methods, exists with the surface spectroscopic techniques such as field emission and electron energy loss.

Vigorous and promising superconducting tunnelling work is now being carried on using unconventional techniques involving coevaporation, quench-condensed films and normal-side proximity effect tunnelling to study the transition-metal superconductor family; using the proximity effect to induce the dilute magnetic alloys into the superconducting state to study the Kondo effect; and in exploring the wide domain of non-equilibrium phenomena in superconductors (Langenberg 1975). This latter work has revealed an enhancement of the superconducting gap by microwave irradiation directly observed in tunnelling.

Probably the most active area in the study of normal systems is the use of IETS to study molecules and their reactions on the Al_2O_3 barrier surface; a well-attended conference and symposium devoted to Inelastic Electron Tunnelling Spectroscopy was held in May 1977 at the University of Missouri, USA, with Proceedings to be published; this field has also been reviewed recently by Hansma (1975, 1977). This work is likely to continue to expand the overlap of normal-metal tunnelling studies with surface physical work.

Acknowledgments

This work was supported by the US Department of Energy, Department of Basic

Energy Sciences, through the Ames Laboratory at Iowa State University. I have benefited from discussions of some of the material with John R Clem, D K Finnemore and J W Osmun of the Ames superconductivity group. I also wish to thank several workers in the field for providing information in advance of publication and R J Noer for a careful reading of the manuscript.

References

Abrikosov A A and Gor'kov 1960 *Zh. Eksp. Teor. Fiz.* **39** 1781 (Engl. trans. *Sov. Phys.–JETP* **12** 1243)
Adkins C J and Kington B W 1966 *Phil. Mag.* **13** 971
—— 1969 *Phys. Rev.* **177** 777
Allen P B and Cohen M L 1972 *Phys. Rev. Lett.* **29** 1593
Allen P B and Dynes R C 1975a *Phys. Rev.* B **11** 1895
—— 1975b *Phys. Rev.* B **12** 905
Anderson P W 1966 *Phys. Rev. Lett.* **17** 95
Andreev A F 1964 *Zh. Eksp. Teor. Fiz.* **46** 1823 (Engl. trans. *Sov. Phys.–JETP* **19** 1228)
Appelbaum J 1967 *Phys. Rev.* **154** 633
Appelbaum J A and Brinkman W F 1969a *Phys. Rev.* **183** 553
—— 1969b *Phys. Rev.* **186** 464
—— 1970 *Phys. Rev.* B **2** 907
Appelbaum J A and Shen L Y L 1972 *Phys. Rev.* B **5** 544
Arnold G B 1978 *Phys. Rev.* B **18** to be published
Arnold G B, Zasadzinski J and Wolf E L 1978 *Phys. Lett.* to be published
Aslamazov L G and Larkin A I 1968 *Phys. Lett.* **26A** 238
Aspen F and Goldman A M 1976 *Cryogenics* **16** 721
Ballay R E 1977 *PhD Thesis* Iowa State University, unpublished
Band W T and Donaldson G B 1973 *Phys. Rev. Lett.* **31** 20
Bardeen J 1961 *Phys. Rev. Lett.* **6** 57
Bardeen J, Cooper L N and Schrieffer J R 1957 *Phys. Rev.* **108** 1175
Bar-Sagi J and Entin-Wohlman O 1977 *Solid St. Commun.* **22** 29
Ben Daniel D J and Duke C B 1967 *Phys. Rev.* **160** 679
Bennett A J, Duke C B and Silverstein S D 1968 *Phys. Rev.* **176** 969
Bermon S 1964 *University of Illinois, Urbana. Tech. Rep.* 1, NSF GP1100
Bermon S and So C K 1978 *Phys. Rev. Lett.* **40** 53
Bermon S, Paraskevopoulos D E and Tedrow P M 1978 *Phys. Rev.* B **17** 2110
Blackford B L and March R H 1968 *Can. J. Phys.* **46** 141
—— 1969 *Phys. Rev.* **186** 397
Blaugher R D, Hein R A, Cox J E and Waterstrat R M 1969 *J. Low Temp. Phys.* **1** 539
Bolz J and Pobell F 1975 *Proc. 14th Conf. on Low Temperature Physics* vol 2, ed M Krusius and M Vuorio (Amsterdam: North-Holland) p425
Bostock, J, Diadiuk V, Cheung W N, Lo K H, Rose R M and MacVicar M L A 1976 *Phys. Rev. Lett.* **36** 603
Brinkman W F, Dynes R C and Rowell J M 1970 *J. Appl. Phys.* **41** 1915
Caroli C, Combescot R, Noziéres P and Saint-James D 1971a *J. Phys. C: Solid St. Phys.* **4** 916
—— 1972 *J. Phys. C: Solid St. Phys.* **5** 21
Caroli C, Combescot R, Lederer D, Noziéres P and Saint-James D 1971b *J. Phys. C: Solid St. Phys.* **4** 2598
Caroli C, Combescot R, Lederer-Rozenblatt D, Noziéres P and Saint-James D 1975 *Phys. Rev.* B **12** 3977
Chaikin P M, Arnold G and Hansma P K 1977 *J. Low Temp. Phys.* **26** 229
Chaikin P M and Hansma P K 1976 *Phys. Rev. Lett.* **36** 1552
Chazalviel J-N and Yafet Y 1977 *Phys. Rev.* B **15** 1062
Chen T T, Chen J T, Leslie J D and Smith H J T 1969 *Phys. Rev. Lett.* **22** 679
Chen T T, Leslie J D and Smith H J T 1971 *Physica* **55** 439

Christopher J E, Coleman R V, Isin A and Morris R C 1968 *Phys. Rev.* **172** 485
Clark T D 1968 *J. Phys. C: Solid St. Phys.* **1** 732
Clarke J and Paterson J L 1974 *J. Low Temp. Phys.* **15** 491
Clem J R 1974 *Proc. 13th Conf. on Low Temperature Physics* vol 3, ed K D Timmerhaus, W J O'Sullivan and E F Hammel (New York: Plenum) p102
Cohen M H, Falicov L M and Phillips J C 1962 *Phys. Rev. Lett.* **8** 316
Cohen R W, Abeles B and Fuselier C R 1969 *Phys. Rev. Lett.* **23** 377
Coleman R V, Morris R C and Christopher J E 1974 *Methods of Experimental Physics* vol 11 (New York: Academic) p123
Collver M M and Hammond R H 1973 *Phys. Rev. Lett.* **30** 92
Combescot R 1971 *J. Phys. C: Solid St. Phys.* **4** 2611
Combescot R and Schreder G 1973 *J. Phys. C: Solid St. Phys.* **6** 1363
—— 1974 *J. Phys. C: Solid St. Phys.* **7** 1318
Conley J W, Duke C B, Mahan G D and Tiemann J J 1966 *Phys. Rev.* **150** 466
Conley J W and Mahan G D 1967 *Phys. Rev.* **161** 681
Conley J W and Tiemann J J 1967 *J. Appl. Phys.* **38** 2880
Cooper J R and Wyatt A F G 1973 *J. Phys. F: Metal Phys.* **3** L120
Cooper L N 1956 *Phys. Rev.* **104** 1189
—— 1960 *Am. J. Phys.* **28** 91
Cullen D E, Wolf E L and Compton W D 1970 *Phys. Rev.* B **2** 3157
Davis L C 1970a *Phys. Rev.* B **2** 1714
—— 1970b *Phys. Rev.* B **2** 4943
Davis L C, Jaklevic R C and Lambe J 1975 *Phys. Rev.* B **12** 798
Dayan M and Deutscher G 1975 *Proc. 14th Conf. on Low Temperature Physics* vol 2, ed M Krusius and M Vuorio (Amsterdam: North-Holland) p421
De Gennes P G 1964 *Rev. Mod. Phys.* **36** 225
De Gennes P G and Saint-James D 1963 *Phys. Lett.* **4** 151
Dew-Hughes D 1975 *Cryogenics* **15** 435
Dietrich I 1964 *Phys. Lett.* **9** 221
Dietz R E, Parisot G I and Meixner A E 1971 *Phys. Rev.* B **4** 2302
Dowman J E, MacVicar M L A and Waldram J R 1969 *Phys. Rev.* **186** 452
Duke C B 1969 *Tunnelling in Solids* (New York: Academic)
Duke C B, Rice M J and Steinrisser F 1969 *Phys. Rev.* **181** 733
Dumoulin L, Guyon E and Nedellec P 1977 *Phys. Rev.* B **16** 1086
Dynes R C 1970 *Phys. Rev.* B **2** 644
Dynes R C and Fulton T A 1971 *Phys. Rev.* B **3** 3015
Dynes R C, Narayanamurti V and Garno J P 1977 *Phys. Rev. Lett.* **39** 229
Dynes R C and Rowell J M 1969 *Phys. Rev.* **187** 821
—— 1975 *Phys. Rev.* B **11** 1884
Eichler A, Wuhl H and Stritzker B 1975 *Proc. 14th Conf. on Low Temperature Physics* vol 2, ed M Krusius and M Vuorio (Amsterdam: North-Holland) p52
Eliashberg G M 1960 *Zh. Eksp. Teor. Fiz.* **38** 966 (Engl. trans. *Sov. Phys.–JETP* **11** 696)
—— 1970 *Zh. Eksp. Teor. Fiz. Pis. Red.* **11** 186 (Engl. trans. *Sov. Phys.–JETP Lett.* **11** 114)
Esaki L 1958 *Phys. Rev.* **109** 603
—— 1974 *Science* **183** 1149
Ewert S, Comberg A, Sander W and Wühl H 1975 *Proc. 14th Conf. on Low Temperature Physics* vol 2, ed M Krusius and M Vuorio (Amsterdam: North-Holland) p407
Falk D S 1963 *Phys. Rev.* **132** 1576
Feuchtwang T E 1974a *Phys. Rev.* B **10** 4121
—— 1974b *Phys. Rev.* B **10** 4135
—— 1975 *Phys. Rev.* B **12** 3979
—— 1976 *Phys. Rev.* B **13** 517
Fisher J C and Giaever I 1961 *J. Appl. Phys.* **32** 172
Flükiger R and Jorda J L 1977 *Solid St. Commun.* **22** 109
Fowler R H and Nordheim L 1928 *Proc. R. Soc.* A **119** 173
Freake S M 1971 *Phil. Mag.* **24** 319
Fuchs J, Epperlein P W, Welte M and Eisenmenger W 1977 *Phys. Rev. Lett.* **38** 919
Fulde P 1969 *Tunnelling Phenomena in Solids* ed E Burstein and S Lundqvist (New York: Plenum) p427

—— 1973 *Adv. Phys.* **22** 667
Fulton T A, Hebard A F, Dunkleberger L N and Eick R H 1977 *Solid St. Commun.* **22** 493
Galkin A A, D'yachenko A I and Svistunov V M 1974 *Zh. Eksp. Teor. Fiz.* **66** 2262 (Engl. trans. *Sov. Phys.–JETP* **39** 1115)
Galkin A A, Svistunov V M and Dikii A P 1969 *Phys. Stat. Solidi* **35** 421
Gamow G 1928 *Z. Phys.* **51** 204
Gavaler J R 1973 *Appl. Phys. Lett.* **23** 480
Geerk J, Gläser W, Gompf F, Reichardt W and Schneider E 1975 *Proc. 14th Conf. on Low Temperature Physics* vol 2, ed M Krusius and M Vuorio (Amsterdam: North-Holland) p411
Giaever I 1960a *Phys. Rev. Lett.* **5** 80
—— 1960b *Phys. Rev. Lett.* **5** 147
—— 1960c *Phys. Rev. Lett.* **5** 464
—— 1969 *Tunnelling Phenomena in Solids* (New York: Plenum) p19
—— 1974 *Science* **183** 1253
Giaever I, Hart H R and Megerle K 1962 *Phys. Rev.* **126** 941
Giaever I and Megerle K 1961 *Phys. Rev.* **122** 1101
Glover R E 1967 *Phys. Lett.* **25A** 542
Gray K E 1974 *J. Low Temp. Phys.* **15** 335
Gregory J A, Bostock J, MacVicar M L A and Rose R M 1973 *Phys. Lett.* **46A** 201
Gregory W D, Averill R F and Straus L S 1971 *Phys. Rev. Lett.* **27** 1503
Griffin A and Demers J 1971 *Phys. Rev.* B **4** 2202
Gurney R W and Condon E U 1929 *Phys. Rev.* **33** 127
Guyon E, Meunier F and Thompson R S 1967 *Phys. Rev.* **156** 452
Hansma P K 1975 *Proc. 14th Conf. on Low Temperature Physics* vol 5, ed M Krusius and M Vuorio (Amsterdam: North-Holland) p264
—— 1977 *Phys. Rep.* **30C** 145
—— 1978 *Inelastic Electron Tunnelling Spectroscopy* ed T Wolfram (Berlin: Springer-Verlag) p186
Hansma P K and Coleman R V 1974 *Science* **184** 1369
Harrison W A 1961 *Phys. Rev.* **123** 85
Haskell B A, Keeler W J and Finnemore D K 1972 *Phys. Rev.* B **5** 4364
Hauser J J 1966 *Physics* **2** 247
Hauser J J, Bacon D D and Haemmerle W H 1966 *Phys. Rev.* **151** 196
Horn G and Saur E 1968 *Z. Phys.* **210** 70
Hubin W N 1970 *University of Illinois, Urbana Tech. Rep.* 182 ARPA SD-131
Hubin W N and Ginsberg D M 1969 *Phys. Rev.* **188** 716
Hulm J K and Blaugher R D 1961 *Phys. Rev.* **123** 1569
Hutchings M T and Samuelson E I 1971 *Solid St. Commun.* **9** 1011
Ivesić T 1975 *J. Phys. C: Solid St. Phys.* **8** 3371
Jackson J E, Briscoe C V and Wühl H 1971 *Physica* **55** 447
Jaklevic R C and Gaerttner M R 1977 *Appl. Phys. Lett.* **30** 646
Jaklevic R C and Lambe J 1966 *Phys. Rev. Lett.* **17** 1139
—— 1973 *Surf. Sci.* **37** 922
—— 1975 *Phys. Rev.* B **12** 4146
Joseph A S, Tomasch W J and Fink H J 1967 *Phys. Rev.* **157** 315
Josephson B D 1962 *Phys. Lett.* **1** 251
—— 1974 *Science* **184** 527
Kaiser A B and Zuckermann 1970 *Phys. Rev.* B **1** 229
Kamitakahara W A, Smith H G and Wakabayashi N 1977 *Ferroelectrics* to be published
Kaplan S B, Kirtley J R and Langenberg 1977 *Phys. Rev. Lett.* **39** 291
Keldysh L V 1964 *Zh. Eksp. Teor. Fiz.* **47** 1515 (Engl. trans. *Sov. Phys.–JETP* **20** 1018)
Kirtley J and Hansma P K 1976 *Phys. Rev.* B **13** 2910
Kirtley J, Scalapino D J and Hansma P K 1976 *Phys. Rev.* B **14** 3177
Klein J, Léger A, Belin M, Défourneau D and Sangster M J L 1973 *Phys. Rev.* B **7** 2336
Knorr K and Leslie J D 1973 *Solid St. Commun.* **12** 615
Koehler W C 1972 *Magnetic Properties of Rare Earth Metals* ed R J Elliot (London: Plenum) p83
Komenou K, Yamashita T and Onodera Y 1968 *Phys. Lett.* **28A** 335
Kommers T and Clarke J 1977 *Phys. Rev. Lett.* **38** 1091

Kondo J 1964 *Prog. Theor. Phys.* **32** 37
Kumbhare P, Tedrow P M and Lee D M 1969 *Phys. Rev.* **180** 519
Kurtin S, McGill T C and Mead C A 1971 *Phys. Rev.* B **3** 3368
Lambe J and Jaklevic R C 1968 *Phys. Rev.* **165** 821
Lambe J and McCarthy S 1976 *Phys. Rev. Lett.* **37** 923
Landolt M and Campagna M 1977 *Phys. Rev. Lett.* **38** 663
Langan J D and Hansma P K 1975 *Surf. Sci.* **52** 211
Langenberg D N 1975 *Proc. 14th Conf. on Low Temperature Physics* vol 5, ed M Krusius and M Vuorio (Amsterdam: North-Holland) p223
Léger A, Klein J, DeCheveigne S, Belin M and Defourneau D 1975 *J. Physique Lett.* **36** L301
Leslie J D, Chen J T and Chen T T 1970 *Can. J. Phys.* **48** 2783
Logan R A and Rowell J M 1964 *Phys. Rev. Lett.* **13** 404
Losee D L and Wolf E L 1971 *Phys. Rev. Lett.* **26** 1021
Lou L F and Tomasch W J 1972 *Phys. Rev. Lett.* **29** 858
Lykken G I, Geiger A L and Mitchell E N 1970 *Phys. Rev. Lett.* **25** 1578
Lykken G I and Soonpaa H H 1973 *Phys. Rev.* B **8** 3186
Machida K 1977 *J. Low Temp. Phys.* **27** 737
Machida K and Dumoulin L 1978 *J. Low Temp. Phys.* **31** 143
MacVicar M L A 1970 *J. Appl. Phys.* **41** 1965
Magno R and Adler J G 1976 *Phys. Rev.* B **13** 2262
Mahan G D 1969 *Tunnelling Phenomena in Solids* (New York: Plenum) p305
Maki K 1964 *Prog. Theor. Phys.* **31** 731
Matthias B T, Geballe T H, Longinotti L D, Corenzwit E, Hull G W Jr, Willens R H and Maiter J P 1967 *Science* **156** 645
McMillan W L 1968a *Phys. Rev.* **167** 331
—— 1968b *Phys. Rev.* **175** 537
—— 1968c *Phys. Rev.* **175** 559
McMillan W L and Anderson P W 1966 *Phys. Rev. Lett.* **16** 85
McMillan W L and Rowell J M 1965 *Phys. Rev. Lett.* **14** 108
—— 1969 *Superconductivity* vol 1, ed R D Parks (New York: Dekker) p561
Meissner H 1960 *Phys. Rev.* **117** 672
Meservey R, Pasaskevopoulos D and Tedrow P M 1977 *Proc. Conf. on Magnetism and Magnetic Materials* (*J. Appl. Phys.* **49** 1405)
Meservey R, Tedrow P M and Fulde P 1970 *Phys. Rev. Lett.* **25** 1270
Meservey R and Tedrow P M 1971 *J. Appl. Phys.* **42** 51
Meyer O 1975 see Buckel W 1975 *Proc. 14th Conf. on Low Temperature Physics* vol 5, ed. M Krusius and M Vuorio (Amsterdam: North-Holland) p150
Mezei F and Zawadowski A 1971a *Phys. Rev.* B **3** 167
—— 1971b *Phys. Rev.* B **3** 3127
Miles J L and Smith P 1963 *J. Electrochem. Soc.* **110** 1240
Millstein J and Tinkham M 1967 *Phys. Rev.* **158** 325
Moore D F and Beasley M R 1977 *Appl. Phys. Lett.* **30** 494
Moore D F, Rowell J M and Beasley M R 1976 *Solid St. Commun.* **20** 305
Morel P and Anderson P W 1962 *Phys. Rev.* **125** 1263
Mott N F 1947 *Trans. Faraday Soc.* **43** 429
Nedellec P, Dumoulin L and Guyon E 1976 *J. Low Temp. Phys.* **24** 663
Nedellec P, Dumoulin L and Noer R J 1974 *J. Phys. F: Metal Phys.* **4** L145
Ngai K L, Economou E N and Cohen M H 1969 *Phys. Rev. Lett.* **22** 1375
Nielsen P 1970 *Phys. Rev.* B **2** 3819
Noer R J 1975 *Phys. Rev.* B **12** 4882
Ochiai S I, MacVicar M L A and Rose R M 1971 *Phys. Rev.* B **4** 2988
Oppenheimer J R 1928 *Phys. Rev.* **31** 66
Owen C S and Scalapino D J 1972 *Phys. Rev. Lett.* **28** 1559
Paraskevopoulos D, Meservey R and Tedrow P M 1977 *Phys. Rev.* B **16** 4907
Parmenter R H 1961 *Phys. Rev. Lett.* **7** 274
Payne R T 1965 *Phys. Rev.* **139** A570
Pessall N and Hulm J K 1966 *Physics* **2** 311
Politzer B A and Cutler P H 1970 *Surf. Sci.* **22** 277
Prange R E 1963 *Phys. Rev.* **131** 1083

Prothero D H 1974 *Phil. Mag.* **29** 829
Reif F and Woolf M A 1962 *Phys. Rev. Lett.* **9** 315
Roberts B W 1976 *J. Phys. Chem. Ref. Data* **5** 581
Robinson B, Geballe T H and Rowell J M 1976 *Superconductivity in d- and f-Band Metals* ed D H Douglass (New York: Plenum) p381
Robinson B and Rowell J M 1978 *Proc. Int. Conf. on Physics of Transition Metals* (*Inst. Phys. Conf. Ser. No. 39*) (Bristol: The Institute of Physics) p666
Rogers J S, Adler J G and Woods S B 1964 *Rev. Sci. Instrum.* **35** 208
Rowell J M 1973 *Phys. Rev. Lett.* **30** 167
Rowell J M and McMillan W L 1966 *Phys. Rev. Lett.* **16** 453
Rowell J M, McMillan W L and Anderson P W 1965 *Phys. Rev. Lett.* **14** 633
Rowell J M, McMillan W L and Dynes R C 1978 *J. Phys. Chem. Ref. Data* to be published
Rowell J M, McMillan W L and Feldman W L 1969 *Phys. Rev.* **178** 897
Rowell J M and Schmidt P H 1976 *Appl. Phys. Lett.* **29** 622
Roy A P and Brockhouse B N 1970 *Can. J. Phys.* **48** 1781
Sahm P R and Pruss T V 1969 *Phys. Lett.* **28A** 707
Saint-James D 1964 *J. Physique* **25** 899
Scalapino D J and Marcus S M 1967 *Phys. Rev. Lett.* **18** 459
Scalapino D J, Schrieffen J R and Wilkins J W 1966 *Phys. Rev.* **148** 263
Schmidt P H, Castellano N R, Barz H, Cooper A S and Spencer E G 1973 *J. Appl. Phys.* **44** 1833
Schmidt P H, Spencer E G, Joy D C and Rowell J M 1976 *Superconductivity in d- and f-Band Metals* ed D H Douglass (New York: Plenum) p431
Schrieffer J R 1964 *Theory of Superconductivity* (New York: Benjamin)
Schrieffer J R, Scalapino D J and Wilkins J W 1963 *Phys. Rev. Lett.* **10** 336
Schrieffer J R and Wolff P A 1966 *Phys. Rev.* **149** 491
Shen L Y L 1970 *Phys. Rev. Lett.* **24** 1104
—— 1972a *Superconductivity in d- and f-Band Metals* (New York: AIP) p31
—— 1972b *Phys. Rev. Lett.* **29** 1082
Shen L Y L and Rowell J M 1967 *Solid St. Commun.* **5** 189
—— 1968 *Phys. Rev.* **165** 566
Skalski S, Betbeder-Matibet O and Weiss P R 1964 *Phys. Rev.* **136** A1500
Solymar L 1972 *Superconductive Tunnelling and Applications* (London: Chapman and Hall)
Steinrisser F, Davis L C and Duke C B 1968 *Phys. Rev.* **176** 912
Strässler S and Wyder P 1967 *Phys. Rev.* **158** 319
Stritzker B 1974 *Z. Phys.* **268** 261
Sutton J 1966 *Proc. Phys. Soc.* **87** 791
Svistunov V M, D'yachenko A I and Belogolovskii 1978 *J. Low Temp. Phys.* **31** 339
Tedrow P M and Meservey R 1971 *Phys. Rev. Lett.* **27** 919
—— 1973 *Phys. Rev.* B **7** 318
Testardi L R, Wernick J H and Royer W A 1974 *Solid St. Commun.* **15** 1
Theuerer H C and Hauser J J 1964 *J. Appl. Phys.* **35** 554
Tinkham M and Clarke J 1972 *Phys. Rev. Lett.* **28** 1366
Tomasch W J 1965a *Phys. Rev. Lett.* **15** 672
—— 1965b *Phys. Rev.* **139** A746
—— 1966 *Phys. Rev. Lett.* **16** 16
Toplicar J R and Finnemore D K 1977 *Phys. Rev.* B **16** 2072
Townsend P and Sutton J 1962 *Phys. Rev.* **128** 591
Tsui D C 1969 *Phys. Rev. Lett.* **22** 293
—— 1970 *Phys. Rev. Lett.* **24** 303
—— 1971 *Phys. Rev.* B **4** 4438
—— 1972 *Proc. 11th Conf. on the Physics of Semiconductors* (Amsterdam: Elsevier) p109
Tsui D C, Dietz R E and Walker L R 1971 *Phys. Rev. Lett.* **27** 1729
von Baltz R and Urban B 1977 *Phys. Stat. Solidi* b **79** 185
Vrba J and Woods S B 1971a *Phys. Rev.* B **3** 2243
—— 1971b *Phys. Rev.* B **4** 87
—— 1972 *Can. J. Phys.* **50** 548
Waldram J R 1976 *Rep. Prog. Phys.* **39** 751
Walmsley D G, Floyd R B and Timms W E 1977 *Solid St. Commun.* **22** 497

Walmsley D G, McMorris I W N and Brown N M D 1975 *Solid St. Commun.* **16** 663
Wolf E L 1968 *Phys. Rev. Lett.* **20** 204
—— 1974 *Phys. Rev.* B **10** 784
—— 1975 *Solid St. Phys.* **30** 1
Wolf E L and Losee D L 1970 *Phys. Rev.* B **2** 3660
Wolf E L and Zasadzinski J 1977 *Phys. Lett.* **62A** 165
—— 1978 *Proc. Conf. on Physics of Transition Metals* (*Inst. Phys. Conf. Ser. No. 39*) (Bristol: The Institute of Physics) pp666–70 and unpublished data
Wolf E L, Zasadzinski J and Arnold G B 1978 to be published
Wolfram T 1968 *Phys. Rev.* **170** 481
Woolf M A and Reif F 1965 *Phys. Rev.* **137** A557
Wright P W and Franck J P 1977 *J. Low Temp. Phys.* **27** 459
Wühl H, Jackson J E and Briscoe C V 1968 *Phys. Rev. Lett.* **20** 1496
Wyatt A F G 1964 *Phys. Rev. Lett.* **13** 401
Wyatt P W, Barker R C and Yelon A 1972 *Phys. Rev.* B **6** 4169
Yoshihiro K and Sasaki W 1968 *J. Phys. Soc. Japan* **24** 426
Zavaritskii N V 1965 *Zh. Eksp. Teor. Fiz.* **48** 837 (Engl. trans. *Sov. Phys.–JETP* **21** 557)
Zawadowski A 1967 *Phys. Rev.* **163** 341
Zeller H R 1972 *Phys. Rev.* B **5** 1813
Zittartz J, Bringer A and Müller-Hartmann E 1972 *Solid St. Commun.* **10** 513